THE INVERSE CONDUCTIVITY PROBLEM: ANISOTROPY, FINITE ELEMENTS AND RESISTOR NETWORKS

A thesis submitted to the University of Manchester
for the degree of Doctor of Philosophy
in the Faculty of Engineering and Physical Sciences

2013

Kyriakos Paridis
School of Mathematics

Contents

Word count 48584

List of Tables

List of Figures

The University of Manchester

Kyriakos Paridis
Doctor of Philosophy
The Inverse Conductivity Problem: Anisotropy, Finite Elements and Resistor Networks
August 26, 2013

EIT is a method of imaging that exists for a century, initially in geophysics and in recent years in medical imaging. Even though the practical applications of EIT go back to the early 20th century the systematic study of the inverse conductivity problem started in the late 1970s, hence many aspects of the problem remain unexplored. In the study of the inverse conductivity problem usually Finite Element Models are used since they can be easily adapted for bodies of irregular shapes. In this work though we use an equivalent approximation, the electrical resistor network, for which many uniqueness results as well as reconstruction algorithms exist. Furthermore resistor networks are important for EIT since they are used to provide convenient stable test loads or phantoms for EIT systems. In this thesis we study the transfer resistance matrix of a resistor network that is derived from n-port theory and review necessary and sufficient conditions for a matrix to be the transfer resistance of a planar network. The so called "paramountcy" condition may be useful for validation purposes since it provides the means to locate problematic electrodes. In the study of resistor networks in relation to inverse problems it is of a great importance to know which resistor networks correspond to some Finite Element Model. To give a partial answer to this we use the dual graph of a resistor network and we represent the voltage by the logarithm of the circle radius. This representation in combination with Duffin's non-linear resistor network theory provides the means to show that a non-linear resistor network can be embedded uniquely in a Euclidean space under certain conditions. This is where the novelty of this work lies.

Declaration

No portion of the work referred to in the thesis has been submitted in support of an application for another degree or qualification of this or any other university or other institute of learning.

Copyright Statement

i. The author of this thesis (including any appendices and/or schedules to this thesis) owns certain copyright or related rights in it (the "Copyright") and s/he has given The University of Manchester certain rights to use such Copyright, including for administrative purposes.

ii. Copies of this thesis, either in full or in extracts and whether in hard or electronic copy, may be made **only** in accordance with the Copyright, Designs and Patents Act 1988 (as amended) and regulations issued under it or, where appropriate, in accordance with licensing agreements which the University has from time to time. This page must form part of any such copies made.

iii. The ownership of certain Copyright, patents, designs, trade marks and other intellectual property (the "Intellectual Property") and any reproductions of copyright works in the thesis, for example graphs and tables ("Reproductions"), which may be described in this thesis, may not be owned by the author and may be owned by third parties. Such Intellectual Property and Reproductions cannot and must not be made available for use without the prior written permission of the owner(s) of the relevant Intellectual Property and/or Reproductions.

iv. Further information on the conditions under which disclosure, publication and commercialisation of this thesis, the Copyright and any Intellectual Property and/or Reproductions described in it may take place is available in the University IP Policy (see http://documents.manchester.ac.uk/DocuInfo.aspx?DocID=487), in any relevant Thesis restriction declarations deposited in the University Library, The University Library's regulations (see http://www.manchester.ac.uk/library/aboutus/regulations) and in The University's policy on Presentation of Theses.

Acknowledgements

Firstly I would like to thank my supervisor Prof. Bill Lionheart for not only being my dreamed supervisor but also for being a good friend. His guidance, knowledge and supervision made this thesis possible and it was an honour to work with him. Furthermore, I have to acknowledge the support of the Engineering and Physical Sciences Research Council of the UK (EPSRC) for the generous financial support. Grateful thanks are extended to my examiners, Dr. Manuchehr Soleimani of the University of Bath and Dr. Oliver Dorn of the University of Manchester firstly for agreeing to be my examiners and secondly for making the viva voce examination a pleasant experience. Moreover, their fruitful comments and suggestions have improved this work.

Additionally, my appreciation and love goes to my office colleagues whose friendship and help contributed in making the last four years a pleasant experience. They are Dr. David Szotten, Dr. Nicola Wadeson, Dr. Will Thompson, Mike Crabb and Russell Miller. Special thanks go also to Dr. Rüdiger Borsdorf for firstly being such a good friend and secondly for all his help mainly in MATLAB programming. Our discussions about economics and politics were always enjoyable. My appreciation goes also to my cousin Dr. Stavros Apostolou for helping me with my first steps in Manchester back in 2006.

I would also like to thank the Andreas C. Ioannou family for being my second family. Special gratitude goes to my family. My mother Maria for always supporting my decisions. In addition I thank my sister Eleni and her husband Neofitos, and my brother Stavros and his wife Eleni for their love and friendship. Last but not least, I thank Myria for her love, patience and understanding. Her visits were always a pleasant way to clear my mind. More importantly her support and encouragement have made this thesis possible.

Dedication

To my mother Maria, my late father Costas and late godfather Theodosis.

List of Acronyms

AC Alternating Current

CEM Complete Electrode Model

CM Continuum Model

CT X-ray Computed Tomography

ECT Electrical Capacitance Tomography

EIDORS Electrical Impedance and Diffuse Optical Reconstruction Software

EIT Electrical Impedance Tomography

EMT Electromagnetic Tomography

EOD Electric Organ Discharge

ERT Electrical Resistivity Tomography

FD Finite Difference

FE Finite Element

FEM Finite Element Method

FVM Finite Volume Method

GM Gap Model

GREIT Graz consensus Reconstruction algorithm for Electrical Impedance Tomography

ICU Intensive Care Unit

MIT Magnetic Induction Tomography

MRI Magnetic Resonance Imaging

SEM Shunt Electrode Model

SVD Singular Value Decomposition

VILI Ventilator-Induced Lung Injury

Chapter 1

Introduction

Ἀγεωμέτρητος μηδεὶς εἰσίτω[1]

Πλάτων

1.1 Inverse problems

The concept of an inverse problem is more easily understood in terms of an example. A classical example involves the heat equation. The heat equation describes the temperature distribution of a body as the time progresses. This is given by the following relation

$$\frac{\partial u}{\partial t} - \alpha \nabla^2 u = 0, \tag{1.1.1}$$

where u is the heat distribution and $\alpha > 0$ is a constant, known as the thermal diffusivity. The function u describes the temperature at a given location (x, y, z). Of course, the temperature will change over time as heat spreads throughout space. This temperature change over time is determined by the heat equation (1.1.1). The idea of finding the temperature distribution after some time consists the forward problem. On the other hand, an inverse problem related to this equation would be to determine the initial temperature distribution from the final distribution, given some conditions. In other words, find the initial temperature from the last measurement. Of course other inverse problems are related to the heat equation. For example the problem of

[1] "Let no one untrained in geometry enter". Motto over the entrance to Plato's Academy

determining the thermal parameters from temperature measurements is also an inverse problem.

From a mathematician's perspective an inverse problem can be described by the statement of J.B. Keller [60]: "We call two problems inverses of one another if the formulation of each involves all or a part of the solution of the other. Often, for historical reasons, one of the two problems has been studied extensively for some time, while the other has never been studied and is not so well understood. In such cases, the former is called the *direct problem*, while the latter is the *inverse problem*".

Generally speaking, the direct and the inverse problem are strongly related, in fact, the data of one problem are the unknowns of the other and vice versa. In this term, it seems arbitrary to decide which problem is the direct and which is the inverse [18].

From a physicist point of view the distinction between direct and inverse problem seems more natural. For a physicist, a direct problem is considered to be more fundamental and oriented along a cause-effect sequence based on well-established physical laws. By contrast, we humans, choose to infer physical problems from certain measured data and this is regarded as an inverse problem.

1.2 Ill-posed problems

The most challenging part of the study of an inverse problem is its ill-posed nature, and in particular the problem of instability. According to the French mathematician Jacques Hadamard [47] a problem is well posed if for all admissible data

1. a solution exists,

2. the solution is unique,

3. the solution depends continuously on the data.

If one or more of the previous conditions is violated then the problem is called ill-posed. The problem of recovering the electrical conductivity from boundary voltage data is extremely ill-posed since the third criterion is not satisfied meaning that it is not possible to obtain a stable algorithm. This can be partially overcomed by imposing additional assumptions (regularization methods).

In practice, the ill-posedness of EIT comes from the fact that for any given measurement precision, there are arbitrarily large changes in the conductivity and this is not detectable by the boundary measurements at the same precision. It is possible to solve the problem if we know *a priori* information about the conductivity distribution, hence the extreme variations causing the instability are ruled out [50].

The existence of a solution is not questioned because we believe that the body has a physical conductivity. The uniqueness of solution is fundamental in inverse problems. The uniqueness of solution is linked to the problem of sufficient data, that is, if we have enough information to uniquely recover the conductivity. During the last three decades many questions have been answered about the uniqueness, mainly for an isotropic conductivity σ [57], but this is not the case for an anisotropic conductivity.

1.3 EIT

EIT is an imaging technique in which a conductivity image of the inside of a body is produced my making surface electrical measurements. It belongs to the family of electromagnetic imaging modalities along with Electrical Capacitance Tomography (ECT), Electromagnetic Tomography (EMT) and Magnetic Induction Tomography (MIT). In EIT electrodes are attached to the body and a sequence of low-frequency current patterns is applied. While the current passes through the body a set of voltage measurements is acquired from the boundary of the body. An Alternating Current (AC) is used in order to avoid polarization effects. EIT is a relatively new method and its invention is attributed to Henderson and Webster who in the late 70s had the idea of an "Impedance Camera" [49]. The first practical medical EIT system was built by the Sheffield group of Barber and Brown [12]. Though EIT is considered to be a medical imaging method it can be found and is used in other disciplines. It is actually used for geophysical surveys under the name Electrical Resistivity Tomography (ERT) and apparently the first electric field imaging experiment was conducted by Conrad Schlumberger (1878-1932), at that time professor at the Ecole des Mines de Paris (now MINES Paristech), in 1912 [10]. Schlumberger's experiments were followed by the first mathematical results in the 1930s (see [64]). The name of Tikhonov is very well known in the inverse problems community due to his work on regularization of

inverse problems but is less known for his contribution in ERT where he explains how to solve the ERT problem in a simple case of 2-layered medium. By the early 1990s the limitation of computer power was less restrictive and the inverse problem of ERT could be solved numerically. The work of Loke and Barker at Birmingham University was among the first such solution, and their approach is still widely used [76], [75]. A similar method to EIT is used for industrial process monitoring under the name Electrical Resistance Tomography. Amazingly EIT can be found in nature too. For example some weakly electric fish use Electric Organ Discharge (EOD), which is typically less than one volt in amplitude, to navigate, hunt their prey and avoid obstacles [83].

An EIT system is typically a compact set of equipment which includes the data acquisition unit with the current source and the sensors attached (electrodes), and a computer with the reconstruction code. Different data acquisition schemes have been developed. For illustration purposes here we describe the Sheffield Mark I system [27]. The system consists of 16 electrodes distributed evenly in the same plane around the body. A constant current of 1-5 mA at 50 kHz is applied to an adjacent pair of electrodes and voltages are measured between the other adjacent pairs. The current is then switched to another pair of electrodes, and a second set of measured voltages is achieved. Usually voltage measurements on current carrying electrodes are avoided. Under this configuration the Sheffield Mark I system can therefore make $13 \times 16 = 208$ measurements. Due to reciprocity only half of these measurements are independent.

1.4 Advantages and disadvantages of EIT

EIT is superior to other medical imaging techniques in terms of cost and speed but inferior in terms of spatial resolution. As we have described in the previous section an EIT system is a simple system in terms of hardware requirements and considering the fact that the main components of an EIT system are getting cheaper this gives EIT an advantage. Of course components for other medical systems are also getting cheaper but it is unlikely that they will ever become as cheap as components for an EIT system. Obviously, an EIT system will never replace other medical imaging systems like X-ray Computed Tomography (CT), Magnetic Resonance Imaging (MRI) or ultrasound

since the information a physician receives from each system is different, hence we must consider different modalities as complimentary rather than competing. Ultimately the user is the one who decides which imaging method will be used depending on the needs. If real time, reliable, portable and cost efficient tool is required then EIT is the obvious choice.

The major disadvantage of EIT is the relatively poor resolution. The resolution of EIT is limited because the number of electrodes is usually limited to 16-32, hence the voltage data set collected is limited. For EIT to compete with other imaging methods in terms of resolution many more electrodes are required. Another factor that limits the resolution and accuracy of EIT is the ill-posedness of the problem, meaning that to achieve small improvement in the image accuracy huge improvement of the measurement accuracy is required. Adding to these, the difficulty of making electrical measurements on a human, it is only natural that EIT is difficult.

1.5 Developments in EIT

The first paper on the use of electrical current for medical imaging appeared in the early 1980s [15]. Due to limitations of computational and memory power the first models were considered to be two dimensional, though the researchers were aware that this was a very simplistic approach. Furthermore, Barber and Brown introduced the linear back-projection method [13], [14], in their first system. This method was considering equipotentials as curves rather than surfaces which in a sense discouraged the development of three dimensional algorithms.

In the early years of medical imaging the electrode modelling was not considered seriously. Probably this is due to the two dimensional models and the unsophisticated algorithms. The transition from the initial Continuum Model (CM) to the model allowing gaps in the boundary (Gap Model (GM)) to the more realistic models like the Shunt Electrode Model (SEM) led the researchers to understand the importance of electrode modelling and the need for a model which would consider and deal with the voltage drop across the non-excited electrodes. Barber and Brown developed the "four-electrode" measurement technique [16], [77]. This specific technique was later used in the Sheffield Mark III system.

In the effort to minimise errors new measurement techniques have been developed. Pidcock et al. [85] suggest to use large drive electrodes while voltage measurements are taken on passive, point electrodes. The suggested configuration eliminates the largest effects of contact impedance on the voltage measurements. Hua et al. [51] in a different approach used electrodes where different parts of the same electrode are used for driving and detection purposes.

In the recent years the electrode models became more precise and realistic with the implementation of the Complete Electrode Model (CEM), which is now the most used model. The CEM is more precise and it adds a complex impedance for each electrode which includes the electrode contact impedance.

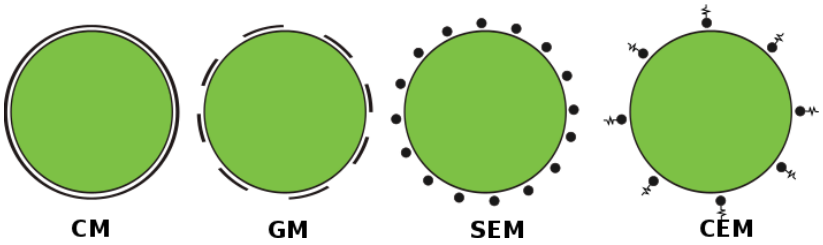

Figure 1.1: The four electrode models used in EIT.

In Figure 1.1 it can be clearly seen how the electrode modelling has changed during the years. From the very simple CM to the very sophisticated CEM.

During the early days of EIT the two scientific communities involved, the engineering and the mathematical, were working in almost complete isolation. The engineers were concentrated on the hardware aspect of EIT along with potential applications. On the other side, mathematicians were concerned about the theoretical aspects of the problem. The question mathematicians were determined to answer was whether or not a set of boundary measurements uniquely determines the conductivity of the body under investigation.

In 1980 Alberto P. Calderón published the revolutionary paper "On an inverse boundary value problem" [28]. This paper is sometimes called "the foundational paper" since it lays the foundations for a mathematical view of the problem. It is worth mentioning that probably Calderón thought of this problem when he was working as an engineer in Argentina for the Yacimientos Petroliféros Fiscales (YPF)[3], the state owned

[3]Treasury Petroleum Fields

oil company, but published it decades later [88]. In this paper, Calderón suggested whether it is possible to reconstruct the conductivity of a body by making current and voltage measurements at the boundary. In his paper Calderón showed that the Fréchet derivative of the forward mapping was an injective function, and therefore a unique inverse could indeed be calculated (see Section 2.1 for more details). Due to Calderón's paper the uniqueness problem for EIT is also called "the Calderón problem". Using the CEM, Somersalo et al. [91] proved the existence and uniqueness of the forward solution for the two dimensional problem. In 1984, Kohn and Vogelius [62] proved that in the case of smooth isotropic conductivity the boundary values and derivatives at the boundary for such conductivity could be determined from the Dirichlet to Neumann map. The same authors have extended their result to piecewise real-analytic conductivities in [63]. Later studies by Sylvester and Uhlmann [93] have proved uniqueness and existence in three dimensional models with $\sigma \in C^2(\bar{\Omega})$. Similar results have been obtained by Isakov [56]. After these promising results Nachman, Sylvester and Uhlmann [80] considered the case where the $\sigma \in C^{1,1}(\bar{\Omega})$ with a positive answer. Later Nachman extended the result to domains with $C^{1,1}$ boundaries [81]. The condition was further relaxed by Alessandrini [9] to Lipschitz boundary.

Until the mid 1990s the existing results for uniqueness under certain conditions were for dimension $n \geq 3$. For the two dimensional case, Nachman [82] proved a global uniqueness result for Calderón's problem for conductivities in the Sobolev space $W^{2,p}(\Omega)$, for $p > 1$, in 1996. Finally, Astala and Päivärinta [11] answered the question of uniqueness in $L^\infty(\Omega)$ using $\bar{\partial}$-methods.

1.6 Resistor networks in EIT

In principle, a finite element approximation is used for EIT. Probably, this is due to the extensive study of Finite Element Method (FEM) and the existence of many reconstruction algorithms (see [88] Chapter 14). The FEM approximation works rather well considering its limitations, but generally no uniqueness results exist. A different approach to the inverse conductivity problem is provided by electrical resistor networks.

A useful illustration of EIT arises from the study of the sensitivity to a small change

in conductivity. In other words, how a small localised change in conductivity affects the voltage. The continuum case is explained in detail in [50] (p.28). The discrete version is based on Geselowitz's sensitivity theorem [44]. The network based version of the sensitivity theorem is due to Murai and Kagawa [79] and Nakayama et al. [59]. This theorem relates a change in the voltage to a change in conductivity for a resistor network. Later, Yorkey [97] used a compensation method in a resistor network and he observed that for a resistor change, the change in voltage to first order is equivalent to the resulting voltage due to a current source applied in parallel with that resistor. Additionally, Yorkey et al. [98] showed how to form a Jacobian matrix entry from the discrete version of the sensitivity theorem. This method of calculation is more efficient and accurate than the standard method.

The connection between resistor networks and EIT was further investigated by Curtis and Morrow. In their studies they considered both rectangular [35] and circular [32] networks proving several uniqueness results along with reconstruction algorithms. Analogous results to the continuous problem were given in [34], namely results about the discrete Green's functions and the maximum principle. Lastly, Curtis and Morrow introduced the process of harmonic continuation. Using this idea they proved that a locally constant harmonic function is not necessarily constant in the whole domain. This property contradicts the continuum case where a locally constant harmonic function guarantees the function to be constant in the whole domain.

In recent years, significant work on resistor networks has been carried out at Rice University by Borcea's group [96], [24], [23]. In [24], Borcea et al. introduced an inversion algorithm for two-dimensional EIT using a model reduction approach. The reduced models are resistor networks obtained from a finite volume discretisation of the elliptic differential equation for the potential on optimal grids. These optimal grids provide the essential connection between the continuum EIT problem and the resistor networks. They prove uniqueness of the solution of the reduced problem and they also propose a method for calculating the unknown conductivity using the resistor networks. Additionally they show how a priori information can be incorporated in the inversion scheme. In a follow up paper [23], the authors show how to construct the optimal grids for EIT with partial information using external quasiconformal transformations of the grid for EIT with full boundary measurements.

1.7 EIT software and hardware

The theoretical developments in EIT enabled researchers to develop code for image reconstruction. A very popular project among the EIT community is the Electrical Impedance and Diffuse Optical Reconstruction Software (EIDORS) project [7], [86], [87], a MATLAB (also Octave) toolbox. EIDORS is a free software released under GNU General Public License that provides algorithms for forward and inverse modelling for EIT and diffusion based optical tomography, in medical and industrial settings. Since one of the main purposes of the EIDORS project it to promote collaboration between groups working in the field of EIT it is relatively easy to use, well documented and deep knowledge of inverse problems is not necessarily required. A similar project that has emerged, mainly from the EIDORS developers is the Graz consensus Reconstruction algorithm for Electrical Impedance Tomography (GREIT) [5]. As we have mentioned EIT is an attractive method for monitoring patients during mechanical ventilation. The problem though was that all the existing algorithms were too simplistic, hence they did not incorporate the advances in inverse problems in the past two decades. A group of experts both from EIT algorithm and clinical applications areas have proposed the following consensus in order of importance: *a*) uniform amplitude response, *b*) small and uniform position error, *c*) small ringing artefacts, *d*) uniform resolution, *e*) limited shape deformation and *f*) high resolution. In the field of geosciences a commercial package for ERT has been developed from Geotomo Software for both 2D [73] and 3D [74] resistivity and induced polarization inversion. The software offers land surface, underwater and cross-borehole surveys. This is based on the work of Loke and Barker at the University of Birmingham [76]. RES3DINV has a finite difference forward solver used when the ground is assumed flat, and a finite element solver for known non-flat topography. The Jacobian is initialized using an analytical initial solution assuming homogeneous conductivity and different regularization methods are used. The penalty function used in the regularization handles horizontal and vertical variations differently. Noisy data can be treated using the one-norm to measure the fit of the data to the forward solution.

At the moment EIT systems for medical monitoring are commercially available from different manufacturers for research purposes. The first system is a Sheffield

Mark 3.5 produced by Maltron International [55]. The EIT group at the University of Göttingen has developed the GOE MF II, distributed by CareFusion, for respiratory monitoring. This is the world's first EIT system suited for and systematically used in experimental validation studies [94]. Breast cancer detection is another area where EIT has been widely tested. Pioneering research has been done at the Research Institute of Radioengineering and Electronics of the Russian Academy of Science who in collaboration with Impedance Medical Technologies have produced the Multifrequency Electrical Impedance Mammography System (MEM) and the Gynecologic Impedance Tomograph (GIT) [53]. The systems typically comply with medical safety legislation and are being used by research groups in hospitals, notably in Intensive Care Unit (ICU) for monitoring ventilation. In 2011, Dräger Medical has made available PulmoVista 500 [78], the first medical system for lung monitoring that is designed for everyday use in the ICU.

1.8 Motivation of this work

Although in the last 30 years the development in EIT is dramatic there are still many issues that need to be investigated. Anisotropy is clearly important, as biological tissue and stratified rock can be anisotropic. However, although there are some theoretical results, the topic has been neglected, especially in terms of practical implementation. Another important issue is the shape deformation. In particular, in the case of pulmonary EIT we know that the chest shape changes with breathing. This change, if not taken into account in the model, causes significant artefacts in the reconstructed images. For these reasons, with this thesis we investigate some of these problems and suggest solutions.

1.9 Thesis organization

In the next chapter we briefly review Calderón's results from his famous paper. Moreover we present a brief introduction to graph theory. The notions presented are very basic and can be found in the first pages of any graph theory textbook, but are necessary to understand the theory of resistor networks. In addition to those we give a

small introduction to the basics of differential geometry. In reality, we just present a series of definitions that lead to the notion of the differentiable manifold.

Chapter 5 gives a general description of resistor networks and we also explain some basics of circuit theory. The important work of Curtis and Morrow is also presented. The most important and novel part of this chapter are the consistency conditions given for transfer resistance matrices of networks. This is extremely helpful, since these consistency conditions may be useful for validating EIT data and fault finding in EIT systems. This chapter also acts as an introduction to the next chapter, where we deal with the problem of the embedding.

Chapter 6 is the main part of this thesis and contains novel work regarding the problem of embedding a resistor network in to the three dimensional space. We start by introducing resistor networks along with some theoretical aspects. We also discuss some uniqueness results due to Curtis and Morrow about rectangular and circular resistor networks. Our main result is stated in Theorem 6.5.1 where we show that a resistor network associated with a FE mesh can be uniquely embedded in the three dimensional space. The novelty of our method lies in the fact that we draw ideas from computer graphics [61] to parameterise a triangular surface and then use non-linear circuit theory [40] on the dual graph of a resistor network, where the voltage is represented by the logarithm of the circle radius.

In Chapter 3 we consider anisotropic conductivities and we start by noting Kohn and Vogelius non-uniqueness result [62]. We also set up the problem in terms of the FEM. Finally we investigate numerically the Singular Value Decomposition (SVD) of the Jacobian for anisotropic EIT and we show that for different mesh sizes and geometries the problem of recovering the conductivity is as ill-conditioned as the isotropic problem.

Chapter 4 deals with the problem of boundary deformations in EIT. We firstly review the progress in recent years. We go on to explain why boundary distortions lead to errors in the reconstruction. Lastly, we build on the two dimensional work of Boyle et al. [25], [26] and construct a conformal vector field that we use for our numerical experiments for image reconstruction of a model under deformation.

In the final chapter we summarise the results of the undertaken research. Additionally we give some ideas on how this research can be expanded and further developed.

All the tests were implemented on my departmental issued workstation running MATLAB R2011a and Linux openSUSE 12.1 on a 2.6GHz quad core AMD Phenom. Some of the tests were implemented on an Apple Macbook Pro with an Intel Core 2 Duo processor clocked at 2.66GHz running the same version of MATLAB.

Chapter 2

Mathematical background and preliminaries

> If I have seen further it is by standing on the shoulders of giants.[1]
>
> Sir Isaac Newton

In this chapter we describe the inverse conductivity problem posed by Calderón and we also outline his findings. In the second part of the chapter we refer to some terminology and give the definitions of the notions used in the thesis. In more detail we start with some basic graph theory where we define a graph and then concentrate on planar graphs and some terminology used by Curtis and Morrow [36]. Lastly, we move to differential geometry and we define the notion of a differentiable manifold. We note here that there is no novelty in this chapter. Its purpose is to give some basic ideas to those unfamiliar with graph theory and differential geometry.

2.1 The inverse conductivity problem

Reconstructing the conductivity inside a body using surface electromagnetic measurements is very important and it has attracted great attention because the problem is simple to state, but extremely ill-posed and non-linear. The problem described here is known as the inverse conductivity problem or Calderón's problem and it can be

[1] Letter from Isaac Newton to Robert Hooke, 5 February 1676, as transcribed in Jean-Pierre Maury (1992) Newton: Understanding the Cosmos, New Horizons

used in many applications such as geophysics, mine detection, industrial and process monitoring and medical imaging.

A mathematical description of the problem follows [95]. Let u be the electrical potential and $\sigma > 0$ be the electrical conductivity in a bounded and smooth domain $\Omega \subseteq \mathbb{R}^n$, $n \geq 2$. Then, in absence of current sources, the conductivity equation is

$$L_\sigma(u) \coloneqq \nabla \cdot (\sigma \nabla u) = 0 \text{ in } \Omega. \tag{2.1.1}$$

Given some Dirichlet data on the boundary, the potential $u \in H^1(\Omega)$ solves the problem

$$\begin{cases} L_\sigma(u) = \nabla \cdot (\sigma \nabla u) = 0 & \text{in } \Omega \\ u = \phi & \text{on } \partial\Omega. \end{cases} \tag{2.1.2}$$

The measurements on the boundary $\partial\Omega$ are given by the Dirichlet to Neumann map, sometimes also called the voltage to current map, since Λ_σ measures the induced current flux at the boundary

$$\Lambda_\sigma : \ u|_{\partial\Omega} \mapsto \sigma \nabla u \cdot \nu, \tag{2.1.3}$$

where ν is the unit outward normal to $\partial\Omega$. The quadratic form Q_σ associated to Λ_σ is defined by

$$\begin{aligned} Q_\sigma(\phi) = \langle \phi, \Lambda_\sigma(\phi) \rangle &= \int_\Omega \sigma |\nabla u|^2 \\ &= \int_{\partial\Omega} \phi \sigma \frac{\partial u}{\partial \nu}. \end{aligned} \tag{2.1.4}$$

Using the polarization identity [20], the bilinear form associated to the quadratic form is obtained

$$\begin{aligned} B_\sigma(\phi, \psi) &= \frac{1}{2} \{ Q_\sigma(\phi + \psi) - Q_\sigma(\phi) - Q_\sigma(\psi) \} \\ &= \frac{1}{2} \left\{ \int_\Omega |\nabla(u+v)|^2 - \sigma |\nabla u|^2 - \sigma |\nabla v|^2 dx \right\} \\ &= \int_\Omega \sigma \nabla u \cdot \nabla v dx, \end{aligned} \tag{2.1.5}$$

where $L_\sigma u = 0$ in Ω and $v|_{\partial\Omega} = \psi \in H^{\frac{1}{2}}(\partial\Omega)$. It is obvious that a complete knowledge of any of Λ_σ, Q_σ and B_σ are equivalent.

Calderón in his revolutionary paper [28] introduced the, now well known, inverse conductivity problem (2.1.2) and he set the following question:

"...decide whether σ is uniquely determined by Q_σ and to calculate σ in terms of Q_σ, if σ is indeed determined by Q_σ.".

The Argentine mathematician was the first who seriously worked on the inverse conductivity problem and he finally proved that the mapping

$$\Phi : \sigma \to \Lambda_\sigma \tag{2.1.6}$$

is analytic as a function of $\sigma \in L^\infty$. For this, he simply considered an expression for the solution of

$$\begin{aligned} L_\sigma(W) = \nabla \cdot (\sigma \nabla W) = 0, \\ W|_{\partial\Omega} = \phi, \\ \sigma = 1 + \delta. \end{aligned}$$

Let $W = u + v$, where $\Delta u = L_1 u = 0$, $u|_{\partial\Omega} = \phi$. Then considering $L_1 u = 0$ it is easy to obtain $L_\sigma W = L_1 v + L_\delta v + L_\delta u = 0$. Furthermore, $v|_{\partial\Omega} = 0$ and $v \in H_0^1(\Omega)$, but since L_1 is an operator from $H_0^1(\Omega)$ into $H^{-1}(\Omega)$, it has a bounded inverse G and hence

$$v + GL_\delta v = -GL_\delta u$$

and

$$v = -\left[\sum_{j=0}^{\infty} (-1)^j \left(GL_\delta\right)^j\right] \left(GL_\delta u\right). \tag{2.1.7}$$

Since $W \in H_0^1(\Omega)$, $||L_\delta W||_{H^1} \leq ||\delta||_\infty ||W||_{H_0^1}$. The series (2.1.7) converges if

$$||\delta||_\infty ||G|| < 1$$

and

$$||v||_{H^{-1}} = \frac{||G||||\delta||_\infty ||\phi||}{1 - ||G||||\delta||_\infty}.$$

Hence Φ is analytic at $\sigma = 1$ and the same argument shows that Φ is analytic for any σ.

Moreover Calderón proved that $d\Phi|_{\sigma=\text{constant}}$ is injective. He also showed that in case the conductivity σ is smooth and nearly constant then it can be approximated using knowledge of Λ_σ. But Calderón was unable to answer his main question, that is if Φ was indeed an injective function, even in a neighbourhood of $\sigma = \text{constant}$.

2.2 Graph theory

In this section we refer to some simple notions of graph theory necessary for understanding the material described in Chapters 5 and 6. The material covered can be found in any graph theory book and we refer to [17], [22], [48] where the reader can find more details.

In simple words a graph is a set of points, typically called vertices or nodes, joined one to another. These links between nodes are called the edges (rarely lines or links) of the graph. Let $V = \{v_i : i = 1, 2, \ldots, n_v\}$ be the set of vertices (sometimes denoted by $V(G)$ or V_G to avoid confusion), and denote by $E = \{\{u, v\} \,|\, u, v \in V,\, u \neq v\}$ the set of edges (similarly denoted by $E(G)$ or E_G).

Definition 2.2.1. *A pair $G = (V, E)$ is called a graph (also simple graph).*

As one would imagine a subgraph of a graph G is a graph whose vertex set is a subset of that of G, and whose adjacency relation is a subset of that of G restricted to this subset. A pair $\{u, v\}$ is usually written simply as uv. Notice that in this case $uv = vu$. The two vertices u and v are called the endpoints (or ends) of the edge $e = uv \in E$. Two vertices u, v are called adjacent or neighbours if $uv \in E$. Two edges $e_1 = uv$ and $e_2 = vw$ sharing an end, are adjacent with each other.

Definition 2.2.2. *The number of vertices in a graph is called the order of the graph and we denote n_v.*

Usually a graph is represented as a plane figure by drawing a line between the points u and v if $e = uv$ is an edge of G (e.g. Figure 2.1).

A graph can also be represented by a matrix. Given an ordering of the vertices $v_1, v_2, \ldots, v_{n_v}$, the matrix with entries

$$M_{ij} = \begin{cases} 1, & v_i v_j \in E \\ 0, & v_i v_j \notin E \end{cases}$$

is called the adjacency matrix of G. For example the graph in Figure 2.1 has an

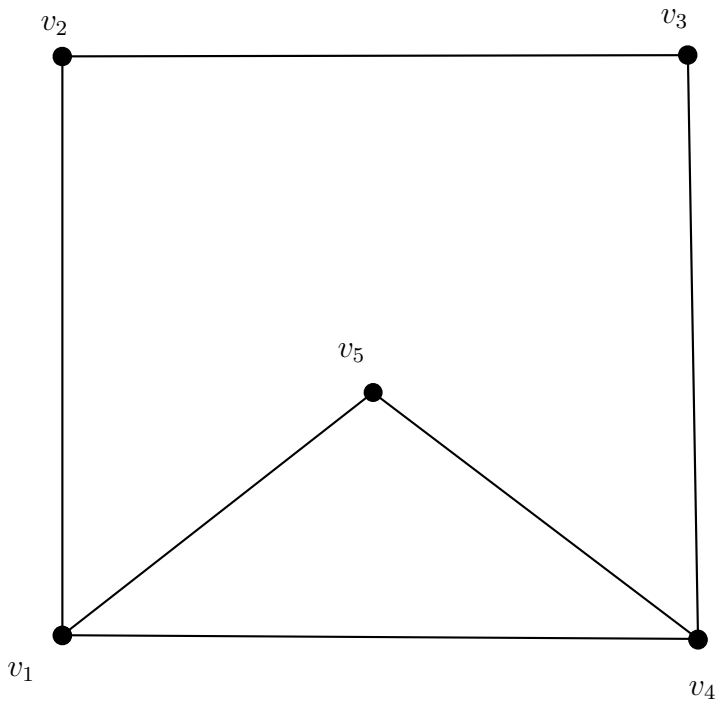

Figure 2.1: A planar graph G with 5 vertices

adjacency matrix

$$\begin{pmatrix} 0 & 1 & 0 & 1 & 1 \\ 1 & 0 & 1 & 0 & 0 \\ 0 & 1 & 0 & 1 & 0 \\ 1 & 0 & 1 & 0 & 1 \\ 1 & 0 & 0 & 1 & 0 \end{pmatrix}.$$

We observe that adjacency matrices are symmetric and the elements of the main diagonal are zeros. Note that a graph has many adjacency matrices, one for each ordering of V. Here we also note the relation between the adjacency matrix of a graph with the Kirchhoff matrix of a resistor network described in Section 5.2.

Definition 2.2.3. *Let $e_i = v_i v_{i+1} \in E$, $i = 1, 2, \ldots, k$ be edges of a graph G. A sequence of edges $W = e_1 e_2 \ldots e_k$ is a walk of length k with start node at v_1 and end node at v_{k+1}.*

Walks are an important notion of graph theory since they give rise to the notions of paths and cycles, which are fundamental for the study of resistor networks.

Planar graphs are a "special" type of graph since such graphs can be embedded in the plane. In plain English, an embedding is defined as a planar graph with a mapping

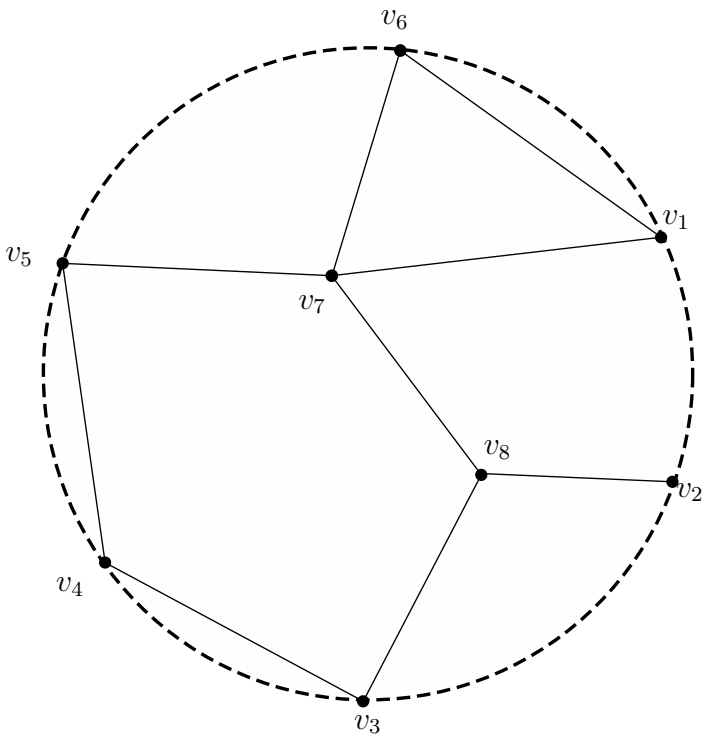

Figure 2.2: A circular planar graph G with 8 nodes

from every node to a point on a plane, and from every edge to a plane curve on that plane, such that the extreme points of each curve are the points mapped from its end nodes, and all curves are disjoint except on their extreme points.

Definition 2.2.4. *A graph $G = (V, E)$ is immersed in the plane if there is a map $f : G \to \mathbb{R}^2$ such that:*

1. *The vertices $v_i \in V$, $i = 1, 2, \ldots, n_v$ are mapped to distinct points in $\mathbb{R}^2$.*

2. *The edges $e_i \in E$, $i = 1, 2, \ldots, n_e$ are mapped to simple curves joining the nodes.*

A planar graph can be simply drawn on the plane in such a way so that its edges intersect only at their endpoints. This kind of drawing is called a plane graph or planar embedding of the graph.

Definition 2.2.5. *An embedding of a graph G in the plane is an immersion such that two edges may intersect only at the endpoints.*

In the study of resistor networks we consider planar graphs with boundary. This means that a planar graph $G = (V, E)$ can be embedded in the plane such that $V_0 \subset V$ is the set of boundary vertices. Naturally the set $V \setminus V_0$ is the set of interior vertices. A

special case are the circular planar graphs, where a graph $G = (V, E)$ can be embedded in the unit disk. Figure 2.2 is an example of a circular planar graph with 6 boundary nodes and 2 interior nodes, totalling 8 nodes and 9 edges.

Definition 2.2.6. *Let $W = e_1 e_2 \dots e_k$ be a walk. Then*

1. *W is closed, if $v_1 = v_{k+1}$,*
2. *W is a path, if $v_i \neq v_j$ for all $i \neq j$,*
3. *W is a cycle, if it is closed and $v_i \neq v_j$ for all $i \neq j$ except $v_1 = v_{k+1}$.*

When a graph is drawn without any crossing, any cycle that surrounds a region without any edges reaching from the cycle into the region forms a face.

Definition 2.2.7. *A connected graph is a graph where for any two vertices v_i and v_j we can find a walk which begins at v_i and ends at v_j.*

A connected graph $G = (V, E)$ is a tree if it has no cycles. Any graph without cycles is a forest.

Definition 2.2.8. *Let $G = (V, E)$ be a connected graph. A spanning tree of G is a tree containing all the vertices and a subset of the edges in G. In other words a tree that spans over all vertices in G. Hence, each spanning tree of a connected graph with n_v vertices has exactly $n_v - 1$ edges. Notation: We denote a spanning tree with (V, E'), where $E' \subset E$.*

A spanning tree rooted at a point $v_0 \in V$ is spanning tree for which the starting vertex is specified to be v_0. The cotree of a spanning tree in a connected graph G is the subgraph of G containing exactly those edges of G which are not in the tree.

In the case of resistor networks from the inverse problems point of view we are generally interested in the paths between boundary nodes. For example in the graph G of Figure 2.2 there are four paths originating from v_1,

$$\begin{aligned} v_1 \leftrightarrow v_2 : \beta_1 &= v_1 v_7 v_8 v_2 \\ v_1 \leftrightarrow v_3 : \beta_2 &= v_1 v_7 v_8 v_3 \\ v_1 \leftrightarrow v_5 : \beta_3 &= v_1 v_7 v_5 \\ v_1 \leftrightarrow v_6 : \beta_4 &= v_1 v_6, \end{aligned}$$

but there is no path from v_1 to v_4 since it is not possible to join the two vertices exclusively with interior nodes. Two paths P and Q are disjoint, if they have no vertices in common.

Lemma 2.2.1. *Let $W : u \xrightarrow{*} v$ with $u \neq v$, be a walk of some length. Then W contains a path $P : u \xrightarrow{*} v$, meaning that P is obtained from W by removing edges and vertices.*

Definition 2.2.9. *If $P = (p_1, p_2, \ldots, p_k)$ and $Q = (q_1, q_2, \ldots, q_k)$ are sequences of boundary vertices, a $k-$connection through G denoted by $P \longleftrightarrow Q$, is a set of paths $\{p_i \leftrightarrow q_i\}$ which are vertex disjoint.*

Referring to Figure 2.2 for $P = (v_1, v_2)$, $Q = (v_5, v_3)$ and $R = (v_6, v_1)$ we see that

1. $(P; Q)$ are 2-connected since

$$\begin{aligned} v_1 \leftrightarrow v_5 : &= v_1 v_7 v_5 \\ v_2 \leftrightarrow v_3 : &= v_2 v_8 v_3 \end{aligned}$$

2. $(R; Q)$ are not 2-connected since the paths $v_6 \leftrightarrow v_5$ and $v_1 \leftrightarrow v_3$ are not disjoint.

Consider a circular planar graph G with boundary in the sense Curtis and Morrow [36] define it, id est the graph is embedded in the plane so that the boundary nodes V_0 lie on a circle C and the remaining nodes are in the interior of C. The boundary nodes are labelled v_i, $i = 1, 2 \ldots, n$ in clockwise order. Now let $P = (p_1, \ldots, p_k)$ and $Q = (q_1, \ldots, q_k)$ be disjoint sequences of boundary nodes.

Definition 2.2.10. *A graph G is well-connected if for every circular pair $(P; Q)$ there is a $k-$connection from P to Q. A graph is called critical if an edge removal breaks a connection.*

When dealing with graphs it is sometimes more convenient to work with the dual graph instead of the original one.

Definition 2.2.11. *Let G be a planar graph. To construct the dual graph G' the following procedure is used:*

1. *To each face of the graph, assign a dual point.*

2. *If two neighbouring faces share a common edge, connect their dual points with a dual edge.*

The term "dual" is used because this property is symmetric, meaning that if G' is a dual of G, then G is a dual of G', assuming that G is connected.

For example in Figure 2.3 the graph G is represented by black, continuous lines and its dual G' by red, dashed lines.

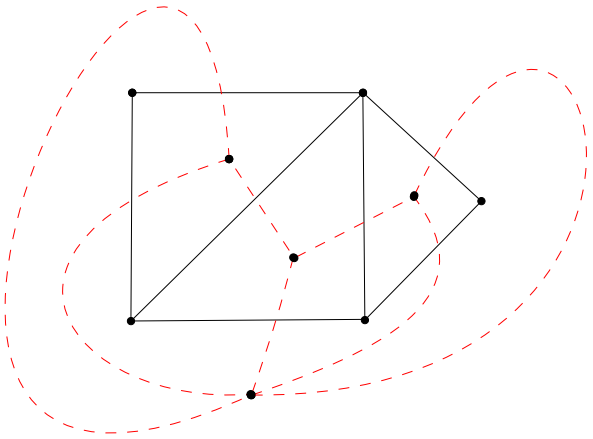

Figure 2.3: A graph G and its dual graph G'

2.3 Differential geometry

In the theoretical study of inverse problems, differential geometry plays a fundamental role. The concept of the differentiable manifold is of great importance in the development of abstract inverse problems theory. A series of definitions (see [38], [3] for more details and examples) follows which will lead to the notion of an n-dimensional smooth manifold.

Let $U \subset X$ be an abstract subset of X and fix a number $n \in \mathbb{N}$.

Definition 2.3.1. *A chart (U, φ) on X is a bijective map $\varphi : U \to V$ where $V \subset \mathbb{R}^n$ is an open set. The inverse map $\varphi^{-1} : V \to X$ is an injection of the open domain V in X. There is a one-to-one correspondence between points in $U \subset X$ and arrays $(x_1, \ldots, x_n) \in V \subset \mathbb{R}^n$ given by the maps φ and φ^{-1}:*

$$X \supset U \ni x = \varphi(x^1, \ldots, x^n) \leftrightarrow (x^1, \ldots, x^n) \in V \subset \mathbb{R}^n.$$

An atlas $\mathcal{A}$ on X is a collection of charts $\mathcal{A} = (U_\alpha, \varphi_\alpha)$, where $\varphi_\alpha : U_\alpha \to V_\alpha \subset \mathbb{R}^n$ for all α, such that the subspaces $\{U_\alpha\}$ cover the whole space X:

$$X = \bigcup_\alpha U_\alpha.$$

Consider sets U_α and U_β, such that $U_\alpha \cap U_\beta \neq \emptyset$. To the intersection $U_\alpha \cap U_\beta$ correspond subsets $\varphi_\alpha^{-1}(U_\alpha \cap U_\beta \subset V_\alpha)$ and $\varphi_\beta^{-1}(U_\alpha \cap U_\beta \subset V_\beta)$. Any point $\mathbf{x} \in U_\alpha \cap U_\beta$, has two coordinate descriptions: $\varphi_\alpha^{-1}(\mathbf{x}) = (x_\alpha^1, \ldots, x_\alpha^n)$ and $\varphi_\beta^{-1}(\mathbf{x}) = (x_\beta^1, \ldots, x_\beta^n)$. Therefore there is an invertible map called the transition map

$$\begin{aligned} \Psi_{\alpha\beta} = \varphi_\alpha \circ \varphi_\beta^{-1} : \ \varphi_\beta(U_\alpha \cap U_\beta) &\to \varphi_\alpha(U_\alpha \cap U_\beta) \\ (x_\beta^1, \ldots, x_\beta^n) &\mapsto (x_\alpha^1, \ldots, x_\alpha^n), \end{aligned}$$

which we call the change of coordinates between charts φ_α and φ_β.

Definition 2.3.2. *An atlas $\mathcal{A} = \{(U_\alpha, \varphi_\alpha)\}$, $\varphi_\alpha : U_\alpha \to X$ is differentiable or smooth if all sets $\varphi_\alpha(U_\alpha \cap U_\beta)$ are open and the functions $\Psi_{\alpha\beta}$ of changing of coordinates are differentiable functions.*

Definition 2.3.3. *A differentiable manifold, or smooth manifold (shortly: manifold) is a set X endowed with a smooth atlas.*

Definition 2.3.4. *Two manifolds M and N are said to be smoothly equivalent or diffeomorphic if there is a bijective map f, called a diffeomorphism, such that both $f : M \to N$ and its inverse $f^{-1} : N \to M$ are smooth.*

A tangent vector $\mathbf{v}$ at a point $\mathbf{x} \in M$ is defined as a rule assigning an array of numbers $(v^1, \ldots, v^n)$ to each coordinate system $x^1, \ldots, x^n$ near $\mathbf{x}$ so that for any two coordinate systems, say, $x^1, \ldots, x^n$ and $x^{1'}, \ldots, x^{n'}$ the respective arrays are related by the transformation

$$v^i = \sum_{i'} \frac{\partial x^i}{\partial x^{i'}} v^{i'}.$$

The numbers v^i are called the components of the vector $\mathbf{v}$ w.r.t a given coordinate system. The set of all tangent vectors at $\mathbf{x} \in M$ is called the tangent space at $\mathbf{x}$ and denoted $T_{\mathbf{x}}M$.

Let $F : M \to N$ be a smooth map, where M and N are manifolds. Let $\mathbf{p} \in M$ and the map $F_* : T_{\mathbf{p}}M \to T_{F(\mathbf{p})}N$. Then $\tilde{\mathbf{v}} = F_*\mathbf{v}$. In components we have

$$\mathbf{v} = \sum_i v^i \frac{\partial}{\partial x^i} \text{ and } \tilde{\mathbf{v}} = \sum_i \tilde{v}^i \frac{\partial}{\partial \tilde{x}^i}.$$

Then $\tilde{v}_i = D(\tilde{\mathbf{x}}^i F \mathbf{x}^{-1})(v_i)$. If F is a diffeomorphism then $F^* = (F^{-1})_*$ is the pull-back of a vector field. Now let $g : M \to T^*M \otimes T^*M$ be a metric on N. Then $(F^*g)(v_\mathbf{p}, w_\mathbf{p}) = g(F_* v_\mathbf{p}, F_* w_\mathbf{p})$. If F is a diffeomorphism then $F_* = (F^{-1})_*$ is the push-forward of the metric g.

Now consider the metric $g = \lambda e$, where e is a flat metric and λ is a positive function.

Definition 2.3.5. *A metric e is called flat or Euclidean if its components in some coordinate system are the Kronecker delta δ_{ij}.*

Definition 2.3.6. *A metric g is called conformally flat if $F_* g = \lambda e$ for some smooth invertible map F and positive scalar function λ.*

Definition 2.3.7. *A conformal mapping of a space with metric g is a smooth invertible mapping F with $F_* g = \lambda g$ for a positive scalar λ. A conformal mapping preserves angles while possibly changing lengths.*

The next definition we give is about the embedding. In simple words an embedding is a map which maps a subspace (smaller structure) to the whole space (larger structure).

Definition 2.3.8. *Let (M_1, g_1) and (M_2, g_2) be Riemannian manifolds. An embedding is a smooth map $F : M_1 \to M_2$ which preserves the metric, that is $g_1 = F^* g_2$.*

Duffin uses the Brouwer's fixed point theorem to prove Lemma 6.4.1 and for this reason we state the theorem.

Theorem 2.3.1 (Brouwer's fixed point theorem)**.** *Fix an integer $n \geq 0$ and let $B \subset \mathbb{R}^n$ be the unit hypersphere*

$$B = \{\mathbf{x} \in \mathbb{R}^n : ||\mathbf{x}|| \leq 1\}.$$

Then any continuous function $f : B \to B$ has a fixed point.

In Section 6.7 we refer to the Gauss-Bonnett condition in Theorem 6.7.1. Here we state the theorem without proof.

Theorem 2.3.2 (Gauss-Bonnett Theorem)**.** *Suppose M is a compact two dimensional Riemannian manifold with boundary ∂M. Let K be the Gaussian curvature of M, and let k_g be the geodesic curvature of ∂M. Then*

$$\int_M K dA + \int_{\partial M} k_g dS = 2\pi\chi(M),$$

where dA is the element of area of the surface, ds is the line element along ∂M and $\chi(M)$ is the Euler characteristic of M.

Chapter 3

FEM and anisotropic EIT reconstruction

Τὰ πάντα ρεῖ καὶ οὐδὲν μένει[1]

Ηράκλειτος

This chapter is an expansion to the conference paper [72] presented at the XIVth International Conference on Electrical Bioimpedance and the 11th Conference on Biomedical Applications of EIT held at the University of Florida, Gainesville, FL, USA on April 4-8, 2010. We start by explaining the meaning of anisotropy in mathematical terms and then we explain why we cannot find a unique solution to the inverse problem of anisotropic conductivity. Afterwards we approach the inverse conductivity problem from the FEM point of view and we calculate the weak form and discuss the system matrix. Lastly, we perform a rank analysis of the Jacobian and present some numerical results showing that the rank of the Jacobian is less than the degrees of freedom in the anisotropic conductivity, hence recovering it is not possible.

3.1 Introduction

It is well known that many body tissues such as muscle have an anisotropic conductivity. It is also known that the inverse problem for anisotropic EIT does not have

[1] "Everything flows, nothing stands still", Heraclitus

a unique solution even with complete data (arbitrarily many, arbitrarily small electrodes) of arbitrary precision [67]. The usual numerical treatment of EIT uses a FE model to solve the forward problem and the conductivity in this model is adjusted to fit the measured data. Extending the usual approach to the anisotropic problem we approximate the potential as piecewise linear on tetrahedra elements and it seems natural to represent the anisotropic conductivity as a constant symmetric matrix on each tetrahedron.

There are two pit-falls with this approach. The finite element system matrix can have non zero elements only for pairs of vertex indices corresponding to an edge in the FE mesh. The diagonal elements are simply the negative of the sum of the off diagonal elements for that row or column so the maximum number of degrees of freedom in our FE model is the number of edges. Representing the anisotropic conductivity as a symmetric matrix on each element gives $6n_t$ degrees of freedom (n_t is number of tetrahedra) – more than n_e the number of edges. This means that even if we knew the FE system matrix (let alone just the boundary data) we still could not uniquely determine the conductivity matrix on each tetrahedron uniquely, however this is not the non-uniqueness that arises in the continuum problem.

3.2 Non-uniqueness

Anisotropy is an important aspect of inverse problems but only researchers recently took it into account. In the case of anisotropic media the conductivity depends on the direction, thus it is represented by a symmetric and positive definite matrix $\sigma = (\sigma_{ij})_{i,j=1}^{n}$.

Since the conductivity is anisotropic the Dirichlet problem (2.1.2) takes the form

$$\begin{cases} \nabla \cdot (\sigma \nabla u) = \sum_{i,j=1}^{n} \frac{\partial}{\partial x^i} \left(\sigma_{ij} \frac{\partial u}{\partial x^j} \right) = 0, & \text{in } \Omega, \\ u = f, & \text{on } \partial\Omega, \end{cases} \tag{3.2.1}$$

where $f \in H^{\frac{1}{2}}(\partial\Omega)$ is the potential at the boundary. For any solution u to the Dirichlet problem (3.2.1) the Dirichlet to Neumann map is

$$\Lambda_\sigma f = \sigma \nabla u \cdot \mathbf{n}|_{\partial\Omega}, \tag{3.2.2}$$

where $\mathbf{n}$ is the unit outward normal to Ω.

Definition 3.2.1. *The Dirichlet to Neumann map associated to* (3.2.1) *is the map*

$$\Lambda_\sigma : H^{\frac{1}{2}}(\partial\Omega) \to H^{-\frac{1}{2}}(\partial\Omega) \tag{3.2.3}$$

given by

$$\langle \Lambda_\sigma f, \eta \rangle = \int_\Omega \sigma(x)\nabla u(x) \cdot \nabla \phi(x) dx, \tag{3.2.4}$$

for any $f, \eta \in H^{\frac{1}{2}}(\partial\Omega)$, $u, \phi \in H^1(\Omega), \phi|_{\partial\Omega} = \eta$.

It is easy to see that a conductivity tensor $\sigma = (\sigma_{ij})$ is isotropic when it is invariant under a rotation, meaning

$$\sigma = P^T \sigma P$$

for all rotations P. It can also be proved that a tensor represents an isotropic conductivity when $\sigma = \alpha I$, where α is a scalar and I is the identity matrix.

In the isotropic case the problem can be considered solved. The reader may refer to [88] for an extensive review of the main results involving the isotropic conductivity case. In contrast, for the anisotropic problem the Dirichlet to Neumann map does not determine the conductivity uniquely in general. Kohn and Vogelius [62] proved the following non-uniqueness result, firstly observed by Tartar.

Proposition 3.2.1. *If* $F : \overline{\Omega} \to \overline{\Omega}$ *is a* C^1 *diffeomorphism such that* $F(x) = x$, *for each* $x \in \partial\Omega$, *then* σ *and* $\tilde{\sigma} = \frac{(DF)\sigma(DF)^T}{\det(DF)} \circ F^{-1}(\sigma)$ *have the same Dirichlet to Neumann map, i.e.* $\Lambda_\sigma = \Lambda_{\tilde{\sigma}}$.

Proof. Consider the change of variables $y = F(x)$ on the Dirichlet integral

$$\int_\Omega \sigma_{ij}(x) \frac{\partial u}{\partial x^i} \frac{\partial u}{\partial x^j} dx = \int_\Omega \tilde{\sigma}_{ij}(x) \frac{\partial \tilde{u}}{\partial y^i} \frac{\partial \tilde{u}}{\partial y^j} dy, \tag{3.2.5}$$

where

$$\tilde{\sigma}(y) = \frac{(DF)\sigma(DF)^T}{\det(DF)} \circ F^{-1}(y)$$

and

$$\tilde{u}(y) = u \circ F^{-1}(y).$$

Since the solution u of the Dirichlet problem (3.2.1) minimizes the left hand side of the Dirichlet integral (3.2.5), then $\tilde{u} = u \circ F^{-1}$ minimizes the right hand side of the same integral. We then conclude that $\tilde{u}$ solves

$$\begin{cases} \nabla \cdot (\tilde{\sigma} \nabla \tilde{u}) = 0 & \text{in } \Omega, \\ \tilde{u} = \tilde{f} = u \circ F^{-1} & \text{on } \partial\Omega. \end{cases}$$

Now, consider the solution ν of

$$\begin{cases} \nabla \cdot (\sigma \nabla \nu) = 0 & \text{in } \Omega, \\ \nu = g & \text{on } \partial\Omega. \end{cases}$$

Applying the change of variable on ν we obtain $\tilde{\nu}$ and therefore as previously,

$$\begin{cases} \nabla \cdot (\tilde{\sigma} \nabla \tilde{\nu}) = 0 & \text{in } \Omega, \\ \tilde{\nu} = \tilde{g} = g \circ F^{-1} & \text{on } \partial\Omega. \end{cases}$$

Similarly due to the change of variables the Dirichlet integral is

$$\int_\Omega \sigma_{ij}(x) \frac{\partial u}{\partial x^i} \frac{\partial \nu}{\partial x^j} dx = \int_\Omega \tilde{\sigma}_{ij}(x) \frac{\partial \tilde{u}}{\partial y^i} \frac{\partial \tilde{\nu}}{\partial y^j} dy,$$

which can be shortened to

$$\int_\Omega \sigma \nabla u \cdot \nabla \nu dx = \int_\Omega \tilde{\sigma} \nabla \tilde{u} \cdot \nabla \tilde{\nu} dy.$$

Using the following identity for u (and similarly for $\tilde{u}$)

$$\begin{aligned} & \nabla \cdot (\nu \sigma \nabla u) = \sigma \nabla u \cdot \nabla \nu + \nu \nabla \cdot (\sigma \nabla u) \\ \Leftrightarrow \quad & \sigma \nabla u \cdot \nabla \nu = \nabla \cdot (\nu \sigma \nabla u) - \nu \nabla \cdot (\sigma \nabla u) \end{aligned}$$

we obtain

$$\int_\Omega \nabla \cdot (\nu \sigma \nabla u) - \nu \nabla \cdot (\sigma \nabla u)\, dx = \int_\Omega \nabla \cdot (\tilde{\nu} \tilde{\sigma} \nabla \tilde{u}) - \tilde{\nu} \nabla \cdot (\tilde{\sigma} \nabla \tilde{u})\, dy.$$

Finally, by the divergence theorem

$$\int_{\partial\Omega} \nu \sigma \nabla u \cdot \mathbf{n} ds = \int_{\partial\Omega} \tilde{\nu} \tilde{\sigma} \nabla \tilde{u} \cdot \mathbf{n} ds.$$

On the boundary now we have

$$\tilde{\nu} = \nu \circ F^{-1} = \nu = g \quad \text{and} \quad \tilde{u} = u \circ F^{-1} = u = f$$

so,

$$\int_{\partial\Omega} g \Lambda_\sigma(f) ds = \int_{\partial\Omega} g \Lambda_{\tilde{\sigma}}(f) ds,$$

hence $\Lambda_\sigma = \Lambda_{\tilde{\sigma}}$. □

Tartar's observation lead the researches to two paths. The first one was to prove uniqueness of the conductivity σ up to a diffeomorphism that fixes the boundary. The other direction was to assume some a priori knowledge of the conductivity distribution.

Let $\sigma(x) = (\sigma_{ij}(x))$ be an anisotropic conductivity on a domain $\Omega \subset \mathbb{R}^3$, and let $F : \Omega \to \Omega$ be a smooth invertible map (diffeomorphism) with $F(x) = x$ for $x \in \partial\Omega$, then the known non-uniqueness in EIT arises as the Neumann-Dirichlet map (transfer impedance) defined by

$$\Lambda_\sigma : \sigma\nabla u \cdot \mathbf{n} \mapsto u|_{\partial\Omega} \tag{3.2.6}$$

(where $\nabla \cdot \sigma\nabla u = 0$) satisfies

$$\Lambda_\sigma = \Lambda_{\tilde{\sigma}} \tag{3.2.7}$$

for another conductivity

$$\tilde{\sigma}(F(x)) = \frac{DF(x)\sigma(x)DF^T(x)}{\det DF(x)} \tag{3.2.8}$$

where $DF(x)$ is the Jacobian matrix of F. Using a fixed finite element mesh does not reveal this non-uniqueness in the inverse problem as a smooth map F does not preserve the mesh. So in this obvious approach we have chosen one of the infinite family of anisotropic conductivities consistent with the data simply by our choice of mesh.

In this study we look at the singular value decomposition of the linearised forward problem (Jacobian) for anisotropic EIT, and we show for a variety of meshes that the problem of determining edge conductances exhibits the same ill-conditioning as the isotropic problem, with no further drop in rank of the Jacobian. This indicates that we are as likely to be as successful in recovering edge conductances from EIT data as we are with isotropic conductivities on elements. This shifts the problem of anisotropic EIT to finding a mesh, and an assignment of anisotropic conductivity matrices on elements, consistent with *a priori* data.

3.3 The Finite Element Method

Typically, solving an inverse problem is analogous to solving a partial differential equation with initial conditions. In the case under investigation this problem is described by (2.1.2). Obviously before attempting to solve the inverse problem, one needs to solve

the forward problem for some conductivity. This is necessary because the measured voltages have to be compared with the predicted voltages. Moreover the calculation of the Jacobian requires the calculation of the interior electric fields. Due to the fact that finding an analytic solution to the forward problem is usually impossible, one has to use numerical methods. Thus, for solving the direct problem for general geometry and arbitrary conductivity distribution we usually use the FEM. To apply the FEM, the domain is decomposed in to polyhedra (for example triangles for 2D and tetrahedra for 3D) called elements, and the unknown potential on each element is represented by a polynomial of fixed order. The potential is assumed continuous at the faces or edges or points of elements intersections. The FEM converges to the solution (or the weak solution) of the partial differential equation as the mesh becomes finer (more, smaller elements) or the order of the polynomial increases.

3.3.1 Weak formulation

The finite element mesh consists of vertices $x_i \in \Omega$ $i = 1, ..., n_v$ and tetrahedra T_k, $k = 1, ..., n_t$. The tetrahedra are the convex hull of the sets of four distinct vertices, and they intersect at most in faces (that is the convex hull of the three vertices they share). The union $\bigcup_k T_k$ is a polyhedron approximating Ω. The nodal basis functions $\phi_i(x)$ are the piecewise linear functions such that

$$\phi_j(x_i) = \begin{cases} 1, & \text{if } i = j, \\ 0, & \text{if } i \neq j. \end{cases}$$

The potential can be represented by the approximation

$$u(x) = \sum_{i=1}^{n_k} u_i \phi_i(x),$$

and assign a positive definite matrix σ^k to each tetrahedron.

It is clear that the basis functions ϕ_i are not differentiable, hence equation

$$\nabla \cdot (\sigma \nabla u) = 0 \tag{3.3.1}$$

is not satisfied directly. To overcome this we derive the weak formulation of (3.3.1)

We start by multiplying (3.3.1) by some test function v and integrating over the domain Ω

$$\int_\Omega v \nabla \cdot \sigma \nabla u dV = 0 \text{ in } \Omega. \tag{3.3.2}$$

Now using the vector identity

$$\nabla \cdot (v\sigma\nabla u) = \sigma\nabla u \cdot \nabla v + v\nabla \cdot \sigma\nabla u, \tag{3.3.3}$$

we get

$$\int_\Omega \nabla \cdot (v\sigma\nabla u)\, dV - \int_\Omega \sigma\nabla u \cdot \nabla v dV = 0. \tag{3.3.4}$$

Finally, applying the divergence theorem

$$\int_\Omega \nabla \cdot (v\sigma\nabla u)\, dV = \int_{\partial\Omega} v\sigma\nabla u \cdot \mathbf{n} dS, \tag{3.3.5}$$

and using the fact the current density is zero off the electrodes we obtain the weak formulation for a test function v

$$\begin{aligned} \int_\Omega \sigma\nabla u \cdot \nabla v dV &= \textstyle\int_{\partial\Omega} \sigma\nabla u \cdot \mathbf{n} dS \\ &= \textstyle\int_\Gamma \sigma\nabla u \cdot \mathbf{n} v dS, \end{aligned} \tag{3.3.6}$$

where $\Gamma = \bigcup_l E_l$ is the union of the electrodes.

3.3.2 Finite element system matrix

In the context of section 3.3.1 the finite element system matrix $K \in \mathbb{R}^{n_v \times n_v}$ is given by

$$K_{ij} = \sum_{k:\{x_i,x_j\}\subset T_k} \nabla\phi_i \cdot \sigma^k \nabla\phi_j |T_k| \tag{3.3.7}$$

where $|T_k|$ is the volume of the tetrahedron and we note that on each tetrahedron $\nabla\phi_i$ is constant. For a boundary current density $J = \sigma\nabla u \cdot \mathbf{n}$ we define the current vector $I \in \mathbb{R}^{n_v}$ by

$$I_i = \int_{\partial\Omega} J\phi_i\, dx, \tag{3.3.8}$$

and the FE system is

$$K\mathbf{u} = I \tag{3.3.9}$$

where $\mathbf{u}$ is the vector of u_i. One additional condition is required for a unique solution as the voltage is only determined up to an additive constant, one way to do this is to choose one ("grounded") vertex i_g and enforce $u_{i_g} = 0$ by deleting the i_g row and column from the system (3.3.9). It is clear from (3.3.7) that for a pair of vertices indexed by i, j that are not both in any tetrahedron, $K_{i,j} = 0$. For an isotropic

conductivity, that is $\sigma^k = \gamma^k \mathbf{I}$ for scalars γ^k and $\mathbf{I}$ the identity matrix, the system (3.3.9) is equivalent to Ohm's and Kirchhoff's law for a resistor network with distinct vertices labelled by i and j connected by a resistor with conductance

$$K_{ij} = 6 \sum_{k:\{x_i,x_j\}\subset T_k} \gamma_k \cot \theta_{ij}^k L_{ij} \tag{3.3.10}$$

(see Appendix A for a derivation of the cotangent formula in 3D) where θ_{ij}^k is the angle between the faces of T_k where they meet the edge *not* containing the vertices indexed by i or j and L_{ij} the length of that edge. Obviously some restrictions on the angles are necessary to ensure the conductances are non-negative, if they are all acute that is certainly sufficient. If we allow negative conductances we can interpret K_{ij} as an "edge conductance" even for anisotropic conductivity and possible non-acute angles. The total Ohmic power for the network will still be non-negative for any solution. The mapping $(\sigma^k) \mapsto K$ is linear, with a domain of dimension $6n_t$ and range of dimension at most n_e. In a typical mesh $6n_t > n_e$.

3.4 Rank analysis of Jacobian

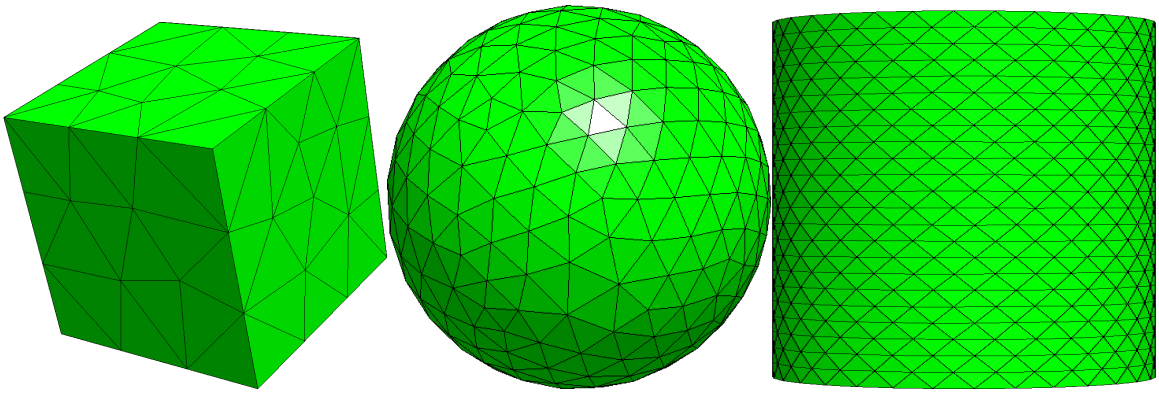

(a) cube, 186 tetrahedra (b) sphere, 2045 tetrahedra (c) cylinder, 7507 tetrahedra

Figure 3.1: Meshes for the three geometric objects used, generated with Netgen

In practical EIT a system of electrodes is used that does not typically cover the whole of $\partial\Omega$ which means some conductivity information at the boundary could be inaccessible in between electrodes. We therefore consider the idealisation that any electrodes can be used. In the finite element context it means that any current vector I can be specified with zero sum and supported on boundary vertices, and all measurements of voltage made at boundary vertices. Without loss of generality we will set

n_t	n_e	rank(J)
6	19	19
28	66	66
48	98	98
168	289	289
224	382	382
384	604	604
1344	1922	1922

(a) Cube

n_t	n_e	rank(J)
40	82	81
70	142	141
122	246	245
320	504	504
336	590	589
560	879	879
976	1529	1529

(b) Sphere

n_t	n_e	rank(J)
89	162	162
251	418	418
361	656	656
712	1049	1049

(c) Cylinder

Table 3.1: Meshes with n_t tetrahedra and n_e edges against the numerical rank of the Jacobian.

a current of -1 at i_g and then apply currents of 1 at each other boundary i vertex in turn. The voltage $V_{ij} = u(x_j)$ is measured at x_j. The Jacobian matrix gives the rate of change of each of these voltages when σ^k_{lm} is changed in tetrahedron T_k. This is

$$\frac{\partial V_{ij}}{\partial \sigma^k_{lm}} = -\int_{T_k} \frac{\partial u^i}{\partial x_l} \frac{\partial u^j}{\partial x_m}\, dx \tag{3.4.1}$$

where $u^i = \sum_q u^i_q \phi_q(x)$ is the finite element approximation to the potential for the current of 1 at vertex x_i.

Using Netgen [89] to generate meshes of geometric objects and a modification of code derived by Abascal [2] from Polydorides' EIDORS-3D [87] to calculate the Jacobian we studied the singular values of the anisotropic Jacobian, see Table 3.1.

We note in Figures 3.2 - 3.4 that sudden fall in the singular values after n_e, and the linear fall on a log scale before that, confirms that the edge conductances can be determined by the transfer impedance data, with a similar degree of ill conditioning as the isotropic inverse problem. We note that this rank of the Jacobian is less than the $6n_t$ degrees of freedom in the anisotropic conductivity and as expected we cannot hope to recover these uniquely.

3.5 The problem with anisotropy

As we know there is no unique solution for anisotropic problems and the problem of anisotropy can be explained in different ways. On one hand, the first thing to consider is that the number of degrees of freedom in a system matrix or a resistor network is smaller than the number of degrees of freedom if we had an anisotropic piecewise

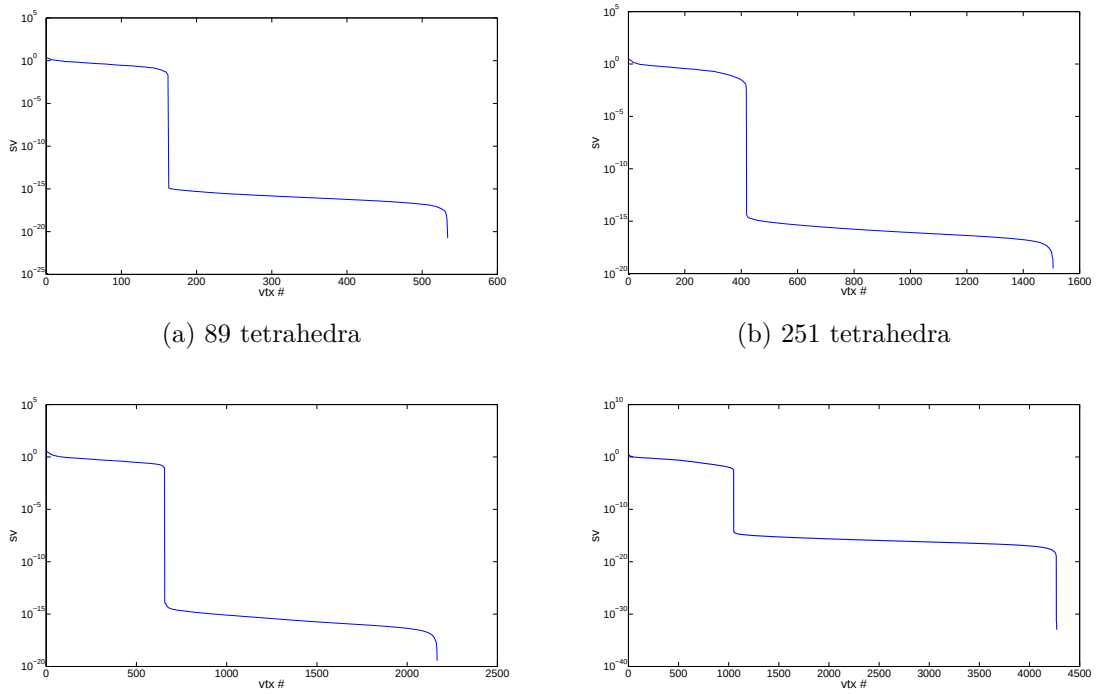

(a) 89 tetrahedra

(b) 251 tetrahedra

(c) 361 tetrahedra

(d) 712 tetrahedra

Figure 3.2: Singular values of the Jacobian for a cylinder

constant conductivity. By considering piecewise constant anisotropic conductivity on elements we immediately have a big null space because the FEM cannot represent the anisotropic conductivity at that level of detail since it only has one degree of freedom per edge. On the other hand, the inverse anisotropic EIT problem has non-unique solution due to the diffeomorphism in the interior, but that does not show up in the FEM formulation because we would have to move the vertices. The are two problems with the non-uniqueness. When solving an inverse problem we have already chosen a FEM which creates a problem that we cannot see. Moreover the SVD of the Jacobian looks like the isotropic case, it is not better or worse. It is still ill-conditioned but there is nothing else we can do, because we do not know uniqueness of solution for the anisotropic case beyond Sylvester's paper in two dimensions [92] and Lee and Uhlmann in three dimensions [67]. What we cannot neglect is that it could be that there is some other source of non-uniqueness for the anisotropic case that we do not know about that is due to the choice of discretisation. To summarise, what we see is that the non-uniqueness appears due to the problem of FEM having only one degree of freedom per edge. It is impossible to see the non-uniqueness due to the diffeomorphism because

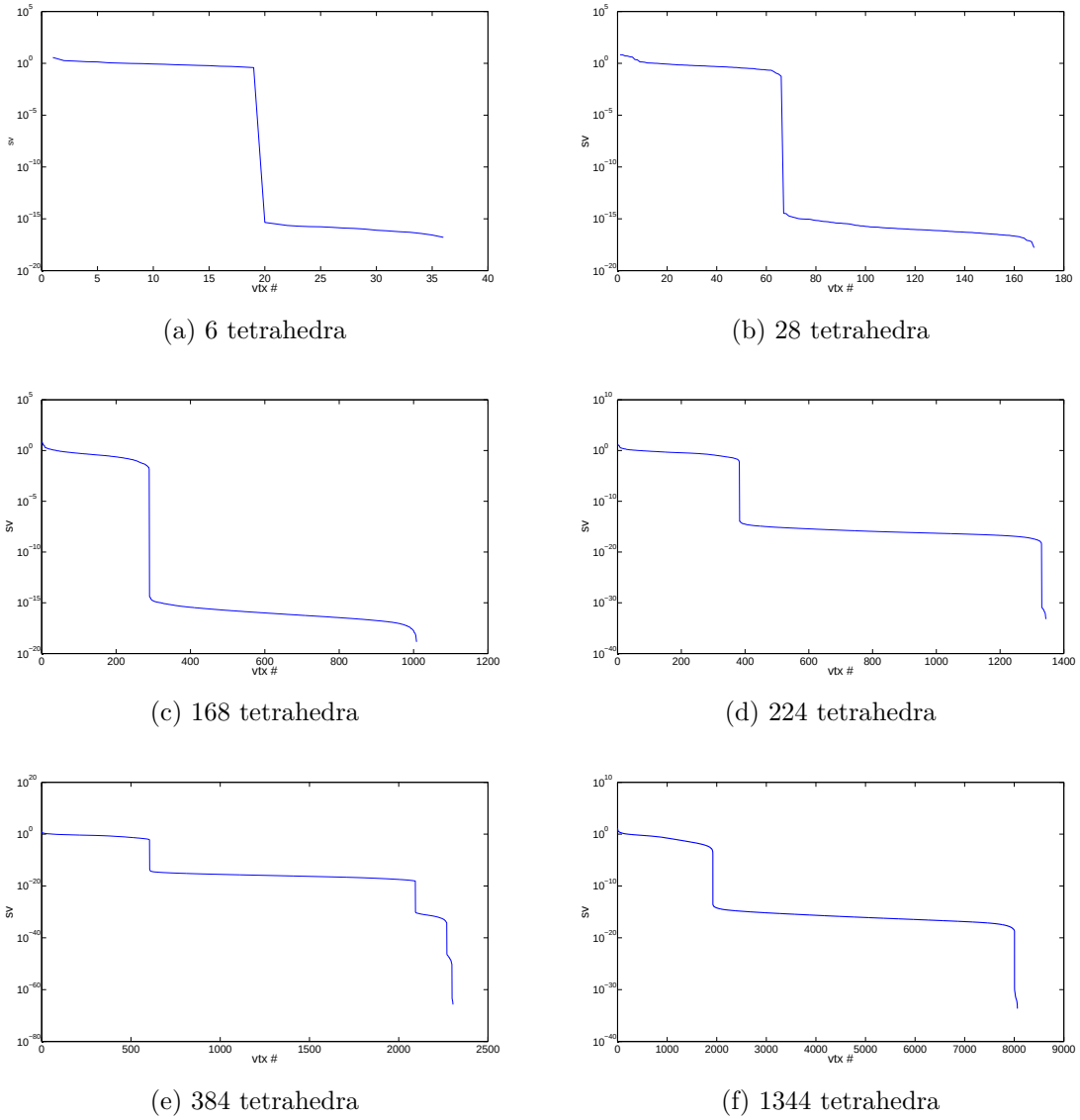

(a) 6 tetrahedra

(b) 28 tetrahedra

(c) 168 tetrahedra

(d) 224 tetrahedra

(e) 384 tetrahedra

(f) 1344 tetrahedra

Figure 3.3: Singular values of the Jacobian for a cube

we fix points, otherwise the SVD looks like the isotropic case.

The next thing to do would be to study what constraints give a unique embedding having done the inverse problem. In this sense, Juan Abascal [1] managed to overcome this by using the argument that we can look at the diagonal case because there is always orthogonal coordinates (DeTurk and Yang coordinates [37]), but we note here that this is not very practical. When we use piecewise constant anisotropic conductivity on elements is not actually correct, in fact it is wrong because it does not show up in the forward model. There is something that we are missing here and from our point of view the problem appears because the conductivity in a Hodge star, which obviously is not a tensor. Furthermore it is wrong geometrically to think conductivity as a matrix

or a tensor because conductivity is actually something that maps current to voltage. In three dimensions it maps 1-forms to 2-forms and in the discrete electromagnetics 1-cochains that have one degree of freedom on each edge.

The natural kind of conclusion to draw is that it is wrong to think of conductivity as piecewise constant on tetrahedra when the voltage is piecewise linear. A piecewise linear voltage means that the currents are on faces and the power density is not defined on tetrahedra. Then for the conductivity you only need one degree of freedom per edge because the expression for the total power is a sum of squared voltage differences on edges times the current source, which is a conductivity. In other words we have Ohm's and Kirchhoff's law in the discrete formulation of a FEM formulation of the forward problem, hence this is the correct way to think of the conductivity. But still, there is something missing though from a practical point of view. How does this relate to eigenvectors of conductivities, because this is the geometric formulation which is independent of position. What we want to do is to relate this to things like muscle fibres or sheets of material that are anisotropic in the same direction. It is interesting to note that our conductivity cannot exactly see down to that level of resolution, so if we are going to define, say eigenvectors of conductivity in elements, then there is a number of conductivity tensors that we fit there that might give the same edge conductance because there are more degrees of freedom.

To summarise we need extra information to determine the conductivity in the continuum case. There are six unknown functions and in reality we can find three functions, so we need three constraints to fit the remaining three components in a diffeomorphism. When we change to the discrete case we face a problem because the voltage and the current do not exist in the same place, so naturally we cannot compare them and this is fundamentally the problem. In FEM the voltage appears on edges and current appears on faces, so it is impossible to compare them at the same point. This is essentially the same problem of representing any kind of Hodge object in electromagnetics. In practice, since we cannot relate voltage and current at the same point, if we do want to represent our conductivity as piecewise linear on triangles we need more information to constrain it than we would for the continuum case. This happens because on one hand it needs to provide the unknown diffeomorphism and on the other hand it also needs to provide the missing components of the conductivity

that we have lost from the discrete model. Consequently, if we are going to represent the conductivity per element, then we need more constraints than we would for the continuum problem. From a different perspective now we do not necessarily expect to get the conductivity on the same resolution we have solved the forward problem. It is not realistic to expect to do that in an ill-posed inverse problem, so in reality we are expected to provide more a priori smoothness from the conductivity so that the values in each tetrahedron are not independent but instead are coupled by some correlation we assume. This means that we can either have bigger pixels for the conductivity or assume that they are correlated more. Using this idea the problem would disappear because we are effectively providing more constraints for the conductivity. The a priori information give enough constraints to provide the extra degrees of freedom to give six per element where as the inverse problem can give no more than one per edge. This is perfectly reasonable although Curtis and Morrow [36] and Colin de Verdière [30] set up the inverse problem for resistor networks, in realistic practical inverse problems we have to assume that the conductivity is not as finely discretised as the forward problem mesh.

3.6 Discussion and conclusion

The relation between finite element meshes and resistor networks only applies to linear tetrahedral elements. It is also not necessarily appropriate to treat the conductivities on elements as each individually variable. In isotropic EIT it is quite usual to use a coarser mesh for the conductivity than for the potential. In this case with fewer degrees of freedom for the conductivity, and perhaps basis functions reflecting *a priori* information, the loss of information we observed going from conductivity matrices to edge conductances is not so important.

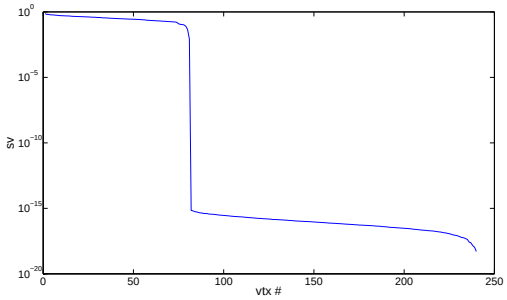

(a) 40 tetrahedra

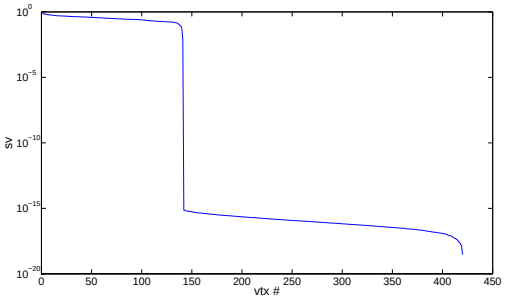

(b) 70 tetrahedra

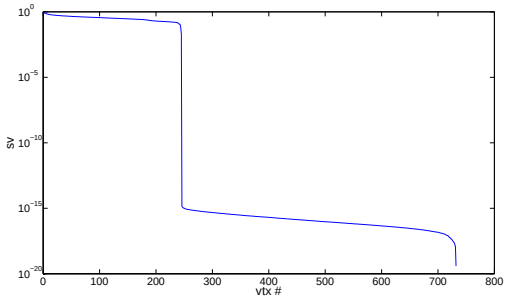

(c) 122 tetrahedra

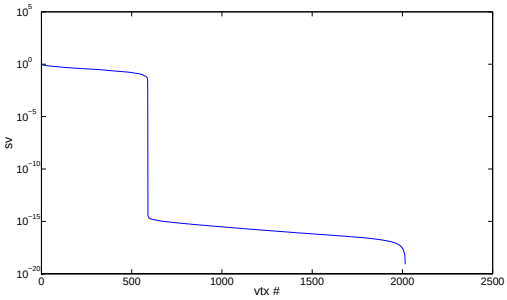

(d) 134 tetrahedra

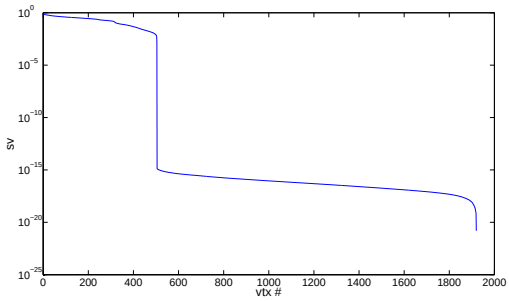

(e) 320 tetrahedra

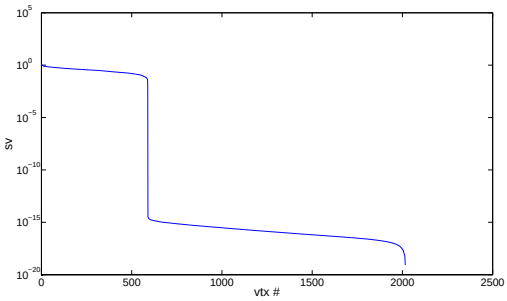

(f) 336 tetrahedra

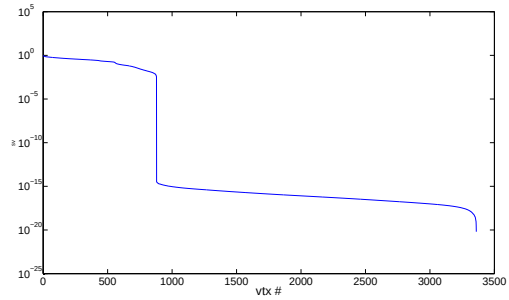

(g) 560 tetrahedra

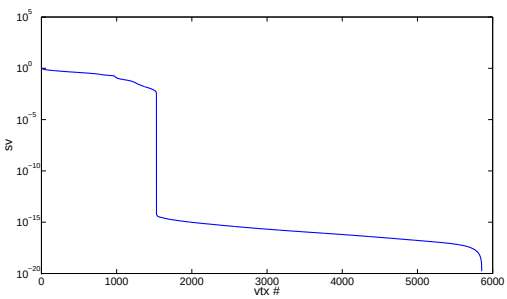

(h) 976 tetrahedra

Figure 3.4: Singular values of the Jacobian for a sphere

Chapter 4

Shape correction in EIT

Ἓν οἶδα ὅτι οὐδὲν οἶδα[1]

Σωκράτης

This chapter is an expansion to the conference paper [84] presented at the XIVth International Conference on Electrical Bioimpedance and the 11th Conference on Biomedical Applications of Electrical Impedance Tomography held at the University of Florida, Gainesville, FL, USA on April 4-8, 2010.

In this chapter we start by reviewing the latest developments regarding shape deformations referring to the work of Lionheart [70], [71], Soleimani et al. [90] and the recent paper by Grychtol et al. [46]. We continue with an explanation as to why a distorted boundary, assuming an isotropic conductivity, leads to significant errors and we refer to the work of Lee and Uhlmann [67]. Furthermore, we refer to the two dimensional work of Boyle et al. [25], [26] and following their work we construct a Möbius transformation vector that we use for our numerical experiments. Finally we present some results which potentially lead to a better reconstruction when deformation of the boundary occurs and we give results of numerical studies analogous to the two dimensional work of Boyle et al. [25], [26] on the effect of electrode movement and shape error in 3D EIT.

[1] "I know one thing, that I know nothing", Socrates

4.1 Introduction

It is well known that one of the possible applications of EIT is cardio-pulmonary monitoring of ICU [42], [5]. At the moment EIT is the only modality to offer real-time, more precise e.g. over hours, monitoring of the lungs. Despite the fact that EIT could be an invaluable asset in lung monitoring and prevention of Ventilator-Induced Lung Injury (VILI) [4], at the moment the clinical use of EIT is delayed because of the difficulties in interpreting the images. Obviously, in pulmonary EIT the patient's chest moves continuously due to breathing and in some extent due to posture changes [6]. It is natural to look for an algorithm that anticipates for this boundary change and use the corrected boundary to find an isotropic conductivity that fits the data.

4.2 Current state of research

Researchers in the inverse problems area have realized the importance of shape in the reconstruction process. Lionheart [71] notes that ideally a 3D model with measured shape should be used when imaging three dimensional bodies. Using an incorrect model shape, assuming an isotropic conductivity distribution, results in conductivity that is inconsistent with the data, in other words there is no consistent conductivity that will fit the data.

The same author in previous work [70] shows that an isotropic conductivity and the shape of the boundary are determined by the boundary electrical data but he notes that it would not be sensible to determine the boundary shape of a body with an unknown conductivity using only electrical measurements. Optical and mechanical measurements are better means for this job. Lastly, Lionheart points out that if we attempt to recover the conductivity but we assumed the wrong shape we generally have no hope to find an isotropic conductivity consistent with the measured data. The exception to this rule is the case where the true shape and the assumed shape are related by a conformal transformation. In practice, if we assume isotropic conductivity and the shape is extremely wrong, the reconstruction algorithms should fail.

Soleimani et al. [90] showed that in some cases a combination of image reconstruction of conductivity and shape changes can be used to recover conductivity and shape

changes. The proposed algorithm reconstructs both electrode movements and conductivity changes for difference EIT, but there is a pitfall in this approach. The problem arises from using fixed electrode models with the nodes for each electrode translating uniformly, without distortion or rotation. Apparently this is not the case for real electrodes where displacements are far more complex and even the electrode contact with the medium might change. This technique, though limited, results in distorted images due to the anisotropy of the human chest but it preserves useful information.

The importance of shape is addressed in a recent paper by Grychtol et al. [46]. The authors discuss the impact of the mismatch between the true shape and the model shape used for the reconstruction and they quantify the errors due to the shape mismatch for popular EIT algorithms. The study shows that the use of a circular model, widely used, sometimes produces undesired results and leads to wrong conclusions. It is encouraging though that according to the study a mismatch of up to 4% is well tolerated, hence there is no need for exact model shapes. The authors point out and conclude that the issue of model shape requires further investigation and future research should seek to answer what causes this phenomenon in order to find strategies to reduce or correct it.

4.3 The problem with the boundary

It is clear that when boundary movement occurs we lose any information about the boundary, hence due to this movement the boundary is unknown. For this reason we consider the body as an abstract three-dimensional manifold M with boundary. Let us assume also that the Dirichlet to Neumann map is known on the manifold M. A configuration is a smooth embedding

$$\Psi : M \to \mathbb{R}^3,$$

where the body is its image $\Psi(M) = \overline{\Omega}$. For the boundary a configuration is an embedding

$$\Psi : \partial M \to \mathbb{R}^3.$$

In electrical impedance tomography we normally attach electrodes on the boundary ∂M to apply current and measure voltage. To be able to get full knowledge

of the Dirichlet to Neumann map, one has to make the electrodes arbitrarily small and numerous. Knowledge of the Dirichlet to Neumann map on the boundary would mean knowledge of the electrodes positions in some coordinate system but without any knowledge on how it is embedded in $\mathbb{R}^3$. According to Lee and Uhlmann's theorem (see Theorem 4.4.1) it is possible to determine some analytic conductivity σ on the manifold, which is consistent with the data, up to some interior distortion $G : M \to M$ with $G(\mathbf{x}) = \mathbf{x}$ for $\mathbf{x} \in \partial M$. Consider two different configurations $\Psi_1(M) = \overline{\Omega_1}$ and $\Psi_2(M) = \overline{\Omega_2}$. Then there exists a smooth invertible map $F = \Psi_2 G \Psi_1^{-1} : \overline{\Omega_1} \to \overline{\Omega_2}$. Let us assume that g_1 and g_2 are two electrical metrics on $\overline{\Omega_1}$ and $\overline{\Omega_2}$ respectively, consistent with the data. Then there must be such an F with $F_* g_1 = g_2$, where F_* is the push-forward.

Obviously, from Definition 2.3.6 the described metric g can be conformally flat but not isotropic. Moreover the push-forward of a conformally flat metric by a smooth invertible map is conformally flat. It is clear now that for two configurations as above, $F : \overline{\Omega_1} \to \overline{\Omega_2}$ is a conformal mapping between domains in Euclidean space, meaning that $F_* e = \lambda e$ for some positive scalar function λ and e is a flat metric.

4.4 Uniqueness up to diffeomorphism

The quest to prove uniqueness to the anisotropic problem led Lee and Uhlmann [67] to the following two conjectures.

Conjecture 4.4.1. *Let $\overline{M}$ be a smooth, compact n-manifold, with boundary, $n \geq 3$ and let g, $\tilde{g}$ be smooth Riemannian metrics on $\overline{M}$ such that*

$$\Lambda_g = \Lambda_{\tilde{g}}.$$

Then there exists a diffeomorphism $\psi : \overline{M} \to \overline{M}$ with $\psi|_{\partial M} = Id$, such that $g = \psi^* \tilde{g}$.

Conjecture 4.4.2. *Let $\overline{M}$ be a smooth, compact 2-manifold, with boundary, and let g, $\tilde{g}$ be smooth Riemannian metrics on $\overline{M}$ such that*

$$\Lambda_g = \Lambda_{\tilde{g}}.$$

Then there exists a diffeomorphism $\psi : \overline{M} \to \overline{M}$ with $\psi|_{\partial M} = Id$, such that $g = \psi^* \tilde{g}$ is a conformal multiple of g, in other words there exists $\phi \in C^\infty(\overline{M})$ such that

$$\psi^* \tilde{g} = \phi g.$$

Lee and Uhlmann have proved Conjecture 4.4.1 in a particular case [67]. Their result is the following

Theorem 4.4.1. *Let $\overline{M}$ be a compact, connected, real-analytic n-manifold with connected real-analytic boundary. Assume that every closed path in $\overline{M}$ with base point in ∂M is homotopic to some path that lies entirely in ∂M. Let g and $\tilde{g}$ be real-analytic metrics on $\overline{M}$ such that*

$$\Lambda_g = \Lambda_{\tilde{g}},$$

and assume that one of the following condition holds:

1. *$\overline{M}$ is strongly convex with respect to both g and $\tilde{g}$.*
2. *Either g or $\tilde{g}$ extends to a complete real-analytic metric on a non-compact real-analytic manifold $\tilde{M}$ (without boundary) containing $\overline{M}$.*

Then there exists a real-analytic diffeomorphism $\psi : \overline{M} \to \overline{M}$ with $\psi|_{\partial M} = Id$, such that $g = \psi^* \tilde{g}$.

Conjecture 4.4.2 was proved by John Sylvester [92] in a particular case. In particular Sylvester showed the following:

Theorem 4.4.2. *Let Ω be a bounded domain in $\mathbb{R}^2$ with a C^3 boundary and let σ_1, σ_2 be anisotropic C^3 conductivities in $\overline{\Omega}$ such that*

$$|| \log (\det \sigma_i) ||_{C^3} < \epsilon(M, \Omega), \quad for \quad i = 1, 2, \tag{4.4.1}$$

with $M \geq ||\sigma_i||_{C^3}$, for $i = 1, 2$ and $\epsilon(M, \Omega)$ sufficiently small. If

$$\Lambda_{\sigma_1} = \Lambda_{\sigma_2},$$

then there exists a C^3 diffeomorphism ψ of $\overline{\Omega}$ such that $\psi|_{\partial\Omega} = Id$ and such that

$$\psi_* \sigma_1 = \sigma_2.$$

The result was extended by Nachman [82] who proved the same without the hypothesis (4.4.1). Lassas and Uhlmann [66] manage to extend the result of [67]. The main result is:

Theorem 4.4.3. *Let us assume that one of the following conditions is satisfied:*

1. *M is a connected Riemannian surface;*

2. *$n \geq 3$ and (M, g) is a connected real-analytic Riemannian manifold and the boundary ∂M is real-analytic in the non-empty set $\Gamma \subset \partial M$.*

Then

1. *For $\dim M = 2$ the $\Lambda_{g,\Gamma} -$ mapping and Γ determine the conformal class of the Riemannian manifold (M, g).*

2. *For a real-analytic Riemannian manifold (M, g), $\dim M > 2$ which boundary is real-analytic in Γ, the $\Lambda_{g,\Gamma} -$ mapping and Γ determine the Riemannian manifold (M, g).*

Note that Theorem 4.4.3 assumes only a connected manifold M in contrast with the assumption in [67] where the manifold was simply connected and its boundary was assumed to be geodesically convex. Lassas, Taylor and Uhlmann have extended Theorem 4.4.3 in [65] using a completeness hypothesis on $\overline{M}$.

4.5 Deformations in two dimensions

Let σ be the conductivity tensor and ϕ the potential throughout a domain Ω. The EIT governing equation is

$$\nabla \cdot \sigma \nabla \phi = \begin{cases} 0, \text{ in } \Omega \\ J_n, \text{ in } \partial\Omega \end{cases} \tag{4.5.1}$$

and the energy integral is

$$\int_\Omega \omega \nabla \cdot \sigma \nabla \phi dV = 0, \tag{4.5.2}$$

for any test function ω chosen to achieve a minimum residual. Now consider a transformation from the cartesian system (x, y) to an arbitrary system (u, v). A deformation of the boundary will obviously cause a change in the conductivity and potential distributions, say σ' and ϕ' respectively. Clearly, the deformation causes a change in the volume dV' too. Introducing a new test function ω' yields,

$$\int_\Omega \omega \nabla \cdot \sigma \nabla \phi dV = \int_\Omega' \omega' \nabla \cdot \sigma' \nabla \phi' dV', \tag{4.5.3}$$

since the measured voltages remain the same. Changing coordinate system gives

$$\begin{bmatrix} \frac{\partial}{\partial x} \\ \frac{\partial}{\partial y} \end{bmatrix} = \begin{bmatrix} a & b \\ c & d \end{bmatrix} \begin{bmatrix} \frac{\partial}{\partial u} \\ \frac{\partial}{\partial v} \end{bmatrix}, \tag{4.5.4}$$

where $a = \frac{\partial u}{\partial x}$, $b = \frac{\partial v}{\partial x}$, $c = \frac{\partial u}{\partial y}$ and $a = \frac{\partial v}{\partial y}$. Inverting (4.5.4) yields,

$$\begin{bmatrix} \frac{\partial}{\partial u} \\ \frac{\partial}{\partial v} \end{bmatrix} = \underbrace{\frac{1}{ad-bc} \begin{bmatrix} d & -b \\ -c & a \end{bmatrix}}_{\mathbf{T}} \begin{bmatrix} \frac{\partial}{\partial x} \\ \frac{\partial}{\partial y} \end{bmatrix}, \tag{4.5.5}$$

where T is the inverse of the transformation matrix (4.5.4). As expected the volume derivative dV is scaled by the determinant of the transformation

$$dV = \det(\mathbf{T})dV'. \tag{4.5.6}$$

It is clear that to have equal voltages before and after the deformation and for relation (4.5.3) to hold, the new conductivity σ' must change. Choose the test functions so that $\omega = \omega'$ and considering the fact that the potential remains the same from (4.5.3) we have

$$\begin{bmatrix} \frac{\partial}{\partial x} & \frac{\partial}{\partial y} \end{bmatrix} \sigma \begin{bmatrix} \frac{\partial}{\partial x} \\ \frac{\partial}{\partial y} \end{bmatrix} \phi dV = \begin{bmatrix} \frac{\partial}{\partial u} & \frac{\partial}{\partial v} \end{bmatrix} \sigma' \begin{bmatrix} \frac{\partial}{\partial u} \\ \frac{\partial}{\partial v} \end{bmatrix} \phi' dV'. \tag{4.5.7}$$

Note that though $\phi = \phi'$, it is now in a different location due to the transformation. Using (4.5.5), (4.5.6), (4.5.7) and simplifying we obtain

$$\sigma' = \mathbf{T}^{-T} \sigma \mathbf{T}^{-1} \det(\mathbf{T}), \tag{4.5.8}$$

which means that a distortion that fixes the boundary leaves the Dirichlet to Neumann map invariant [62].

The last relation shows that for an arbitrary conductivity σ and an arbitrary transformation $\mathbf{T}$, the new conductivity distribution σ' will be adjusted in some way so that the new boundary data will fit the old.

Assuming that both conductivities are isotropic gives

$$\begin{aligned}
& \sigma' = \sigma \mathbf{T}^{-T} \mathbf{T}^{-1} \det(\mathbf{T}) \\
\Leftrightarrow \quad & \mathbf{T}^{-T} \mathbf{T}^{-1} \det(\mathbf{T}) = \kappa \mathbf{I} \\
\Leftrightarrow \quad & \tfrac{1}{ad-bc} \begin{bmatrix} a^2+c^2 & ab+cd \\ ab+cd & b^2+d^2 \end{bmatrix} = \kappa \mathbf{I} \\
\Rightarrow \quad & ab+cd = 0, \quad a^2+c^2 = b^2+d^2 \\
\Rightarrow \quad & a = \pm d, \quad c = \mp b \quad \text{and} \quad \kappa = 1.
\end{aligned}$$

Taking the first solution $a = d$ and $c = b$ we get the Cauchy-Riemann equations

$$\frac{\partial u}{\partial x} - \frac{\partial v}{\partial y} = 0, \tag{4.5.9}$$

$$\frac{\partial u}{\partial y} + \frac{\partial v}{\partial x} = 0. \tag{4.5.10}$$

Choosing the second solution corresponds to the opposite direction. Clearly, this shows that only a conformal deformation returns an isotropic conductivity if the initial one was also isotropic [25].

Let $\mathbf{V}$ be a sufficiently smooth vector field. A distortion can be linearised by adding a vector field $\mathbf{V}$ to each point. In the case of distortions that preserve the angles (that is, conformal mappings) then $\mathbf{V}$ is called conformal vector field. A vector field $\mathbf{V}$ is conformal if and only if

$$\frac{\partial V_i}{\partial x_j} + \frac{\partial V_j}{\partial x_i} = (\nabla \cdot \mathbf{V})\, \delta_{i,j} \tag{4.5.11}$$

is satisfied. In two dimensions it is straight forward (set $i, j \in \{1, 2\}$) to show that the Killing field equation (4.5.11) satisfies the Cauchy-Riemann equations

$$\frac{\partial V_1}{\partial x_1} - \frac{\partial V_2}{\partial x_2} = 0 \tag{4.5.12}$$

$$\frac{\partial V_1}{\partial x_2} + \frac{\partial V_2}{\partial x_1} = 0. \tag{4.5.13}$$

Now, since $\mathbf{V} = V_1 + \mathrm{i}V_2$ is differentiable and its derivatives are continuous and moreover it satisfies the Cauchy-Riemann equations (4.5.12)-(4.5.13) then $\mathbf{V}$ is a holomorphic (also called analytic) function [8] as a function of $x + \mathrm{i}y$, hence $\mathbf{V}$ is a conformal vector field.

Since V_1 and V_2 satisfy Laplace's equation and (4.5.12)-(4.5.13), they are harmonic conjugate functions and V_1 is arbitrarily specified at the boundary. Moreover the tangential derivative $\frac{dV_1}{ds}$, where s is the arc length, is determined. Furthermore V_2 is the solution of Laplace's equation with Neumann boundary data determined up to a constant.

Simulated results [26] show that non-conformal distortions cause significant artefacts in the reconstruction of the conductivity. On the other hand conformal movements do not show any benefit in reconstruction and the algorithm is unable to detect such movements. In addition to the simulations, experimental results [26] also suggest that in the case of non-conformal mappings it is possible to reconstruct electrode

movement and boundary distortions based on conductivity changes. This method is limited to isotropic domains and hence it cannot be used for muscle tissue or flowing blood.

4.6 Deformations in three dimensions

Our task is to calculate a conformal vector field on S^3. This can be done by stereographicly projecting the hypersphere S^3 on $\mathbb{R}^3$ and then applying a rotation about an arbitrary hyperplane. Finally back projection is required. This process will finally return a conformal vector field since stereographic projections and rotations are conformal mappings, meaning that they preserve angles.

4.6.1 Conformal vector field construction

We will start by calculating the stereographic projection of the 4-dimensional sphere S^3 onto $\mathbb{R}^3$.

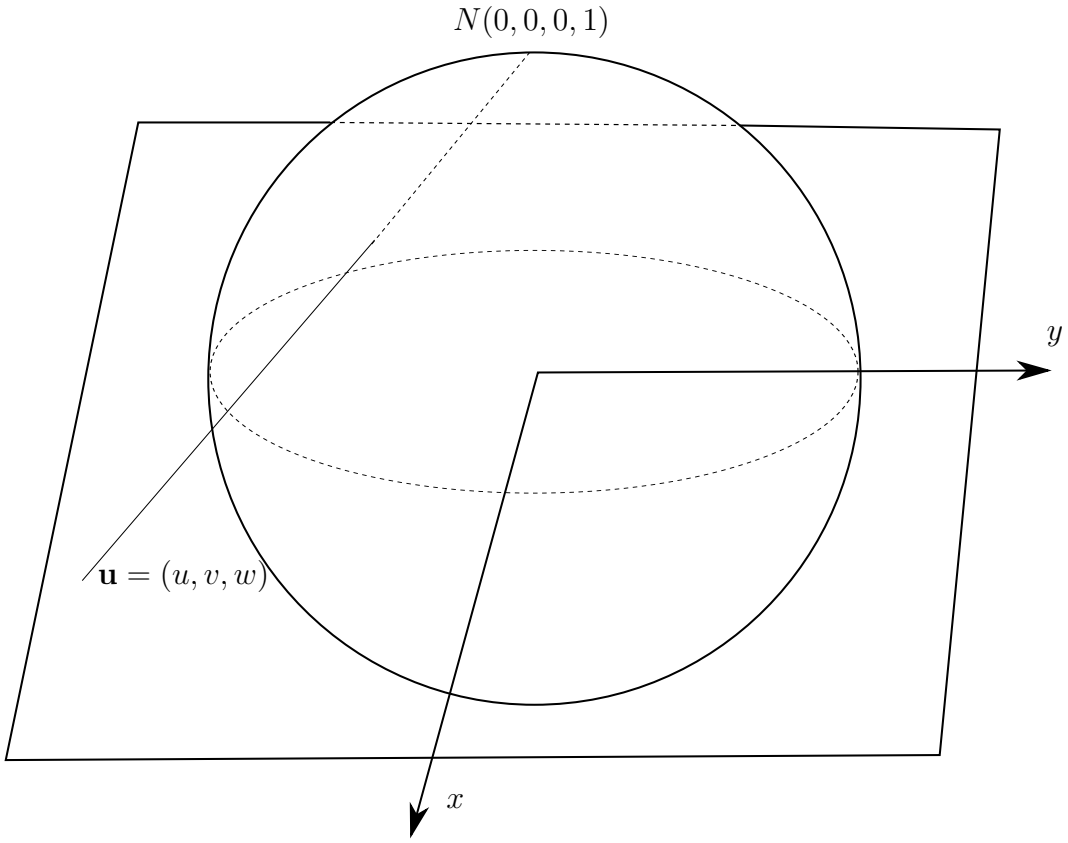

Figure 4.1: Stereographic projection

Let $S^3 \subset \mathbb{R}^4$ be the 4-dimensional sphere and $N(0,0,0,1)$ be the north pole. Suppose $(x,y,z,t) \in S^3$ is an arbitrary point on the hypersphere. Then the equation of the line passing through the north pole and (x,y,z,t) is given by

$$\begin{pmatrix} x \\ y \\ z \\ t \end{pmatrix} = \begin{pmatrix} 0 \\ 0 \\ 0 \\ 1 \end{pmatrix} + \kappa \begin{pmatrix} u \\ v \\ w \\ -1 \end{pmatrix}, \tag{4.6.1}$$

where $\kappa \in \mathbb{R}$. Then, we easily obtain

$$\frac{x}{u} = \frac{y}{v} = \frac{z}{w} = 1 - t = \kappa. \tag{4.6.2}$$

Solving the linear system

$$\begin{cases} \frac{x}{y} = \frac{u}{v}, \\ \frac{y}{z} = \frac{v}{w}, \\ w = \frac{z}{1-t}, \\ x^2 + y^2 + z^2 + t^2 = 1. \end{cases} \tag{4.6.3}$$

we find the stereographic projection $P : \mathbb{R}^3 \to S^3 \setminus \{N\}$, $(u,v,w) \mapsto (x,y,z,t)$

$$\begin{cases} x = \frac{2u}{u^2+v^2+w^2+1}. \\ y = \frac{2v}{u^2+v^2+w^2+1}, \\ z = \frac{2w}{u^2+v^2+w^2+1}, \\ t = \frac{u^2+v^2+w^2-1}{u^2+v^2+w^2+1}. \end{cases} \tag{4.6.4}$$

Then the inverse mapping $T : S^3 \setminus \{N\} \to \mathbb{R}^3$ is

$$\begin{cases} u = \frac{x}{1-t}, \\ v = \frac{y}{1-t}, \\ w = \frac{z}{1-t}. \end{cases} \tag{4.6.5}$$

To continue, a 4-dimensional rotation is required. Without loss of generality and to keep the calculations simple, we use a rotation about the $x-t$ plane. Then $R_\theta \in SO(4)$ is given by

$$R_\theta = \begin{pmatrix} \cos(\theta) & 0 & 0 & \sin(\theta) \\ 0 & 1 & 0 & 0 \\ 0 & 0 & 1 & 0 \\ -\sin(\theta) & 0 & 0 & \cos(\theta) \end{pmatrix}.$$

Now, let F_θ represent a curve, where θ is the angle of rotation. Then,

$$F_\theta = TR_\theta P(\mathbf{x}), \tag{4.6.6}$$

where $\mathbf{x} = (x, y, z, t) \in S^3$, $P : \mathbb{R}^3 \to S^3 \setminus \{N\}$. Finally, we differentiate with respect to θ and set $\theta = 0$,

$$\left.\frac{dF_\theta}{d\theta}\right|_{\theta=0} = DT \left.\frac{dR_\theta}{d\theta}\right|_{\theta=0} P(\mathbf{x}) = \begin{pmatrix} -\frac{u^2+v^2+w^2-1}{(t-1)(u^2+v^2+w^2+1)} \\ -\frac{2uy}{(t-1)(u^2+v^2+w^2+1)} \\ -\frac{2uz}{(t-1)(u^2+v^2+w^2+1)} \end{pmatrix},$$

where DT is the Jacobian of the inverse mapping $T : S^3 \setminus \{N\} \to \mathbb{R}^3$. Substituting (4.6.4) we get a Möbius transformation vector

$$\left.\frac{dF_\theta}{d\theta}\right|_{\theta=0} = DT \left.\frac{dR_\theta}{d\theta}\right|_{\theta=0} P(\mathbf{x}) = \begin{pmatrix} \frac{-u^2+v^2+w^2-1}{2} \\ -uv \\ -uw \end{pmatrix}.$$

Permuting the axes generates other independent Möbius vector fields, and we can

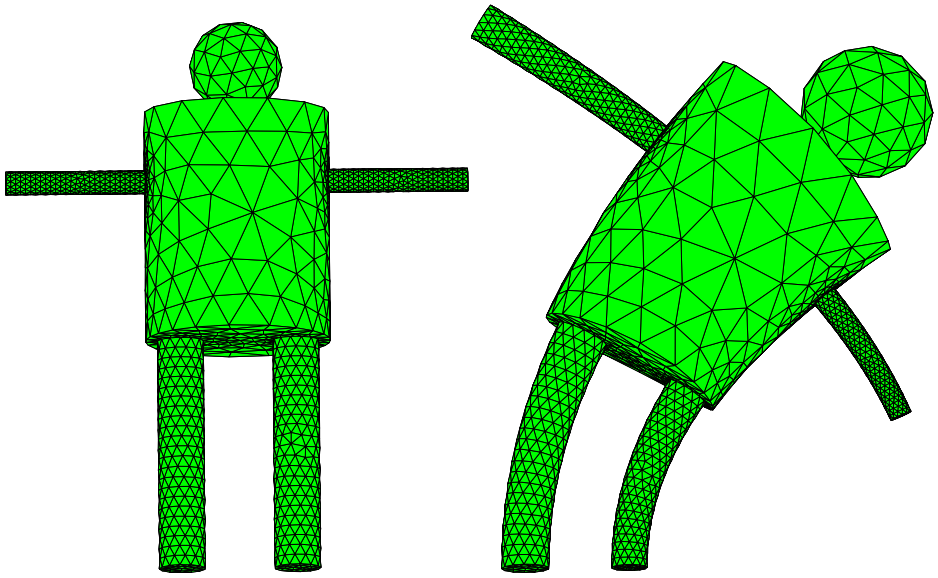

Figure 4.2: A simplified body shape and its image under the Möbius transformation specified in the text (see also [70]). Note how the transformation acts on the body, circles and spheres are preserved while straight lines are taken to circles.

thus construct a basis of the conformal vector fields. The theory predicts that any vector field orthogonal to the space of Möbius vector fields can be determined from

complete boundary data while a distortion by a Möbius vector field will produce data for which there is a consistent isotropic conductivity, which is distorted from the true one by the Möbius vector field.

As a first test of this in the context of finitely many electrodes and a finite element mesh we will simply verify that data subject to a conformal distortion results in a recognisable but distorted reconstruction of the true conductivity but a non-conformal distortion of the same size produces a reconstruction with more artefacts.

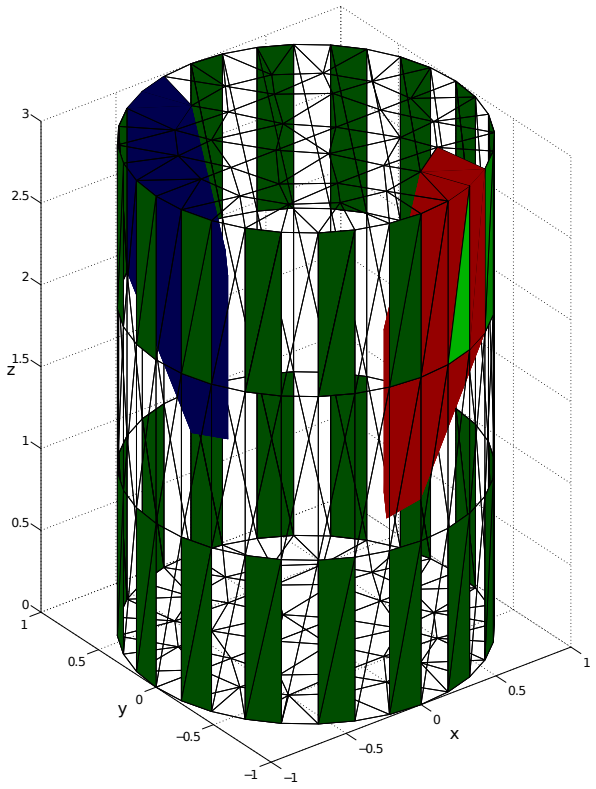

Figure 4.3: Finite element mesh with electrodes and simulated inhomogeneities.

4.6.2 Numerical experiments

In order to verify the theoretical results we used the familiar demonstration model demo_real from EIDORS [7]. Specifically, for our initial test we use a finite element mesh with electrode positions (green) and simulated inhomogeneities (blue and red) (Figure 4.3). In order to be able to apply conformal and non-conformal distortions on the inhomogeneities we modified the existing code. The code was later further developed to exploit some new features of later EIDORS releases. Using the new EIDORS function ng_mk_cyl_models we are able to call Netgen [89] within EIDORS and hence different inhomogeneities can be tested (see Appendix C).

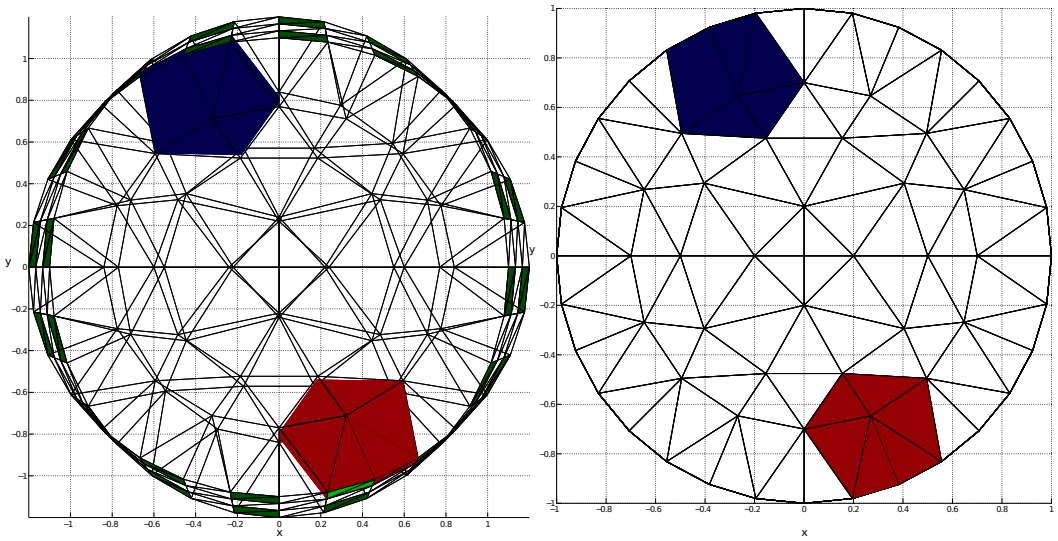

(a) Non-Conformal (b) Conformal

Figure 4.4: Top view of the model after applying the distortions

In detail, we started by applying the following non-conformal perturbation

$$(x, y, z) \to \left(x + \epsilon\left(x\frac{z+3}{3}\right), y + \epsilon\left(y\frac{-z+6}{3}\right), z\right), \tag{4.6.7}$$

where ϵ is small enough and it was chosen so that the L^2-norms of the perturbations are equal. The non-conformal transformation was chosen so that it transforms circles to ellipses, that is a transformation which is "very" non-conformal. For the conformal distortion we used the Möbius vector (4.6.1) we have constructed before. The applied perturbation is given by

$$(x, y, z) \to \left(x + \epsilon\frac{-x^2 + y^2 + z^2 - 1}{2}, y - \epsilon xy, z - \epsilon xz\right). \tag{4.6.8}$$

The reconstruction was a standard regularized linear reconstruction using the undistorted mesh.

The simulated results shown in Figures 4.5-4.9 confirm the theory. It is clear that non-conformal movements cause significant artefacts in the conductivity reconstruction. On the other hand, conformal distortions do not affect the conductivity reconstruction, at least not as importantly as with non-conformal distortions.

4.7 Discussion and conclusion

This chapter deals with the effect of conformal and non-conformal distortions on the conductivity reconstruction in EIT. The simulated results show an important difference

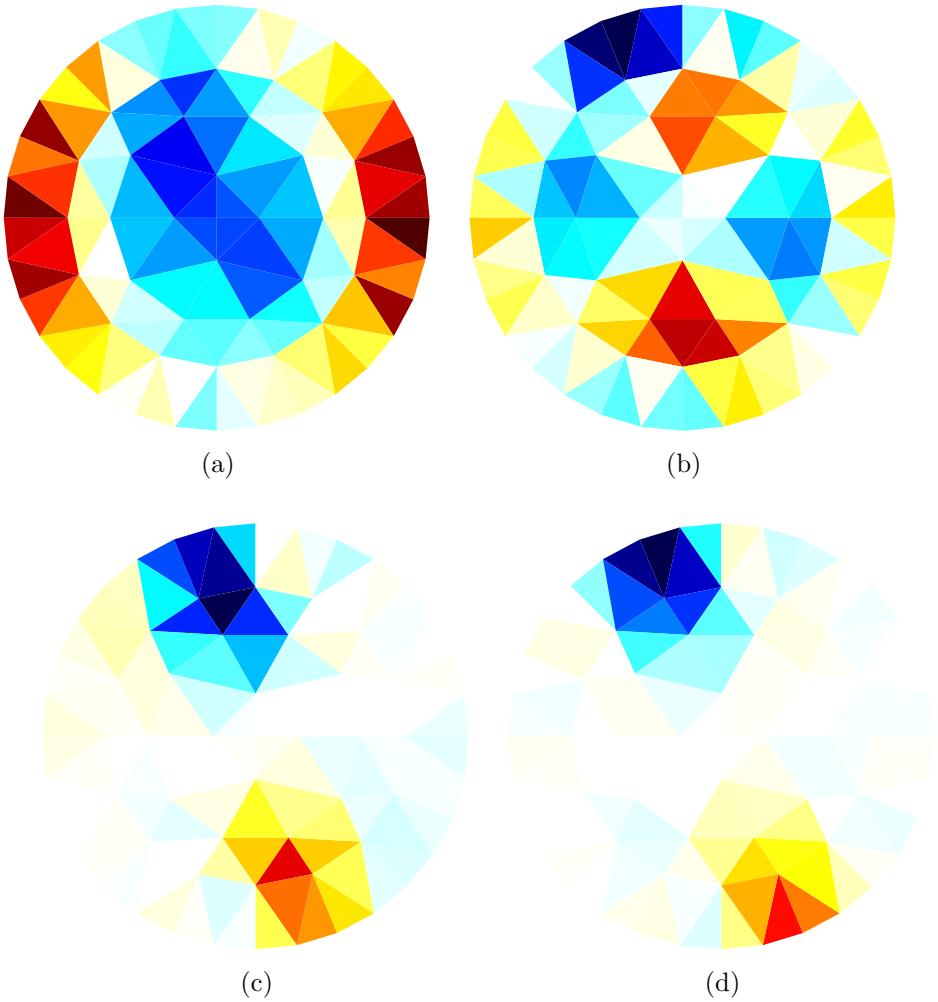

Figure 4.5: Reconstructed conductivity distributions at z=1 *(left)* and z=2 *(right)*. *Top* (4.5a), (4.5b) Non-conformal distortion applied. *Bottom* (4.5c), (4.5d) Conformal distortion applied.

in the conductivity reconstruction for the two distortions and suggest that conformal vector fields (Möbius transformations) tend to give a better reconstruction, avoiding artefacts.

It is hoped that the idea in this chapter can be used to reduce artefacts in chest EIT images caused by variable chest shape. The idea is to start with an initial realistic chest shape, but to compensate for the breathing component by calculating a non-conformal shape perturbation which is adjusted along with the conductivity to fit the data at each time frame. The error will be a conformal map, which can either be determined by a small number of mechanical measurements, or if undetermined will result in a distortion of the conductivity image that will still be clinically useful.

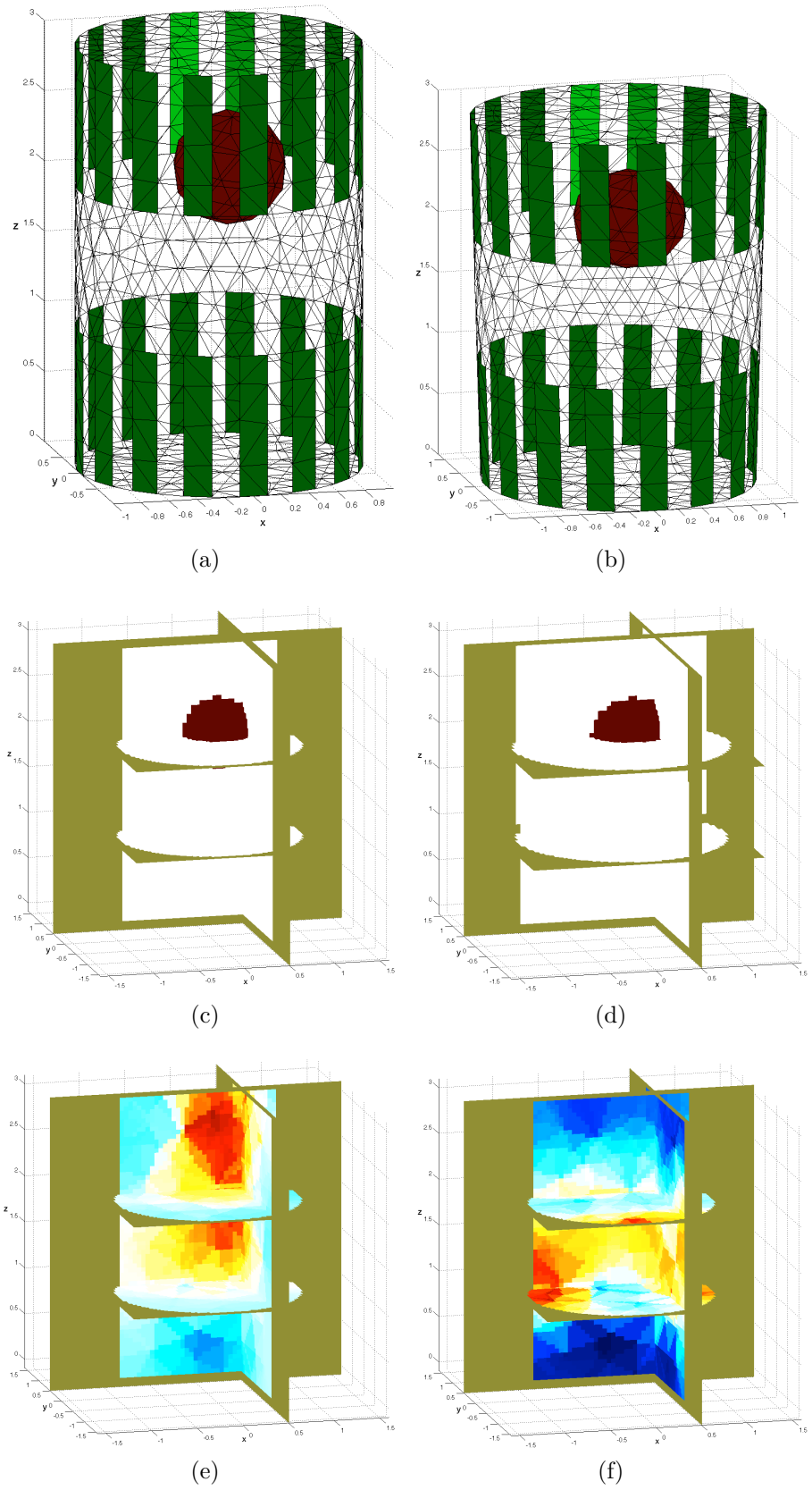

Figure 4.6: Conformal *(left)* and non-conformal *(right)* distortion applied. *Top*, Finite element mesh with electrodes and a conductive ball. *Middle*, 3D images of the simulated inhomogeneity. *Bottom*, 3D images of the reconstructed inhomogeneity.

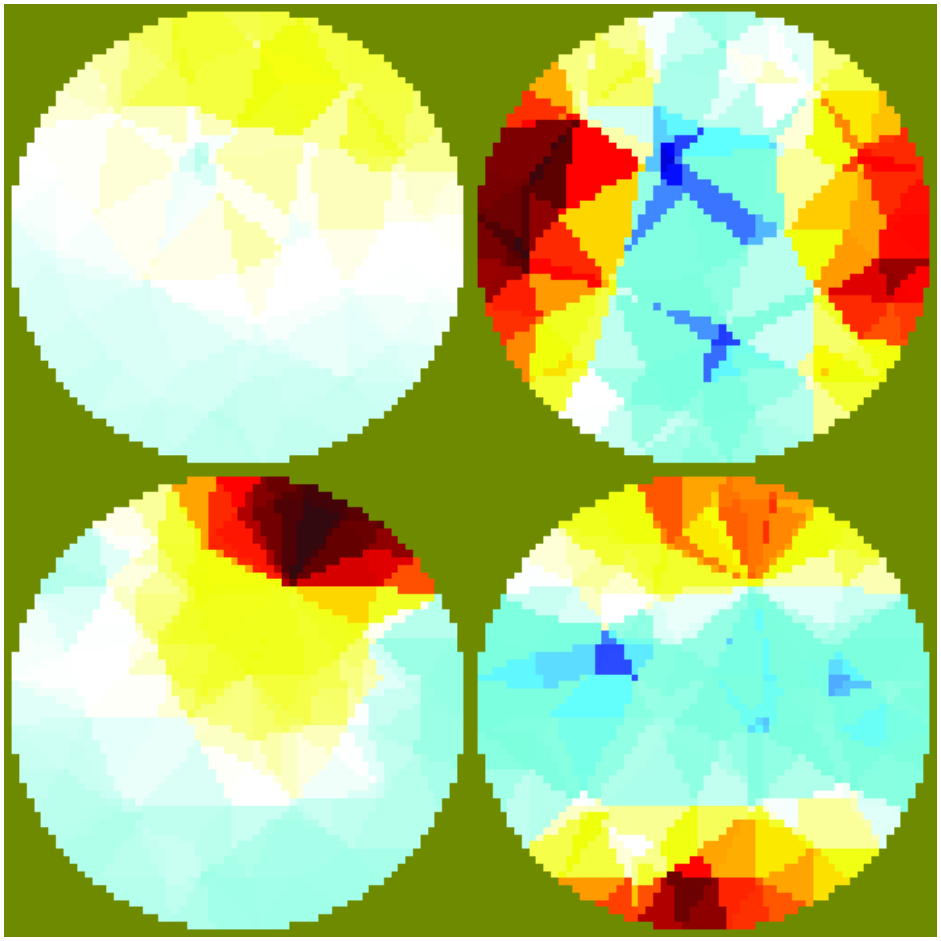

(a) (b)

Figure 4.7: Reconstructed conductivity distributions at z=1 *(top)* and z=2 *(bottom)* for conformal *(left)* and non-conformal *(right)* distortion.

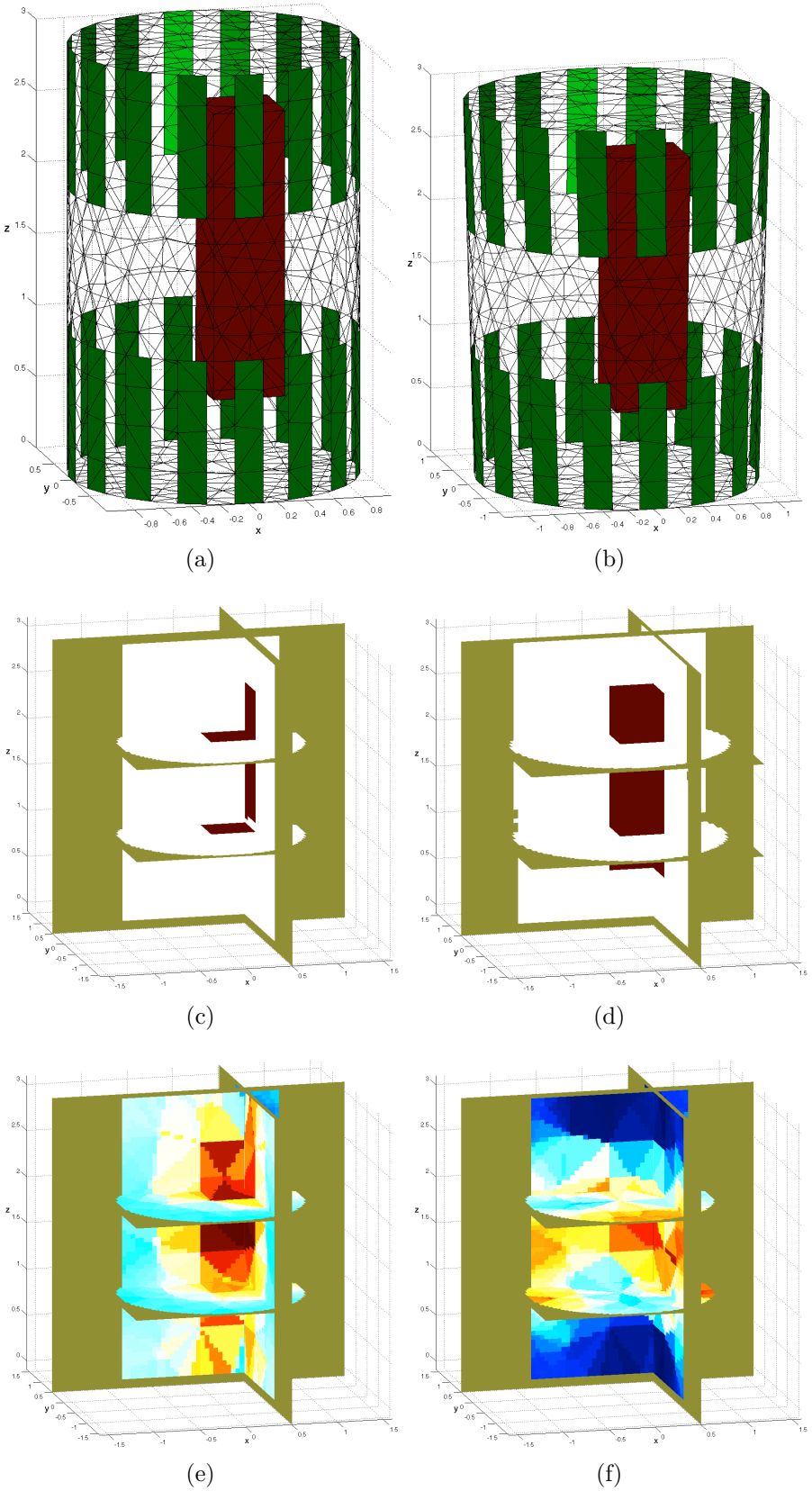

Figure 4.8: Conformal *(left)* and non-conformal *(right)* distortion applied. *Top*, Finite element mesh with electrodes and a conductive cuboid. *Middle*, 3D images of the simulated inhomogeneity. *Bottom*, 3D images of the reconstructed inhomogeneity.

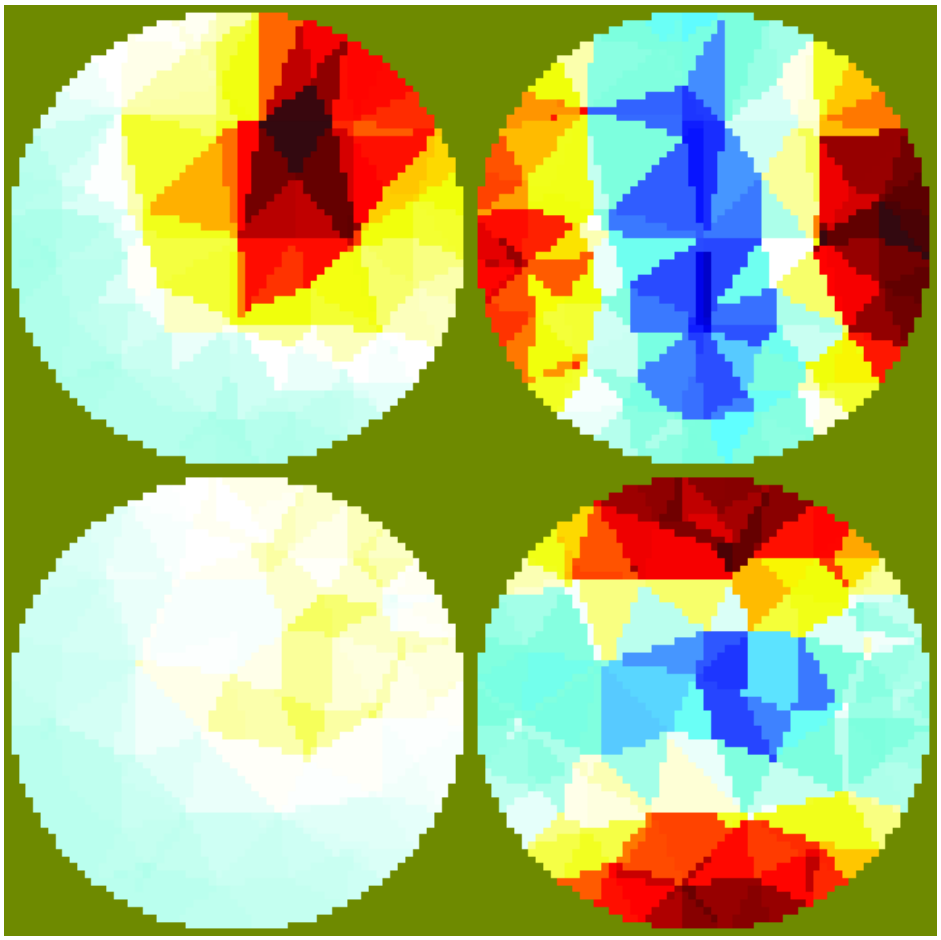

(a) (b)

Figure 4.9: Reconstructed conductivity distributions at z=1 *(top)* and z=2 (*bottom*) for conformal *(left)* and non-conformal *(right)* distortion.

Chapter 5

Resistor networks and transfer resistance matrices

Το λαχωνίζειν εστί φιλοσοφείν[1]

This chapter is an expansion to the conference paper [69] presented at the 13th Conference on Biomedical Applications of Electrical Impedance Tomography held at Tianjin University, Tianjin, China on May 23-25, 2012.

Resistor networks are important for EIT for two reasons. They are used to provide convenient stable test loads or phantoms for EIT systems [45], [43], [58] and they provide a lumped approximation to a conductive body that includes FE, Finite Difference (FD) and Finite Volume Method (FVM) as special cases. In this chapter we start by explaining how a resistor network is acquired from a graph and we outline the basic electrical principles related with resistor networks. In addition, we describe the response and Kirchhoff matrices of a network and their properties. Later we present the uniqueness results for circular and rectangular networks as those were proved by Curtis and Morrow. Finally, we give a consistency condition on transfer resistance matrices of networks derived from n-port theory and review necessary and sufficient conditions for a matrix to be the transfer resistance of a planar network. We give an example to show that there are three dimensional conductivity distributions for which

[1]Literally, "Talking like Lacons talk is philosophical". Lacons is another name for Spartans. It means brief and correct speech (like ancient Spartans) is philosophical. Ancient Greek proverb

the transfer resistance matrix for electrodes on a plane cannot be represented by a planar resistor network.

5.1 Introduction to resistor networks

In this section we present some theoretical results on resistor networks. These are taken from the book "Inverse problems for electrical networks" of Curtis and Morrow [36].

Let $G = (V, E)$ be a graph, where V is the set of vertices and E is the set of edges. To define a resistor network we need a function $\gamma : E \to \mathbb{R}^+$, which assigns to each edge $e \in E$ a positive real number $\gamma(e) = \gamma_e$.

Definition 5.1.1. *A pair $\Gamma = (G, \gamma)$, as defined above, is called a resistor network.*

Similarly to the case of graphs, the set V is called the set of nodes or vertices. Each edge $e \in E$ is a resistor with resistance $1/\gamma_e$. Resistor networks from the inverse problem point of view are networks with boundary. We denote V_0 the set of boundary vertices and $V_I = V \setminus V_0$ the set of interior vertices.

Using Ohm's law the current passing through the conductance $\gamma(pq)$ is given by

$$I(pq) = \gamma(pq)[u(p) - u(q)]. \tag{5.1.1}$$

According to Kirchhoff's law the currents entering an interior node $p \in V_I$ are equal to the algebraic sum of the currents leaving the node p,

$$(L_\gamma u)(p) = \sum_{q \in \mathcal{N}(p)} \gamma(pq)[u(p) - u(q)] \tag{5.1.2}$$

where $\mathcal{N}(p)$ denotes the set of the neighbouring nodes of the node p. If $(L_\gamma u)(p) = 0$ of a node $p \in G \setminus \partial G$, u is said to be γ-harmonic at the node p. Obviously, summing over all the nodes $p \in G$ and considering that currents across each edge occur twice with opposite signs we have

$$\sum_{p \in G} (L_\gamma u)(p) = 0. \tag{5.1.3}$$

If (5.1.3) holds, we say that the function u is γ-harmonic. In the case of γ-harmonic functions Kirchhoff's law becomes

$$(L_\gamma u)(p) = \sum_{q \in \mathcal{N}(p)} \gamma(pq)[u(p) - u(q)] = 0 \tag{5.1.4}$$

and the sum of the currents over the boundary is

$$\sum_{p\in\partial G} \left(L_\gamma u\right)(p) = 0. \tag{5.1.5}$$

Assuming that u is γ-harmonic from (5.1.4) we have

$$\left(\sum_{q\in\mathcal{N}(p)} \gamma(pq)\right) u(p) = \sum_{q\in\mathcal{N}(p)} \left(\gamma(pq)u(q)\right), \tag{5.1.6}$$

hence

$$u(p) = \frac{\displaystyle\sum_{q\in\mathcal{N}(p)} \left(\gamma(pq)u(q)\right)}{\left(\displaystyle\sum_{q\in\mathcal{N}(p)} \gamma(pq)\right)}. \tag{5.1.7}$$

Noting that the conductivity function γ is real-valued the last equation implies that $u(p)$ is a weighted average of the values at the neighbouring nodes. Now if $u(q) < u(p)$ for some nodes $q \in \mathcal{N}(p)$, then $u(r) > u(p)$ for some other neighbouring nodes $r \in \mathcal{N}(p)$ [34]. This leads to the following lemma:

Lemma 5.1.1. *Suppose u is a γ-harmonic function on Γ, and let $p \in V_I$. Then either $u(p) = u(q)$ for all nodes $q \in \mathcal{N}(p)$ or there is at least one node $q \in \mathcal{N}(p)$ for which $u(p) > u(q)$ and there is at least one node $r \in \mathcal{N}(p)$ for which $u(p) < u(r)$.*

In other words, for a resistor network a γ-harmonic function attains its maximum and minimum values at the boundary, which gives the following theorem,

Theorem 5.1.1 (Maximum principle for harmonic functions)**.** *Suppose u is a γ-harmonic function on Γ, then the maximum and minimum values of u occur on the boundary.*

As a consequence of this theorem, any γ-harmonic function that is zero at the boundary is identically zero everywhere [36].

5.2 The response and Kirchhoff matrix of a network

Consider a resistor network $\Gamma = (G, \gamma)$ with n boundary nodes. If a voltage function u is applied at the boundary nodes then a current will pass through the network. The

voltage to current function is an $n \times n$ matrix, called the response matrix, denoted by $\Lambda = \Lambda_\gamma$, with the following properties:

1. Λ is symmetric,

2. the row-sum is equal to zero for each row

3. all the elements with the exception of those in the main diagonal are negative.

Now consider a similar resistor network with edge conductances γ_{ij}. Let $v_i, v_j \in V$. If $v_i v_j \in E$ then $\gamma_{ij} > 0$, otherwise $\gamma_{ij} = 0$. The Kirchhoff matrix is an $n \times n$ matrix with elements

1. $k_{ij} = -\gamma_{ij}$ if $i \neq j$ and

2. $k_{ii} = \sum_{i \neq j} \gamma_{ij}$.

Clearly the Kirchhoff matrix depends on the network Γ and the conductivity function γ. Moreover, if u is a voltage applied on the nodes of G then $\phi = Ku$ is the current in the network.

5.3 Uniqueness results for resistor networks

The existing uniqueness results for resistor networks are mainly due to the work of Edward B. Curtis and James A. Morrow. The two mathematicians of the University of Washington considered the uniqueness problem for a resistor network in the late 1980s when they started working on rectangular networks.

5.3.1 Global uniqueness for rectangular resistor networks

The innovative idea was to introduce the notion of γ-harmonic function (see Section 5.1) and a process they called harmonic continuation. The basic idea is that the boundary values and currents are known for some nodes. Now assume p is an interior node with four neighbouring nodes as in Figure 5.1. Then using Kirchhoff's law and assuming that the potential u is $\gamma-$harmonic and knowing the value of four nodes gives the value of the fifth. In the case where the potentials are known at the surrounding nodes and the current is known at p then Ohm's law is used. Continuing

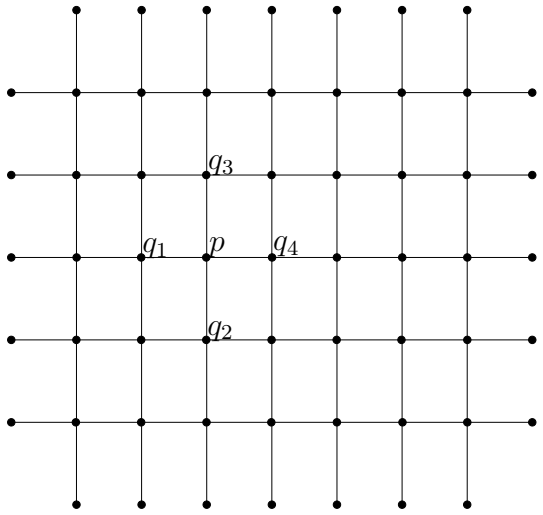

Figure 5.1: Rectangular graph

in this manner we determine the network [36]. Harmonic continuation enabled Curtis and Morrow to prove global uniqueness and continuity of the Dirichlet to Neumann map. A procedure for recovering the conductivity from the Dirichlet to Neumann map is also given [34].

5.3.2 Uniqueness for circular resistor networks.

Curtis and Morrow along with Ingerman later considered circular planar resistor networks [33]. As we have mentioned earlier a planar graph G with boundary is called circular planar if its boundary is embedded in a disc D in the plane so that the boundary nodes lie on the circle C. For their study they introduced the notion of k-connection (Definition 2.2.9). In this work they calculate the possible number of pairs of sequences that are connected through the graph. Moreover, they define the critical graph as the graph produced when removing any edge breaks any connection through G (Definition 2.2.10). Furthermore, they show that two circular planar graphs are $Y-\Delta$ (see [36] for more details) equivalent if and only if they have the same connections. In the same paper the concept of medial graph, described by Colin De Verdière [30] is used to show that two circular planar graphs are $Y-\Delta$ equivalent if and only if their medial graphs are equivalent. In addition, a reconstruction algorithm of the conductivity using the Dirichlet to Neumann map is given.

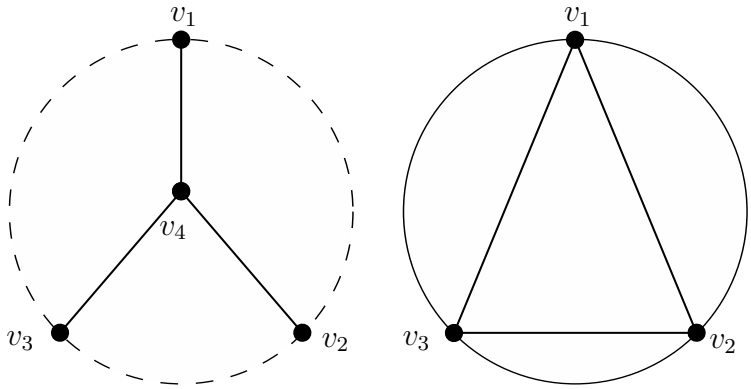

Figure 5.2: Y-Δ transformation

5.4 Transfer resistance matrices

Given a system of L electrodes attached to a conductive body to which a vector of currents $\mathbf{I} \in \mathbb{R}^L$, $\sum_{\ell=1}^{L} I_\ell = 0$ is applied, the resulting vector of voltages $\mathbf{V} \in \mathbb{R}^L$ satisfies

$$\mathbf{V} = \mathbf{R}\mathbf{I}, \tag{5.4.1}$$

where $\mathbf{R}$ is the (real symmetric) transfer resistance matrix. Without loss of generality this is chosen so that $\sum_{\ell=1}^{L} V_\ell = 0$. Restricted to this subspace, $\mathbf{R}$ has an inverse – the transfer conductance matrix.

In EIT of course, $\mathbf{R}$ represents the complete data that can be obtained with this system of electrodes at zero frequency, and it is typically calculated for a known conductivity using the complete electrode model and the finite element method. Such a finite element model gives rise to a resistor network of which the electrodes are considered as terminals. In the general case of a body of arbitrary topology in three dimensional space we can deduce some properties of the matrix $\mathbf{R}$ from general results in circuit theory. In particular the theory of n-port networks.

5.5 n-port networks

An n-port network is a connected resistor network with $m > 2n$ terminals in which n pairs of terminals have been chosen, and within each pair one is labelled $+$ and one $-$. The *open circuit resistance matrix* of this n-port network is the matrix $\mathbf{S}$ such that

$$\mathbf{V} = \mathbf{S}\mathbf{I} \tag{5.5.1}$$

where here $\mathbf{I} \in \mathbb{R}^n$ is a current applied across each pair of terminals and $\mathbf{V} \in \mathbb{R}^n$ the resulting voltages across those terminals. Here $\mathbf{S}$ is a real symmetric $n \times n$ matrix and indeed

$$\mathbf{S} = \mathbf{C}^T \mathbf{R} \mathbf{C}, \tag{5.5.2}$$

where $\mathbf{R}$ is the transfer resistance of the network with the $L = 2n > 4$ distinguished terminals and where the i-th column of the matrix $\mathbf{C}$ has a 1 in the row corresponding to the $+$ terminal of the i-th port and -1 in the row corresponding to the $-$ terminal and is otherwise zero.

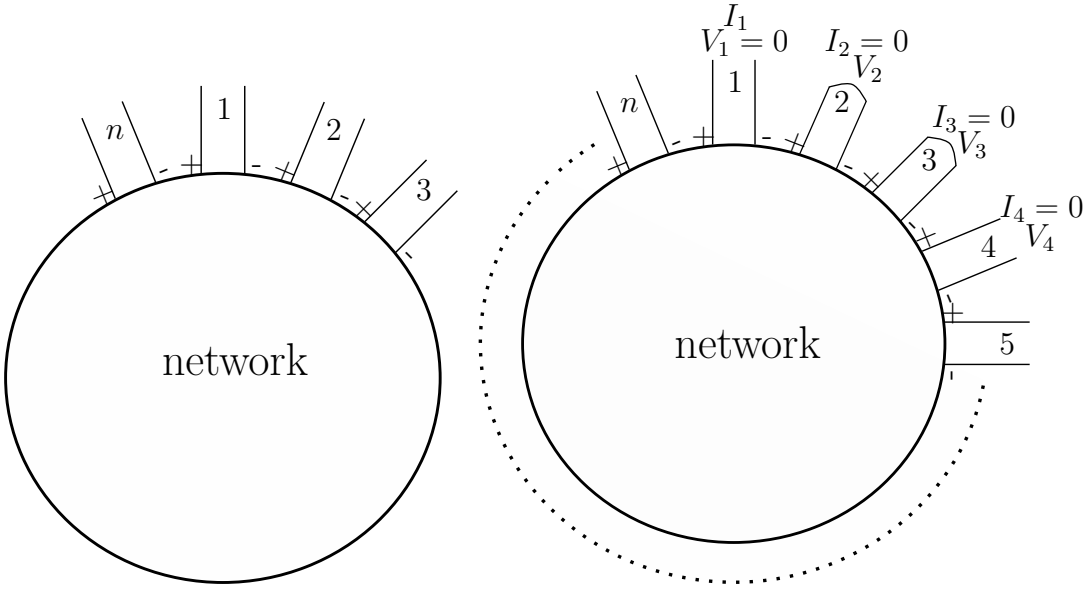

Figure 5.3: *Left*: An n-port network. Each port consists of two terminals of the network labelled $+$ and $-$ but those terminals do not need to be in any sense adjacent and can be chosen arbitrarily. *Right*: The paramountcy condition is derived for applying a current through one port while the other ports are short circuited or open circuit

Cederbaum [29] noticed that the open circuit resistance matrix of an n-port has a property known as paramountcy (see Figure 5.3).

Definition 5.5.1. *Let* $\mathbf{A}$ *be a real symmetric* $n \times n$ *matrix with elements* a_{ij}. *Let* $I = (i_1, i_2, ..., i_k)$ *be an ordered set* $k < n$ *of indices between* 1 *and* n *and* A_{II} *the determinant of the submatrix of rows and columns indexed by* I. *Suppose* J *is another ordered subset of* k *indices and denote by* A_{IJ} *the determinant with rows indexed by* I *and columns by* J. *We say the matrix* $\mathbf{A}$ *is paramount if* $A_{II} \geq |A_{IJ}|$ *for all such* I *and* J.

Most EIT systems use each electrode as both positive and negative current and

voltage terminal, so to apply this definition we choose a subset of the measurements used to define an n-port open circuit resistance matrix where $n \leq L/2$. We thus have a consistency condition on a set of EIT data. For any such designation of a subset of electrodes as ports the resulting $\mathbf{S}$ must be paramount.

This condition may be useful for validating EIT data and fault finding in EIT systems. In particular, if paramountcy fails for a given subset of electrodes chosen as ports but not for others, suspicion falls on the current drive and voltage measurement circuits for the electrodes in those subsets.

5.6 Planar networks

The case of planar networks is much better understood. Consider a connected planar graph embedded in the unit disk in the plane such that L of the vertices fall on the unit circle. The resistor network that results from assigning non zero resistances has a transfer resistance matrix $\mathbf{R}$ with generalized inverse $\mathbf{A}$ (the transfer conductance or "Dirichlet-to-Neumann" matrix). Given that the graph has sufficient connections between the electrodes (see [30], [33]) $\mathbf{A}$ satisfies

$$\det(-1)^k \mathbf{A}_{P,Q} > 0, \tag{5.6.1}$$

where $\mathbf{A}_{P,Q}$ is the matrix restricted to subsets $P, Q \subset \{1, ..., L\}$, $P \cap Q = \emptyset$, $|P| = |Q| = k > 1$ and on the circle the electrodes in P and Q are ordered as $p_1, .., p_k, q_k, ..., q_1$. The sets P and Q should be thought of as two ordered and not interleaved sets of electrodes. The condition of "sufficient connections" required is for all P and Q such that there are disjoint paths through the resistor network joining each p_i to q_i.

Indeed any matrix with this property is the transfer conductance matrix for such planar resistor network and [31] give a canonical topology for this network. Of course given a network and transfer conductance, other networks with the same transfer conductance can be derived using $Y - \Delta$ and resistors in series and parallel transformations, but up to such transformations the resistor mesh is determined by the transfer conductance.

For the continuum case of a simply connected conductive domain in the plane and assuming point electrodes [54] show that the transfer conductance matrix has the same property (5.6.1).

The well known consistency condition for two dimensional EIT data with adjacent pair drives, that the voltages decrease from the current source to the sink, is a consequence of (5.6.1), but the full set of inequalities provides a wider range of consistency conditions that might be applied to the data. Clearly the paramountcy is a weaker condition and might be expected to be less useful.

It was claimed by [58] that a planar resistor network could be used as a realistic test for an EIT system applied to a three dimensional body. The system in question was intended to be used with the electrodes in a single plane on the chest. It is not known if there are conditions on a three dimensional conductivity that guarantee that the transfer conductance on electrodes on a single plane satisfy (5.6.1). It is clear however that for a given pair drive current there are locations of electrodes, specifically on the equipotential on the surface, that have the same voltage and so for some arrangement of electrodes (5.6.1) fails. As a consequence, non-planar resistor networks are needed to test EIT systems for more general arrangements of electrodes. We have already mentioned that for a planar network if you use a pair drive, then the voltage decreases from source to sink. To show that there are some three dimensional conductivities where the data from electrodes on the plane is not consistent with any two dimensional conductivity, it is sufficient to find a conductivity distribution such that the voltage is not monotonically decreasing where that plane intersects the surface between the source and sink electrodes. To construct such an example we simply need a sufficiently complicated variation in the conductivity that bends the equipotential on the surface so that they intersect the plane more than twice. Adler's example shown in Figure 5.4, created for [69], shows that this can happen even in the plane of electrodes.

5.7 Which resistor networks correspond to some FEM?

It is well known that the system matrix for an isotropic first order (two or three dimensional) FEM model with non-obtuse elements is the Ohm-Kirchhoff matrix of a resistor network with the same topology as the FE mesh and resistors given by a cotangent formula (see e.g. [72]). It is interesting in this context to ask the converse

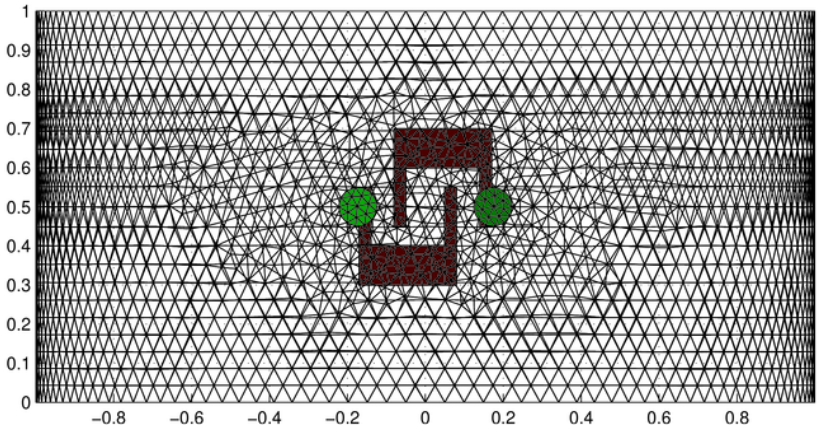

(a) An asymmetrical conductivity anomaly in a cylindrical domain.

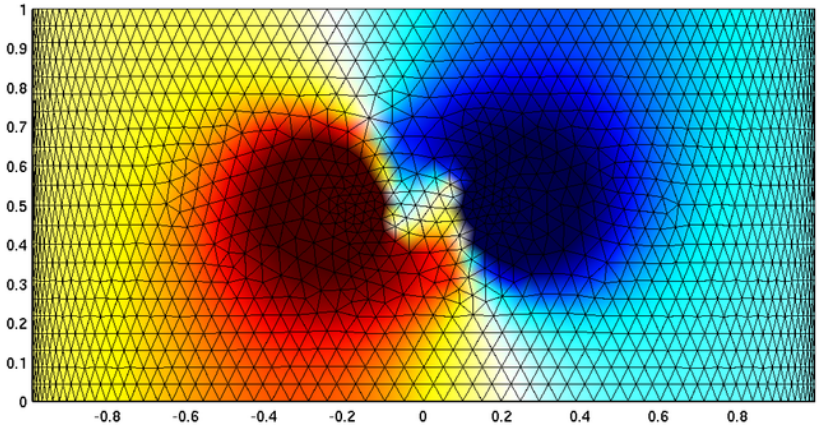

(b) The equipotential lines on the surface resulting from driving current between the two electrodes.

Figure 5.4: An illustration where the transfer resistance matrix for electrodes on a plane cannot be represented by a planar resistor network.

question of which resistor networks (with the topology of a FE mesh) have an assignment of node positions and conductivities that give rise to a system matrix equal to the Ohm-Kirchhoff matrix. A partial answer to this was given by [52] who showed that for a fairly general two dimensional family of layered meshes an open set of resistances resulted in an equivalent isotropic planar FE model. In the next chapter some more results are presented.

5.8 Conclusion

Our contribution involves the paramountcy condition and the consistency conditions for a matrix to be the transfer resistance of a resistor network. The paramountcy condition provides an easy method to check if EIT data is valid. For example we choose

a subset of electrodes as a $n-$port and check if this satisfies the paramountcy condition. If the chosen $n-$port is not paramount, then the problem is in that subset. For the case of planar networks the condition (5.6.1) gives a set of consistency conditions that might be applied to the data. In addition to that it verifies that for two dimensional EIT data with adjacent pair drives, the voltage decreases from the current source to the sink.

Chapter 6

Determination of an embedding consistent with discrete Laplacian on a triangular graph

῞Οπερ ἔδει δεῖξαι[1]

In this chapter we discuss the consistency conditions necessary to find an embedding for a resistor network. Then we use a method used for computer graphics to find a circumcircle representation of a triangulated surface. This representation enable us to "eliminate" some equations by including them in to the parameterisation. We then prove our main result using Duffin's theorem that guarantees a solution for a non-linear resistor network. This is done by considering the dual graph of a resistor network and using the logarithm of the circle radius to represent the voltage. This is where the novelty of our work lies. Finally, we present some numerical results.

6.1 Introduction

Let $G = (V, E)$ be a connected planar graph that can be embedded in the unit disk such that $V_0 \subset V$ lies on the unit circle (we will call them boundary vertices). We will say the graph is *triangular* if each interior face in the embedding is bounded by three

[1]Quod erat demonstrandum

edges. In this case we will denote by T the set of these triangular faces, where $t \in T$ is a set of three edges. For a positive function $C : E \to \mathbb{R}^+$, which we call the *edge conductance*, we define the Laplacian[3] $\Delta_C : \mathbb{R}^V \to \mathbb{R}^V$

$$(\Delta_C u)_v = \sum_{w \in N_v} C_{\{v,w\}}(u_w - u_v) \tag{6.1.1}$$

where $N_v = \{w \in V | \{v, w\} \in E\}$.

This Laplacian arises from considering an electrical network with graph G and each edge e a resistor with resistance $1/C_e$. If the electric potential is U_v at each vertex then combining Ohm's and Kirchhoff's law the current at the vertices is $\Delta_C U$.

Such a Laplacian on a triangular graph also arises as in the FEM. In this case the graph is embedded in $\mathbb{R}^N$, $N \geq 2$ so that the image of each $t \in T$ is a Euclidean triangle and these triangles intersect only in edges and vertices; that is the image forms a simplicial surface. Those edges in only one triangle (*boundary edges*) we will denote by E_0 and clearly these are pairs from V_0.

For a given embedding $\iota : V \to \mathbb{R}^N$ we have an edge length $\ell : E \to \mathbb{R}_+$ given by $\ell_{\{v,w\}} = ||\iota(v) - \iota(w)||$. We note that when we refer to an embedding we mean that we are embedding straight lines. This is slightly different from the general embedding where we embed curves (see Definition 2.2.5). For each triangle t with edges e, f, g we define ϕ_e^t to be the (unsigned) angle between the embedded edges f and g. The FEM problem we have in mind is to solve Laplace's equation on a surface with boundary, given Dirichlet or Neumann boundary conditions. We take a triangulation of the surface and approximate the solution of Laplace's equation by functions that are continuous and piecewise linear on triangles, and hence determined by the values at the vertices. The FEM or cotangent Laplacian arising from this discretisation is $\Delta_{\mathscr{C}(\ell)}$, where

$$\mathscr{C}_e(\ell) = \begin{cases} \frac{1}{2}\left(\cot \phi_e^t + \cot \phi_e^{t'}\right), & \text{where } e \in E - E_0,\ e \subset t \cap t', \\ \frac{1}{2} \cot \phi_e^t, & \text{where } e \in E_0,\ e \subset t. \end{cases} \tag{6.1.2}$$

This formula, though widely used, its origins are not clear. As far as we know, this representation appears for the first time in literature in 1959, and is due to Duffin [41].

[3]We will generally not distinguish between functions on a finite set and tuples indexed by a finite set and use subscripts from the index set to denote the values of both.

The aim of this section is given triangular G and conductance C, determine if there is an assignment of edge lengths ℓ such that $C = \mathscr{C}(\ell)$. This is especially of interest in discrete approximations to the inverse conductivity problem. On resistor networks this problem is well studied (see e.g. [36], [30]) however in many practical applications (such as electrical resistivity tomography in geophysics, electrical impedance tomography in medical imaging and electrical resistance and capacitance tomography in industrial process monitoring) the finite element approximation is used.

It is clear that a necessary condition for the lengths to correspond to some embedding is the triangle inequality. For triangle $t = \{e, f, g\}$ this is

$$\ell_e + \ell_f > \ell_g. \tag{6.1.3}$$

Conversely it is straightforward to verify that any assignment of ℓ satisfying (6.1.3) are the lengths for an embedding in $\mathbb{R}^{n_v-1}$. There is an extensive literature on existence and uniqueness (up to rigid motion) of embeddings in the important case of $\mathbb{R}^3$.

6.2 Consistency conditions

In this section we analyse two consistency conditions we use to solve the optimisation problem. The third condition we use is that the angles in a triangle add up to π. This is a trivial result from Euclidean geometry.

6.2.1 Sine constraint

The sine rule consistency condition is due to Al Humaidi who describes it in his thesis [52]. We start with a set of triangles that all share an interior vertex. We call this a wheel in the triangulation. The edges are denoted with e_i with respective edge length ℓ_{e_i}, $i = 1, \ldots, n$. Referring to Figure 6.1 we apply the sine rule to the triangles and we move anti-clockwise. Starting with the first triangle we have

$$\frac{\ell_{e_1}}{\ell_{e_2}} = \frac{\sin\beta_1}{\sin\alpha_1}. \tag{6.2.1}$$

Moving to the next triangle and applying the sine rule gives

$$\frac{\ell_{e_2}}{\ell_{e_3}} = \frac{\sin\beta_2}{\sin\alpha_2}. \tag{6.2.2}$$

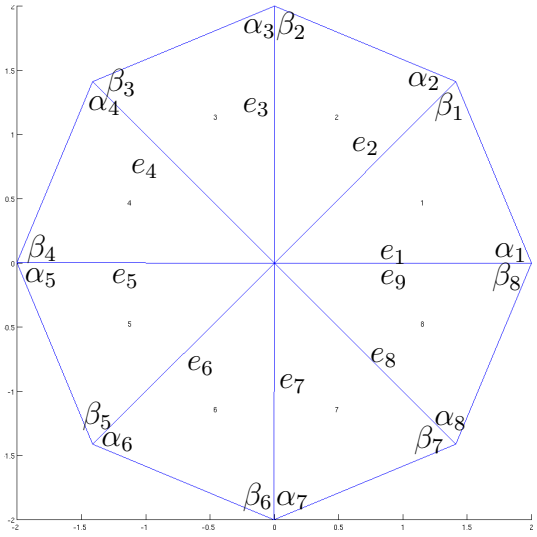

Figure 6.1: Illustration of sine rule

Combining the two relations we get

$$\frac{\ell_{e_1}}{\ell_{e_3}} = \frac{\ell_{e_1}}{\ell_{e_2}}\frac{\ell_{e_2}}{\ell_{e_3}} = \frac{\sin\beta_1}{\sin\alpha_1}\frac{\sin\beta_2}{\sin\alpha_2}. \tag{6.2.3}$$

Assume now that this is true for n triangles enclosing an interior vertex. Then

$$\frac{\ell_{e_1}}{\ell_{e_n}} = \frac{\ell_{e_1}}{\ell_{e_2}}\frac{\ell_{e_2}}{\ell_{e_3}}\cdots\frac{\ell_{e_{n-1}}}{\ell_{e_n}} = \frac{\sin\beta_1}{\sin\alpha_1}\frac{\sin\beta_2}{\sin\alpha_2}\cdots\frac{\sin\beta_n}{\sin\alpha_n}. \tag{6.2.4}$$

Finally, for $n+1$ we have

$$\frac{\ell_{e_1}}{\ell_{e_{n+1}}} = \frac{\ell_{e_1}}{\ell_{e_2}}\frac{\ell_{e_2}}{\ell_{e_3}}\cdots\frac{\ell_{e_{n-1}}}{\ell_{e_n}}\frac{\ell_{e_n}}{\ell_{e_{n+1}}} = \frac{\sin\beta_1}{\sin\alpha_1}\frac{\sin\beta_2}{\sin\alpha_2}\cdots\frac{\sin\beta_n}{\sin\alpha_n}\frac{\sin\beta_{n+1}}{\sin\alpha_{n+1}} = 1, \tag{6.2.5}$$

since the last edges e_1 and e_{n+1} coincide. For convenience we take logarithms and relation (6.2.5) becomes

$$\sum_{i=1}^{n}(\ln\sin\beta_i - \ln\sin\alpha_i) = 0. \tag{6.2.6}$$

Obviously this proves that the sine constraint is satisfied for an interior vertex. Now let us consider the case where a cycle is formed by a union of basic cycles (Figure 6.2). By basic cycle we mean a cycle around an interior vertex. Then in a similar way we can prove that the sine constraint is valid for any cycle in the graph. We use the same notation as before, that is e_i, and ℓ_i, $i = 1, 2, \ldots, n$ are the edges and there lengths respectively. Then for the first and second triangles T_1 and T_2 we have

$$\frac{\ell_{e_1}}{\ell_{e_2}} = \frac{\sin\beta_1}{\sin\alpha_1} \text{ and } \frac{\ell_{e_2}}{\ell_{e_3}} = \frac{\sin\beta_2}{\sin\alpha_2},$$

hence,

$$\frac{\ell_{e_1}}{\ell_{e_3}} = \frac{\sin\beta_1}{\sin\alpha_1}\frac{\sin\beta_2}{\sin\alpha_2}.$$

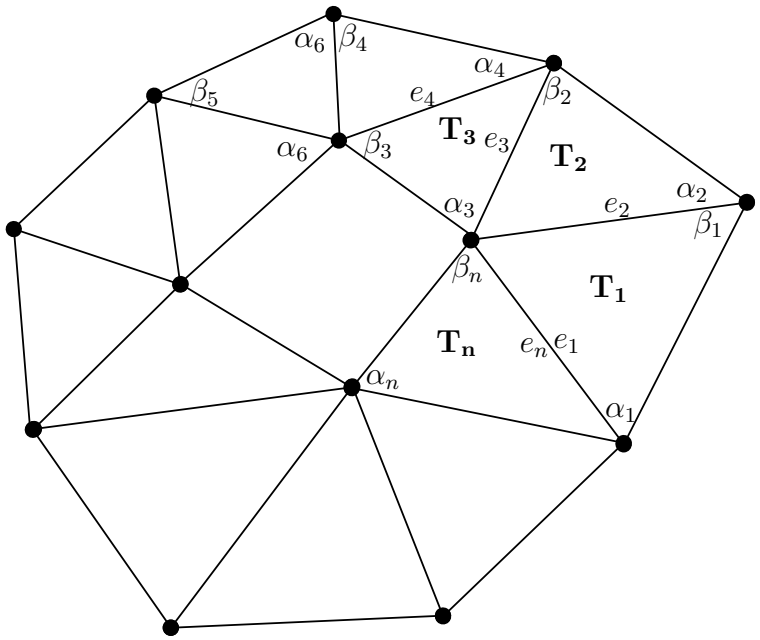

Figure 6.2: Illustration of sine rule

Moving in the same way in the cycle we reach the final triangle T_n that closes the cycle. Applying the sine rule we have.

$$\frac{\ell_{e_{n-1}}}{\ell_{e_n}} = \frac{\sin\beta_n}{\sin\alpha_n}.$$

Notice that $e_1 = e_n$ so we have

$$\frac{\ell_{e_1}}{\ell_{e_n}} = \frac{\ell_{e_1}}{\ell_{e_2}} \cdots \frac{\ell_{e_{n-1}}}{\ell_{e_n}} = \frac{\sin\beta_1}{\sin\alpha_1} \cdots \frac{\sin\beta_n}{\sin\alpha_n} = 1. \tag{6.2.7}$$

This proves that the sine constraint is satisfied in any cycle of the graph.

6.2.2 Cotangent constraint

To construct a resistor network equivalent to a FEM model replace each edge by a resistor. When the triangles are assembled in to a mesh the conductances add in parallel summing the contribution from triangles both sides of an edge (Figure 6.3).

Now we have to determine the conductances. The FE mesh is related to the Dirichlet to Neumann map Λ_σ (Definition 3.2.1) through the system matrix K. The construction of the system matrix is discussed in subsection 3.3.2 where the reader may refer for more details. The system matrix $K \in \mathbb{R}^{n_v \times n_v}$ is given by

$$K_{ij} = \sum_{k:\{x_i,x_j\}\subset T_k} \nabla\phi_i \cdot \sigma^h \nabla\phi_j |T_k|, \tag{6.2.8}$$

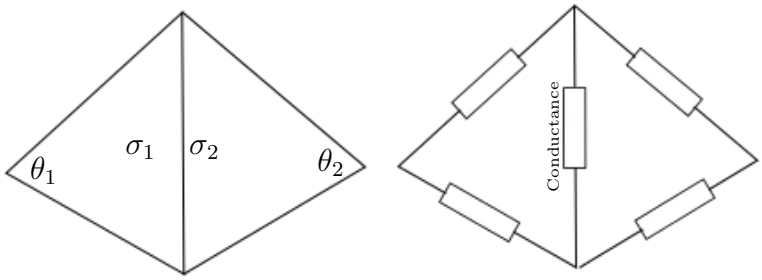

Figure 6.3: A resistor network assembled from a FE mesh

where $|T_k|$ is the area of the triangular element and ϕ_i is a piecewise linear function. Since the potential is piecewise linear then $\nabla\phi_i$ is constant on elements.

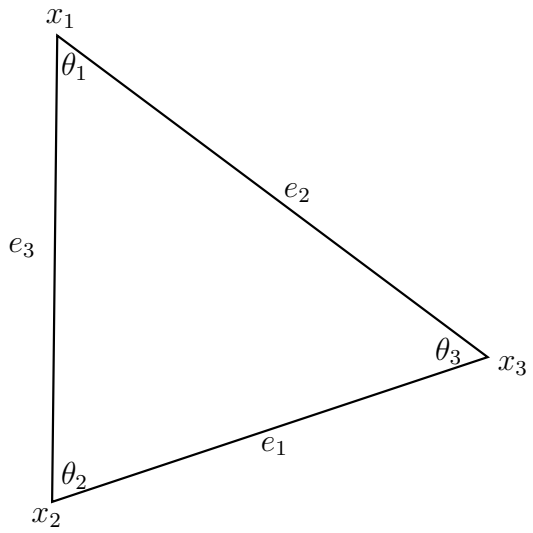

Figure 6.4: Cotangent formula

We refer to Figure 6.4 for the derivation of the formula. Denote the vertex positions with x_i, $i = 1, 2, 3$. Clearly the edge lengths are

$$\begin{aligned} \ell_{e_1} &= |x_3 - x_2|, \\ \ell_{e_2} &= |x_3 - x_1|, \\ \ell_{e_3} &= |x_2 - x_1|. \end{aligned}$$

Now the gradient of the normal to e_1 is given by

$$\nabla N_1 = \frac{(x_2 - x_3)^\perp}{(x_1 - x_2) \cdot (x_2 - x_3)^\perp},$$

where $\perp$ denotes an anticlockwise perpendicular vector. Similarly, we have

$$\nabla N_2 = \frac{(x_3 - x_1)^\perp}{(x_2 - x_3) \cdot (x_3 - x_1)^\perp}.$$

Multiplying the two relations yields

$$\begin{aligned}
\nabla N_1 \cdot \nabla N_2 &= \frac{(x_2 - x_3)^\perp \cdot (x_3 - x_1)^\perp}{(x_1 - x_2) \cdot (x_2 - x_3)^\perp \cdot (x_2 - x_3) \cdot (x_3 - x_1)^\perp} \\
&= \frac{(x_2 - x_3) \cdot (x_3 - x_1)}{(x_1 - x_2) \cdot (x_2 - x_3)^\perp \cdot (x_2 - x_3) \cdot (x_3 - x_1)^\perp} \\
&= \frac{\ell_{e_1}\, \ell_{e_2}\, \cos\theta_3}{\ell_{e_3}\, \ell_{e_1}\, \sin\theta_2\, \ell_{e_1}\, \ell_{e_2} \sin\theta_3} \\
&= \frac{\cot\theta_3}{\ell_{e_1}\, \ell_{e_3}\, \sin\theta_2} \\
&= \frac{\cot\theta_3}{2\,|T_k|}.
\end{aligned}$$

Hence, locally $k_{12} = \frac{\sigma}{2}\cot\theta_3$. In total, $K_{ij} = 0$ if i and j do not share an edge and $K_{ii} = -\sum_{i \neq j} k_{ij}$ otherwise. Note also that K is symmetric.

6.3 Parameterisation of a triangulated surface

From the point of view of a cotangent Laplacian it is of course convenient to work with the angles ϕ_e^t rather than lengths.

Lemma 6.3.1. *Consider a triangle $t = \{e, f, g\}$, where e, f and g are the edges with lengths ℓ_e, ℓ_f and ℓ_g respectively. The angle opposite the edge e is denoted by ϕ_e^t. Then ϕ_e^t is related to the edge lengths through*

$$\tan\phi_e^t/2 = \sqrt{\frac{(\ell_e + \ell_f - \ell_g)(\ell_e + \ell_g - \ell_f)}{(\ell_f + \ell_g - \ell_e)(\ell_e + \ell_f + \ell_g)}}. \tag{6.3.1}$$

Formula (6.3.1) is easy to prove but since we were unable to find a published proof we give one.

Proof. Consider a triangle $t = \{e, f, g\}$ with edge lengths ℓ_e, ℓ_f, ℓ_g respectively (Figure 6.5). As usual denote the angle opposite to the side e by ϕ_e^t. Then apply the cosine rule for the angle ϕ_e^t, hence $\cos\phi_e^t = \frac{\ell_e^2 + \ell_g^2 - \ell_e^2}{2\ell_f\ell_g}$. It is known that the tangent half-angle formulae are given by

$$\tan\frac{\phi_e^t}{2} = \frac{\sin\phi_e^t}{1 + \cos\phi_e^t} = \frac{1 - \cos\phi_e^t}{\sin\phi_e^t}. \tag{6.3.2}$$

Multiplying the equations (6.3.2) we obtain $\tan^2\frac{\phi_e^t}{2} = \frac{1-\cos\phi_e^t}{1+\cos\phi_e^t}$. Lastly, substituting $\cos\phi_e^t$ from the cosine rule, simplifying and applying basic polynomial identities we

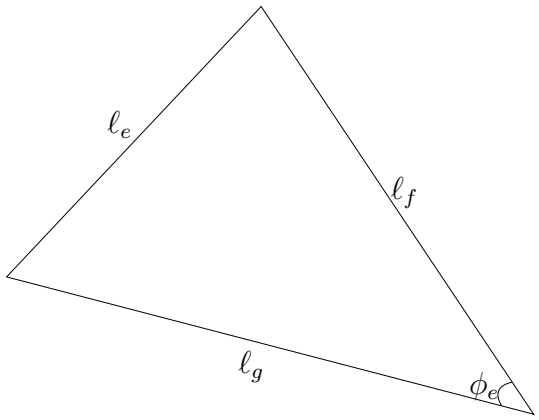

Figure 6.5: Calculation of angle ϕ_e with respect to edge lengths.

get

$$\tan^2 \frac{\phi_e^t}{2} = \frac{(\ell_e + \ell_f - \ell_g)(\ell_e + \ell_g - \ell_f)}{(\ell_f + \ell_g - \ell_e)(\ell_e + \ell_f + \ell_g)}. \tag{6.3.3}$$

The result follows. □

The triangle inequality guarantees that the term under the square root is positive and (6.3.1) then implies

$$\phi_e^t + \phi_f^t + \phi_g^t = \pi. \tag{6.3.4}$$

It is well known that if there is an embedding in $\mathbb{R}^2$ then ϕ_e^t determines the embedding up to similarity, indeed this is the classical triangulation survey problem studied by Tycho Brahe (see also [52]). There is a simple explicit construction of a ℓ satisfying the triangle inequality given ϕ_e^t satisfying (6.3.4).

6.3.1 The edge lengths from corner angles

Given ϕ and a spanning tree (T, S) of G' rooted at $t_0 \in T_0$ one calculates ℓ restricted to the edges dual to the edges in S recursively using the sine rule

$$\ell_f = \frac{\sin \phi_f^t}{\sin \phi_e^t} \ell_e. \tag{6.3.5}$$

Each edge f in the cotree $E \setminus S$ has the property that $S \cup \{f\}$ has exactly one cyclic path C in G'. One can then calculate ℓ_f using the sine rule for e, the edge either side of f in the cyclic path. Provided that the corner angles satisfy (6.3.10) the answer will be independent of this choice.

The triangle inequality (6.1.3) follows immediately from $\phi_e^t + \phi_f^t + \phi_g^t = \pi$ where $t = \{e, f, g\}$ as

$$\ell_e + \ell_f = \frac{\sin \phi_e^t + \sin \phi_f^t}{\sin(\phi_e^t + \phi_f^t)} > \ell_g \tag{6.3.6}$$

provided $\phi_e^t, \phi_f^t \in (0, \pi)$.

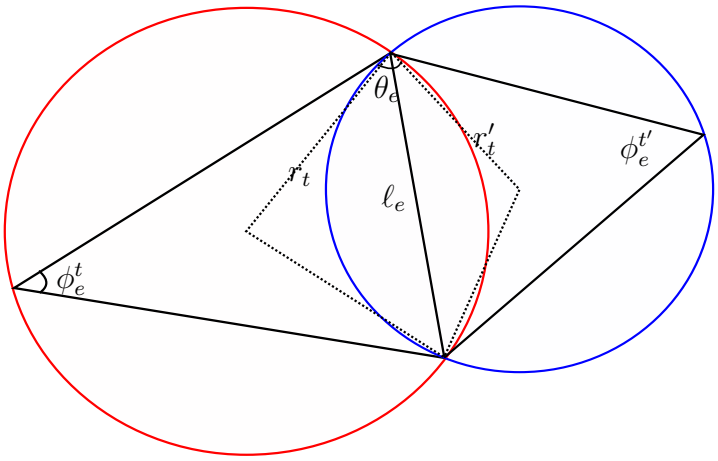

Figure 6.6: Intersecting circles with circumscribed adjacent triangles

6.3.2 Circumcircle representation of a triangulated surface

We will find it more convenient to represent the embedding in terms of the radius and angles between circumcircles of the triangles because this representation includes the sine constraints in to the parameterisation. Kharevych et al. [61] use this method for the construction of discrete conformal mappings from surface meshes of arbitrary topology to the plane. Following this method we denote by r_t the circumcircle radius of the embedded triangle and note that for each $t \in T$ from the sine rule

$$2r_t = \frac{\ell_e}{\sin \phi_e^t} \tag{6.3.7}$$

for each $e \in t$. We define for any $e \in E$

$$\theta_e = \begin{cases} \pi - \phi_e^t - \phi_e^{t'} & \text{where } e \in E - E_0,\ e \subset t \cup t' \\ \pi - \phi_e^t & \text{where } e \in E_0,\ e \subset t \end{cases} \tag{6.3.8}$$

which has the following interpretation: for $e \in E - E_0$ the quadrilateral defined by the embedded t and t' can be isometrically embedded in the plane and then θ_e is the angle between the radii of the circumcircles of the two triangles.

Let $G' = (T, E')$ be the dual graph, where $\{t, t'\} \in E' \Leftrightarrow \exists e \in E - E_0$, $e \subset t \cup t'$ or $\exists e \in E_0$, $e \subset t$. Clearly there is a natural one-to-one correspondence between E' and E. The dual graph is also connected and planar and can be embedded in the unit disk with vertices T_0 on the unit circle where each triangle $t \in T_0$ has an edge in E_0. We will equip G' with an arbitrary orientation on edges so $\tilde{G}' = (T, \tilde{E}')$, where $\tilde{E}' \subset T \times T$. We then identify $\mathbb{R}^T$ with $C^0(\tilde{G}')$ the space of zero-cochains. Specifically $\rho_t = \log r_t$ is a zero cochain and its exterior derivative is $\omega = d\rho$, where d is the coboundary operator, specifically

$$\omega_e = \log(r'_t/r_t) \quad \text{where } e = (t, t') \in \tilde{E}'. \tag{6.3.9}$$

The following is immediate

Lemma 6.3.2. *Let S be any spanning tree of G' rooted at $t_0 \in T$. ρ is uniquely determined by its restriction to $\tilde{S}$, which is S inheriting the orientation from $\tilde{G}'$, and ρ_{t_0}.*

The corner angles cannot be assigned arbitrarily as they must satisfy (6.3.4). We now show that they must also satisfy another set of relations. Let $(e'_1, e'_2, ...e'_k)$ be a cyclic path in the dual graph, that is a sequence of triangles $(t_1, t_2, ..., t_k)$ where t_i and t_{i+1}, and t_k and t_1 share an edge in G, then from the sine rule we have

$$\prod_i^k \frac{\sin \phi_{e_i}^{t_i}}{\sin \phi_{e_i}^{t_{i+1}}} = 1. \tag{6.3.10}$$

In the circumcircle parameterisation this is expressed more succinctly. Let c be the chain in $C_1(\tilde{G}')$ corresponding to the cyclic path, then

$$\langle \omega, c \rangle = 0, \tag{6.3.11}$$

where the angle brackets are the dual pairing between chains and cochains. By definition $\langle d\rho, c \rangle = \langle \rho, \partial c \rangle$. This shows succinctly that the number of independent constraints due to the sine rule are exactly the dimension of the first cohomology group of G', which is precisely $|V - V_0|$, the number of interior vertices.

We define the cotangent $\cot : (0, \pi) \to \mathbb{R}$ so that it is monotonically decreasing, bijective and continuous. We can then recover the corner angles ϕ from the circle parameters ω, ρ. Consider the triangle formed by the centres of the circumscribed

circles and a point of intersection. Applying the sine rule on the triangle

$$\frac{\sin\phi_e^t}{r_t'} = \frac{\sin\theta_e}{D} \Leftrightarrow \sin\phi_e^t = \frac{r_t'}{D}\sin\theta_e, \tag{6.3.12}$$

where D is the distance between the two centres. Now using the cosine rule

$$r_t'^2 = r_t^2 + D^2 - 2r_t D\cos\phi_e^t \Leftrightarrow \cos\phi_e^t = \frac{r_t^2 + D^2 - r_t'^2}{2r_t D}. \tag{6.3.13}$$

Similarly

$$D^2 = r_t^2 + r_t'^2 - 2r_t r_t'\cos\theta_e. \tag{6.3.14}$$

By the definition of cot we have

$$\cot\phi_e^t = \frac{\cos\phi_e^t}{\sin\phi_e^t} = \frac{\frac{r_t^2+D^2-r_t'^2}{2r_t D}}{\frac{r_t'}{D}\sin\theta_e} = \frac{\frac{r_t^2+D^2-r_t'^2}{2r_t r_t'}}{\sin\theta_e}. \tag{6.3.15}$$

Eliminating D we have

$$\phi_e^t = \cot^{-1}\left(\frac{\frac{r_t^2 - r_t r_t'\cos\theta_e}{r_t r_t'}}{\sin\theta_e}\right) = \cot^{-1}\left(\frac{\frac{r_t}{r_t'} - \cos\theta_e}{\sin\theta_e}\right). \tag{6.3.16}$$

Now since $\rho = \log r_t$ and $\rho' = \log r_t'$ we have $\omega_e = \rho - \rho' = \log\frac{r_r}{r_t'} \Leftrightarrow \frac{r_r}{r_t'} = \mathrm{e}^{\omega_e}$. Repeating for the opposite angle $\phi_e^{t'}$ we get $\cot^{-1}\frac{\mathrm{e}^{-\omega_e'} - \cos\theta_e}{\sin\theta_e}$. Hence,

$$\phi_e^t = \begin{cases} \cot^{-1}\frac{\mathrm{e}^{-\omega_e'} - \cos\theta_e}{\sin\theta_e} & \text{for } e \in E - E_0,\ e' \text{ an oriented edge dual to } e, \\ \pi - \theta_e & \text{for } e \in E_0. \end{cases} \tag{6.3.17}$$

While for $N > 2$ the problem of finding an embedding given ℓ is hard, we can nevertheless construct the ℓ explicitly up to a single scale factor given a consistent set of ϕ or θ and $d\rho$ on a spanning tree of the dual graph routed at $t_0 \in T_0$. The construction is given in subsection 6.3.1.

6.4 Non-linear resistor networks

In this section we describe the work of Richard Duffin from 1947 [39]. Duffin's work on non-linear resistor networks is essential in our study, because by applying his theorem on our non-linear system of equations (6.5.1) we are able to find a unique solution to the problem and hence find a three dimensional embedding for a planar resistor network. Since the paper is relatively old, it is written in an old style that makes

reading difficult. For this reason we try to modernize it, make it easier to read and bring Duffin's important work to surface.

Consider map $S : R^n \to R^n$. The idea is to show that this map has a unique inverse by imposing certain conditions on the S. The conditions are chosen in such a manner so that the map is a generalization of the equations describing the steady flow of a current in electrical networks with quasi-linear conductors.

Obviously, it is possible to express S in the form

$$y_i = P_i(z_i), \tag{6.4.1}$$

where

$$(z_i)_k = \begin{cases} x_i & \text{for } i = k, \\ x_k - x_i & \text{otherwise.} \end{cases}$$

Definition 6.4.1. *The set of functions $P_i(t_1, t_2, \ldots, t_n)$, $i = 1, 2, \ldots, k$ is called an n-dimensional connected foundation if for $i, j \in \mathbb{N}$ and all values of the variables:*

1. *P_i is a continuous function of n variables,*
2. *P_{ij} is either an increasing function unbounded at $\pm\infty$, or is constant,*
3. *there is a sequence of integers $a, b, \ldots, g, h$ (dependent on i) such that in the chain $P_{ab}, P_{bc}, \ldots, P_{gh}, P_{hh}$ each function is unbounded at $\pm\infty$.*

Notation: P_{i_j} indicates P_i as a function of t_j with the rest of the variables fixed at arbitrary values

Definition 6.4.2. *If the set of functions P_i forms a connected foundation, then transformation* (6.4.1) *will be called a connected transformation.*

Lemma 6.4.1 (Duffin's Lemma)**.** *Transformation* (6.4.1) *has at least one solution if*

1. *P_i is a continuous function,*
2. *P_{ij} is nondecreasing,*
3. *for each i there is a chain in which the functions are unbounded at $+\infty$ and for each i there is a chain in which the functions are unbounded at $-\infty$.*

Proof. Let y be a constant vector and let $\epsilon > 0$. The relations

$$v_i = \epsilon \mathbf{x} + P_i(z_i) - y_i, \quad i = 1, \ldots, n$$

define a continuous vector field v when $\mathbf{x}$ ranges in and on a cube with corners at $(\pm k, \pm k, \ldots, \pm k)$, $k \geq 0$. For $x_1 = k > 0$, that

$$v_1 = \epsilon k + P_1(k, k - x_2, \ldots, k - x_n) - y_1. \tag{6.4.2}$$

Since P_{ij} is nondecreasing (condition 2) we have

$$P_1(k, k - x_2, \ldots, k - x_n) \geq P_1(0, 0, \ldots, 0). \tag{6.4.3}$$

Hence,

$$v_1 \geq \epsilon k + P_1(0, 0, \ldots, 0) - y_1. \tag{6.4.4}$$

Similarly, with $x_1 = -k$

$$v_1 \leq \epsilon k + P_1(0, 0, \ldots, 0) - y_1. \tag{6.4.5}$$

Consequently, for $k > \max |P_i(0, 0, \ldots, 0) - y_i| \epsilon^{-1}$ the vector $\mathbf{v}$ on the surface of the cube is pointing outwards. Recall now that Brouwer's fixed point theorem (see Theorem 2.3.1) states that every continuous function from a closed ball of a Euclidean space to itself has a fixed point. At this point

$$y_i = P_i(x_i - x_1, \ldots, x_i, \ldots, x_i - x_n) + \epsilon x_i. \tag{6.4.6}$$

The next step is to show that x_i, $i = 1, 2, \ldots, n$ are bounded independent of ϵ. For some integer i, $x_i \geq x_j$, $j = 1, 2, \ldots, n$. Let $i, a, b, \ldots, g, h$ be a chain sequence such that $P_{ia}, P_{ab}, \ldots, P_{gh}$ satisfy condition 3 and assume that $x_i, x_a, \ldots, x_h$ are all positive. Then since $x_i > 0$ and $x_i \geq x_j$ for all j

$$\begin{aligned} y_i &\geq P_i(x_i - x_1, \ldots, x_i - x_a, \ldots, x_i - x_n) \\ &\geq P_i(0, \ldots, x_i - x_a, \ldots, 0). \end{aligned}$$

Thus, there is a constant $c_i > 0$ (independent of ϵ) such that $x_i - x_a \leq c_i$. Now, since $x_j \leq x_i \Leftrightarrow x_j - x_a \leq x_i - x_a \leq c_i$, hence $x_a - x_j \geq -c_i$ for any j. Therefore,

$$\begin{aligned} y_a &\geq P_a(x_a - x_1, \ldots, x_a - x_b, \ldots, x_a - x_n) \\ &\geq P_a(-c_i, \ldots, x_a - x_b, \ldots, -c_i). \end{aligned}$$

Thus, there is a constant $b_a > 0$ such that $x_a - x_b \leq b_a$. Obviously, as before,

$$\begin{aligned} x_j - x_a \leq c_i &\Leftrightarrow x_j - x_b - x_a \leq c_i - x_b \\ &\Leftrightarrow x_j - x_b \leq c_i + x_a - x_b \\ &\Leftrightarrow x_j - x_b \leq c_i + b_a = c_a. \end{aligned}$$

Continuing the process gives

$$\begin{aligned} y_h &\geq P_h(x_h - x_1, \ldots, x_h, \ldots, x_h - x_n) \\ &\geq P_h(-c_g, \ldots, x_h, \ldots, -c_g), \end{aligned}$$

and finally there is a constant $c_h > 0$ such that $x_h \leq c_h$. Clearly,

$$\begin{aligned} x_i &= (x_i - x_a) + (x_a - x_b) + \ldots + (x_g - x_h) + x_h \\ &\leq c_i + c_a + \ldots + c_g + c_h. \end{aligned}$$

Note that the last inequality is valid even if some members of the sequence $x_i, \ldots . x_h$ are negative. Lets assume that x_e is the first non-positive member of the sequence, then

$$\begin{aligned} x_i &= (x_i - x_a) + (x_a - x_b) + \ldots + (x_d - x_e) + x_e \\ &\leq c_i + c_a + \ldots + c_d. \end{aligned}$$

The constants c depend only on y and the growth of P_i, and for each i there are such constants so the components of x have a finite upper bound.

Using a symmetrical argument and chains unbounded at $-\infty$ it can be shown that the components of x have a finite lower bound too. As ϵ goes to zero, it follows that x has at least one limit point and since P_i is continuous this proves Lemma 6.4.1. □

Lemma 6.4.2 (Duffin's Lemma)**.** *Transformation* (6.4.1) *may not have more than one solution if:*

1. *P_{ij} is nondecreasing.*

2. *For each i there is a chain in which each of the functions is an increasing function.*

Proof. If P_i, $i = 1, \ldots, n$ are homogeneous linear functions, i.e $P_i(\alpha x) = \alpha^k P_i(x)$, for some multiplicative factor α, then transformation (6.4.1) becomes

$$\mathbf{y} = A\mathbf{x}, \tag{6.4.7}$$

where A is the matrix

$$A_{ij} = \begin{cases} \sum_{k=1}^{n} p_{ik} & \text{if } i = j, \\ -p_{ij} & \text{otherwise.} \end{cases}$$

Let x and x' be two vectors with transforms y and y' respectively and $\delta x_i = x'_i - x_i$, $\delta y_i = y'_i - y_i$. Let also,

$$t_1 = x_1, t_2 = x_1 - x_2, \ldots, t_n = x_1 - x_n,$$
$$t'_1 = x'_1, t'_2 = x'_1 - x'_2, \ldots, t'_n = x'_1 - x'_n.$$

Then,

$$\begin{aligned} \delta y_1 &= y'_1 - y_1 \\ &= P_1(t'_1, t'_2, \ldots, t'_n) - P_1(t_1, t_2, \ldots, t_n) \\ &= [P_1(t'_1, t'_2, \ldots, t'_n) - P_1(t_1, t'_2, \ldots, t'_n)] + \\ &\quad [P_1(t_1, t'_2, \ldots, t'_n) - P_1(t_1, t_2, \ldots, t'_n)] + \\ &\quad \vdots \qquad\qquad \vdots \qquad\qquad + \\ &\quad [P_1(t_1, t_2, \ldots, t_{n-1}, t'_n) - P_1(t_1, t_2, \ldots, t_n)]. \end{aligned}$$

Now, let

$$p_{1j} = \begin{cases} \frac{[P_1(t_1,\ldots,t'_j,t'_{j+1},\ldots,t'_n) - P_1(t_1,\ldots,t_j,t'_{j+1},\ldots,t'_n)]}{(t'_j - t_j)}, & t'_j - t_j \neq 0, \\ 1, & t'_j - t_j = 0. \end{cases}$$

Finally,

$$\begin{aligned} \delta y_1 &= p_{11}(t'_1 - t_1) + p_1 2(t'_2 - t_2) + \ldots + p_{1n}(t'_n - t_n) \\ &= p_{11}(x'_1 - x_1) + p_1 2(x'_1 - x'_2 - x_1 + x_2) + \ldots + p_{1n}(x'_1 - x'_n - x_1 + x_n) \\ &= p_{11}\delta x_1 + p_1 2(\delta x_1 - \delta x_2 + \ldots + p_{1n}(\delta x_1 - \delta x_n). \end{aligned}$$

Continuing in a similar manner the expressions for $\delta y_2, \ldots, \delta y_n$ can be calculated. The constants p_{ij} define a linear connected transformation and hence, by Lemma 6.4.1 this transformation has an inverse. But a linear transformation with an inverse has a unique inverse and we conclude that if $\delta y = 0$, then $\delta x = 0$. □

Duffin's Theorem. *For any assigned values of $y_1, y_2, \ldots, y_n$ a connected transformation has a unique solution $x_1, x_2, \ldots, x_n$.*

Proof. The theorem is an obvious consequence of Lemma 6.4.1 that proves the existence of such solution and Lemma 6.4.2 that proves the uniqueness. □

6.5 The main result

Now that we have established all the necessary components we can proceed to our main result.

Theorem 6.5.1. *Let G be a planar triangular graph and ι_0 some embedding in $\mathbb{R}^N$ with embedded lengths ℓ^0, and resulting edge conductances C^0. Then there is an open neighbourhood $\mathcal{U} \subset \mathbb{R}_+^E$, $C^0 \in \mathcal{U}$ such that for each $C \in \mathcal{U}$*

$$\sum_{e \subset t} H_{C_e}((d\rho)_e) = \pi. \tag{6.5.1}$$

Notice that ϕ_e^t and θ_e are immediately determined on boundary edges. For interior edges using (6.1.2) and (6.3.17) we have

$$\begin{aligned} \frac{\mathrm{e}^{\omega_e} - \cos\theta_e}{\sin\theta_e} + \frac{\mathrm{e}^{-\omega_e} - \cos\theta_e}{\sin\theta_e} &= 2C_e \\ \Leftrightarrow \frac{\frac{\mathrm{e}^{\omega_e} + \mathrm{e}^{-\omega_e}}{2} - \cos\theta_e}{\sin\theta_e} &= C_e \\ \Leftrightarrow \frac{\cosh\omega_e - \cos\theta_e}{\sin\theta_e} &= C_e. \end{aligned} \tag{6.5.2}$$

Now $\cos^2\theta_e + \sin^2\theta_e = 1, \quad \Rightarrow \cos^2\theta_e + \frac{(\cosh\omega_e - \cos\theta_e)^2}{C_e^2} = 1$. Expanding and collecting terms gives,

$$(C_e^2 + 1)\cos^2\theta_e - 2\cosh\omega_e \cos\theta_e + (\cosh^2\omega_e - C_e^2) = 0. \tag{6.5.3}$$

Similarly, by eliminating $\cos\theta_e$ we obtain

$$(C_e^2 + 1)\sin^2\theta_e - 2C_e \cosh\omega_e \sin\theta_e + (\cosh^2\omega_e - 1) = 0. \tag{6.5.4}$$

Finally by solving the quadratic equations (6.5.3)-(6.5.4) we obtain

$$\cos\theta_e = \frac{\cosh\omega_e - C_e\sqrt{1 + C_e^2 - \cosh^2\omega_e}}{1 + C_e^2}, \tag{6.5.5}$$

$$\sin\theta_e = \frac{C_e\cosh\omega_e + \sqrt{1 + C_e^2 - \cosh^2\omega_e}}{1 + {C_e}^2}, \tag{6.5.6}$$

which determine θ_e given ω_e and C_e for an interior edge e. Note that the sign of the solutions is chosen so that the solutions indeed satisfy the initial equation.

Obviously for θ_e to be real we need $\cosh^2\omega_e \leq 1 + C_e^2$. Moreover, $0 < \cos\theta_e \leq 1$, so

$$0 < \cosh\omega_e - C_e\sqrt{1 + C_e^2 - \cosh^2\omega_e} \leq 1 + C_e^2. \tag{6.5.7}$$

From the first inequality we have

$$\begin{aligned} 0 &< \cosh\omega_e - C_e\sqrt{1 + C_e^2 - \cosh^2\omega_e}, \\ \Leftrightarrow \cosh\omega_e &> C_e\sqrt{1 + C_e^2 - \cosh^2\omega_e}, \\ \Leftrightarrow \cosh^2\omega_e &> C_e^2\left(1 + C_e^2 - \cosh^2\omega_e\right), \\ \Leftrightarrow (1 + C_e^2)\cosh^2\omega_e &> C_e^2\left(1 + C_e^2\right), \\ \Leftrightarrow \cosh^2\omega_e &> C_e^2, \end{aligned} \tag{6.5.8}$$

hence $\cosh\omega_e > C_e$. From the second inequality

$$\begin{aligned} 1 + C_e^2 &\geq \cosh\omega_e - C_e\sqrt{1 + C_e^2 - \cosh^2\omega_e}, \\ \Leftrightarrow \cosh\omega_e &\leq 1 + C_e^2 + C_e\sqrt{1 + C_e^2 - \cosh^2\omega_e}, \end{aligned}$$

which is true for all ω_e and $C_e > 0$ since $\cosh\omega_e \leq \sqrt{1 + C_e^2} \leq 1 + C_e^2$.
Clearly, $0 < \sin\theta_e \leq 1$, so

$$0 < C_e\cosh\omega_e + \sqrt{1 + C_e^2 - \cosh^2\omega_e} \leq 1 + C_e^2. \tag{6.5.9}$$

The inequality on the left hand side gives

$$\begin{aligned} 0 &< C_e\cosh\omega_e + \sqrt{1 + C_e^2 - \cosh^2\omega_e}, \\ \Leftrightarrow \cosh\omega_e &> -\frac{\sqrt{1 + C_e^2 - \cosh^2\omega_e}}{C_e}, \end{aligned}$$

which is clearly true for any ω_e and positive C_e. Now on the right hand side we have

$$\begin{aligned} 1 + C_e^2 &> C_e\cosh\omega_e + \sqrt{1 + C_e^2 - \cosh^2\omega_e}, \\ \Rightarrow 1 + C_e^2 - C_e\cosh\omega_e &> \sqrt{1 + C_e^2 - \cosh^2\omega_e} > 0. \end{aligned}$$

Squaring both sides of the inequality

$$\begin{aligned} (1 + C_e^2 - C_e\cosh\omega_e)^2 &> 1 + C_e^2 - \cosh^2\omega_e, \\ \Leftrightarrow 1 + C_e^4 + C_e^2\cosh^2\omega_e + 2C_e^2 - 2C_e\cosh\omega_e - 2C_e^3\cosh\omega_e &> 1 + C_e^2 - \cosh^2\omega_e. \end{aligned}$$

Finally, simplifying and collecting terms gives

$$\begin{aligned} 0 &< (1+C_e^2)\cosh^2\omega_e - 2C_e(1+C_e^2)\cosh\omega_e + C_e^2(1+C_e^2) \\ &= \cosh^2\omega_e - 2C_e\cosh\omega_e + C_e^2 = (\cosh\omega_e - C_e)^2 \end{aligned}$$

which is also true for all ω_e and $C_e > 0$.

Hence, $|\omega_e| < \cosh^{-1}\sqrt{1+{C_e}^2}$, while $\cosh\omega_e > C_e$ ensures $\theta_e \in (0, \pi/2)$. Substitution in to (6.3.17) gives

$$\phi_e^t = \cot^{-1}\frac{(1+C_e^2)\mathrm{e}^{-\omega_e} - \cosh\omega_e + C_e\sqrt{C_e^2 - \sinh^2\omega_e}}{C_e\cosh\omega_e + \sqrt{C_e^2 - \sinh^2\omega_e}} := H_{C_e}(\omega_e). \tag{6.5.10}$$

We take $\cot : (0,\pi) \to \mathbb{R}$ so that ϕ_e^t is defined for all

$$\omega_e \in (-\cosh^{-1}\sqrt{1+C_e^2}, \cosh^{-1}\sqrt{1+C_e^2}).$$

The remaining constraint is that the angles within each triangle t sum to π

$$\sum_{e\subset t} H_{C_e}(\omega_e) = \pi. \tag{6.5.11}$$

Noting that $\omega_e = (d\rho)_e$ this can be seen as Ohm-Kirchhoff law for a network (on the dual graph of G) of non-linear resistors with current voltage law given by H_{C_e} and a current of π input at each vertex. The boundary conditions are the Neumann boundary conditions that ϕ_e^t is specified on boundary edges and one Dirichlet condition is chosen (one circumradius) which determines an overall scale factor of the embedding.

$$\frac{d}{d\omega}\cot H_C(\omega) = -\frac{C(1+C^2)}{\sqrt{C^2-\sinh^2\omega}\left(C\cosh\omega + \sqrt{C^2-\sinh^2\omega}\right)} < 0 \tag{6.5.12}$$

The condition $|\omega_e| < \sinh^{-1} C_e$ could be considered as the operating voltage. The problem of existence and uniqueness of solution for a non-linear resistor network is one that has received considerable attention since Duffin in 1947. We will prove the necessary result directly rather than relying on this literature.

Let $F_C(\rho)_t = \sum_{e\subset t} H_{C_e}((d\rho)_e) - \pi$

We see that $DF_t(\rho)\eta = \sum_{e\subset t} H'_{C_e}((d\rho)_e)d\eta$ and we notice that solving

$$DF_t(\rho)\eta = Y$$

for known Y is exactly Poisson's equation for the Ohm-Kirchhoff Laplacian on the dual graph G' with homogeneous Neumann boundary conditions and edge conductance $H'_{C_e}((d\rho)_e)$.

6.6 Number of equations

In this section we use three relations that are satisfied for any triangular mesh and we calculate the number of equations. This is necessary to do because though our theorem proves that the system of equations is solvable our numerical implementation uses a different approach, though equivalent. For this reason we have to check that the equations we are solving are independent. We denote with n_t the number of triangles, n_e the number of edges and $n_v = n_{v_i} + n_{v_\partial}$ the number of vertices, where n_{v_i} and n_{v_∂} are the number of interior and boundary vertices respectively. Using this notation, for any triangulation the following relations are valid:

1. $n_v - n_e + n_t = 1$,
2. $3n_t + n_{v_\partial} = 2\, n_e$,
3. $n_v = n_{v_i} + n_{v_\partial}$.

It is worth mentioning here that $\chi = n_v - n_e + n_t$ is the Euler characteristic. For general polyhedra the number of triangles is replaced with the number of faces. We know that we have a π constraint per triangle, thus n_t equations, a sine constraint per interior vertex, thus n_{v_i} equations and a cotangent constraint per edge, thus n_e equations. So the total number of equations is:

$$\begin{aligned}
n_t + n_{v_i} + n_e &= n_t + n_{v_i} + \frac{3n_t + n_{v_\partial}}{2} \\
&= \frac{5n_t}{2} + n_{v_i} + \frac{n_{v_\partial}}{2} \\
&= \frac{5n_t}{2} + n_v - \frac{n_{v_\partial}}{2} \\
&= \frac{5n_t}{2} + 1 - n_t + n_e - \frac{n_{v_\partial}}{2} \\
&= \frac{3n_t}{2} + 1 + n_e - \frac{n_{v_\partial}}{2} \\
&= \frac{3n_t}{2} + 1 + \frac{3\, n_t + n_{v_\partial}}{2} - \frac{n_{v_\partial}}{2} \\
&= 3n_t + 1
\end{aligned}$$

This means that we have one extra equation since we have $3n_t$ number of variables, that is the number of angles in the triangulation.

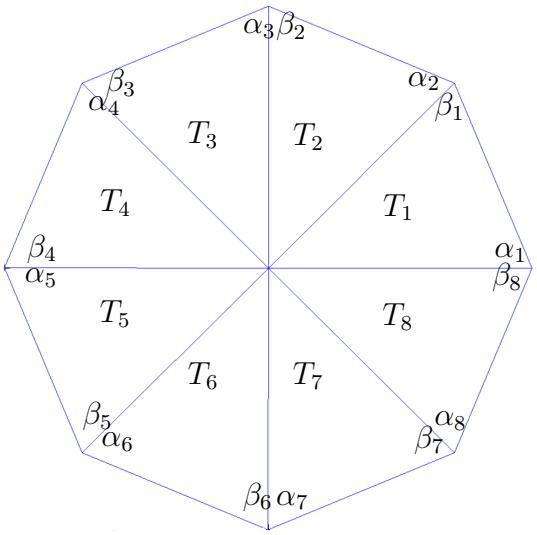

Figure 6.7: 1-wheel resistor network

6.6.1 Removing one π constraint

Before giving a formal reasoning of the π constraint removal we explain in simple words why this is possible using an extreme case. Consider the case of having a resistor network with one interior vertex only as in Figure 6.7. Then all the angles with endpoint the interior vertex (those opposite to the boundary edges) are known from the cot formula. Then we use the sine constraint. Doing this will force the last and first edges to meet, so that the cycle will close and the sine constraint will be satisfied. The next step is to use the cotangent constraints in all the interior edges. It is clear now that the cotangent constraints will give a relation between the angles α_7 and β_8 and between the angles α_8 and β_1, making the use of the π constraint in the last triangle T_8 redundant.

Now we formally show why one π constraint is redundant. For this we use the notation and construction of Biggs [19]. Let $G = (V, E)$ be a graph with n_v vertices and n_e edges with an incidence function $i : E \to V^{(2)}$, where $V^{(2)}$ is the set of unordered pair of vertices. Let $h : E \to V$ be an orientation of G such that $h(e) \in i(e)$, for all edges e. The vertex $h(e)$ is called the head of the edge e. The tail is denoted by $t(e)$ and obviously $i(e) = \{h(e), t(e)\}$ is an oriented edge. Now consider the edge adjacency

(also called incidence) matrix $D = (d_{\text{ve}}) \in \mathbb{R}^{n_v \times n_e}$ such that

$$(d_{\text{ve}}) = \begin{cases} 1, & \text{if } v = h(e), \\ -1, & \text{if } v = t(e), \\ 0 & \text{if } v \notin i(e). \end{cases}$$

Let $C^0(G;\mathbb{R})$ and $C^1(G;\mathbb{R})$ denote the vector spaces of real-valued functions defined on V and E, respectively. Interpreting the elements of these spaces as column vectors, we have the linear operator

$$D : C^0(G;\mathbb{R}) \to C^1(G;\mathbb{R}) \text{ and } D^T : C^1(G;\mathbb{R}) \to C^0(G;\mathbb{R}).$$

Given $\alpha \in C^0$, the transpose of the adjacency matrix is given by

$$(D^T\alpha)(e) = \alpha(h(e)) - \alpha(t(e)). \tag{6.6.1}$$

Suppose that $\alpha \in C^0$ such that $(D^T\alpha)(e) = 0$, then from the relation (6.6.1), α takes the same value on the head and tail of any edge. If v and w are in the same component of G, then there is a walk from v to w and $\alpha(v) = \alpha(w)$. This simply means that α is constant on each component of G. On the other hand, if α is constant on each component, then $D^T\alpha = 0$. Altogether, $\ker(D^T)$ is the space of functions which are constant on each component of G.

Using Biggs notation the Kirchhoff Laplacian is $\Delta = DCD^T$, where the matrix $C \in \mathbb{R}^{n_e \times n_e}$ is the diagonal matrix of the edge conductances. Following his construction of the kernel of D^T we construct the kernel of the Laplacian and since it is symmetric, then for a constant vector v we have

$$\Delta v = \Delta^T v = 0. \tag{6.6.2}$$

This shows that a constant vector gives a relation between the rows of Δ. From this we determine that one equation (any row of Δ) can be written as the sum of the remaining rows with a negative sign. Hence, any equation can be neglected. Finally, this is applied to the linearised version of $\sum_{e \subset t} H_{C_e}((d\rho)_e) = \pi$.

6.7 Embedding in $\mathbb{R}^3$ vs. $\mathbb{R}^N$

Finding an embedding in $\mathbb{R}^N$, for N big enough is an easy process. Consider a graph with n_t triangular elements. Naturally the first triangle (formed by three connected

vertices) is embeddable in $\mathbb{R}^2$. Then for the next triangle we can add one dimension (i.e. we are now in $\mathbb{R}^3$) and thus the second triangle is embeddable. The process of adding a dimension is repeated until all the triangles are embedded. Hence, for dimension $N > n_t$ we can easily find an embedding.

The non-uniqueness of an embedding in $\mathbb{R}^3$ is related to the curvature. Regions of positive curvature can be "up" or "down", causing a problem in the choice of direction. To explain this let us use the following example. The areas A and B represent a finite set of triangular elements for which the curvature is positive for both. Area C has zero curvature (see Figure 6.8). Under these circumstances, it is clear that we can embed area C in to the plane, say we choose the $x-y$ plane. Then for the other two we have to choose how we will embed them. This can be done in different ways, meaning that the z-coordinates of A and B can be either positive or negative. This simple example shows that an embedding in $\mathbb{R}^3$ is not unique.

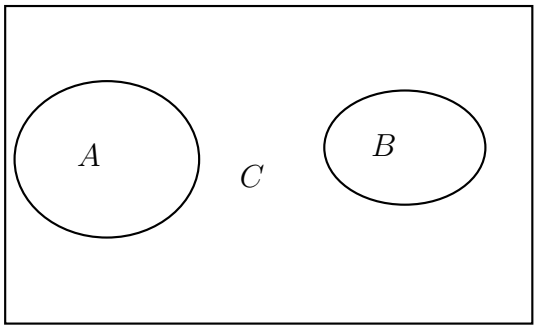

Figure 6.8: Non-uniqueness of an embedding in $\mathbb{R}^3$.

Alexandrov's theorem is an important result that gives conditions under which a polygon will fold into a convex polyhedron.

Alexandrov's Theorem. *Let S be a sphere with a convex Euclidean polyhedral metric. Then there exists a convex polytope $P \subset \mathbb{R}^3$ such that the boundary of P is isometric to S. Moreover, P is unique up to a rigid motion.*

Bobenko and Izmestiev give a constructive proof of the theorem in [21].

A consequence of Alexandrov's theorem is the following theorem.

Theorem 6.7.1. *Suppose that the boundary of an abstract triangulated surface can be isometrically embedded (i.e. the lengths are the same) in the plane as a convex polygon such that when this polygon is a face added to the surface to form a polyhedron*

1. *the curvatures on the boundary are all positive, and*

2. *the Gauss-Bonnet condition is satisfied.*

Then this is a polyhedron with a positive curvature and Alexandrov's theorem guarantees that it is embeddable in $\mathbb{R}^3$*, and this embedding is unique.*

6.8 Numerical experiments

In this section we present a few numerical tests we have conducted. Naturally the first test is to check how much we can perturb the z-dimension of the initial mesh. The second test is to check whether we can still find an embedding after we have applied some perturbation on the edge conductances. Lastly, we perturb the x and y coordinates of the mesh while the perturbation in the z-dimension is retained. It is obviously expected for small enough perturbations to be able to find an embedding. Before presenting our numerical results we explain why our code is equivalent to our theory.

6.8.1 Uniqueness theorem vs. Numerical implementation

Our theoretical result suggests that an embedding can be uniquely determined. The reader though will notice that our existence and uniqueness theorem was proved using a slightly different method from the one we use for the numerical tests. The main difference lies in the way we have chosen to parameterise the triangulation using the circumcircle representation as this is described in Section 6.3. Defining the variable $\omega = \log \frac{r}{r'}$, where r and r' are the radii of the circumcircles of adjacent triangles enabled us to build-in the sine constraints in to the parameterisation. This suggests that we still have the same constraints and the same number of equations to solve. One could then suggest why we do not solve numerically the equation

$$\sum_{e \subset t} H_{C_e}((d\rho)_e) = \pi. \tag{6.8.1}$$

It is clear that this can be done, but we must have in mind that this is a non-linear problem and trying to avoid it is desirable. Even if we exclude the fact of non-linearity of equation (6.8.1), solving it will only give the circumradii of the triangulation. We

would still have to calculate the angles of the triangulation to determine the embedding. In contrast to this, our numerical implementation returns the final answer, that is the required angles. For these reasons we choose to implement the code in the way we describe in the next subsection.

6.8.2 Explanation of the code in Appendix D

For the embedding calculation we use the two MATLAB codes in Appendix D. The first one is the main code where the mesh angles, to be passed to the constraints function, and the edge conductances are calculated. An explanation of the code follows.

1. Construct a planar mesh and find all the angles (angles2d)
2. Perturb the z-coordinate so that the mesh "buckles up" from the plane and calculate the angles (angles3d), retaining the mesh geometry (i.e. same geometry as in step 1)
3. Calculate the edge conductances on the perturbed mesh.
4. Find the fixed angles, i.e. angles opposite a boundary edge.
5. The remaining angles are those we want to calculate, so we vectorize them (angles_vec) and pass to myfunc

Obviously the angles we will get after we optimize must be close to the angles of the perturbed mesh, that is angles3d.

We note here that the code is a modification of Al Humaidi's code [52] and it uses Vauhkonen's cirgrid_eit to create the circular meshes. The second code, containing all the constraints is again a modified version of Al Humaidi's code. The difference between Al Humaidi's implementation and ours is that Al Humaidi is looking for a two dimensional embedding, so he has an extra set of constraints, the fact that the angles with an interior vertex as an endpoint add up to 2π. In our case this is not the case, as we are trying to find an embedding in three dimensions.

6.8.3 Numerical tests

Test 1 - Perturbation in the z-dimension

As a first test we check for two different meshes if the algorithm converges to a solution when we perturb by ϵ in the z coordinate. The first mesh (mesh 1) is a two layered circular mesh with seven interior vertices and ten boundary. For the second mesh (mesh 2) we add a third layer with twenty vertices. In Tables 6.1-6.2 we present the results for a variety of perturbations. Figures 6.9 and 6.11 show the two meshes used. Figures 6.10 and 6.12 show the calculated embedding for selected cases.

ϵ	Convergence	Iterations	$f(x)$
0.1	Yes	7	8.92224e-14
0.5	Yes	7	1.09489e-22
1	Yes	8	6.75122e-13
1.5	Yes	7	4.14266e-23
2	Yes	9	1.69736e-20
2.5	No		

Table 6.1: Test 1, mesh 1, 2-layered circular mesh.

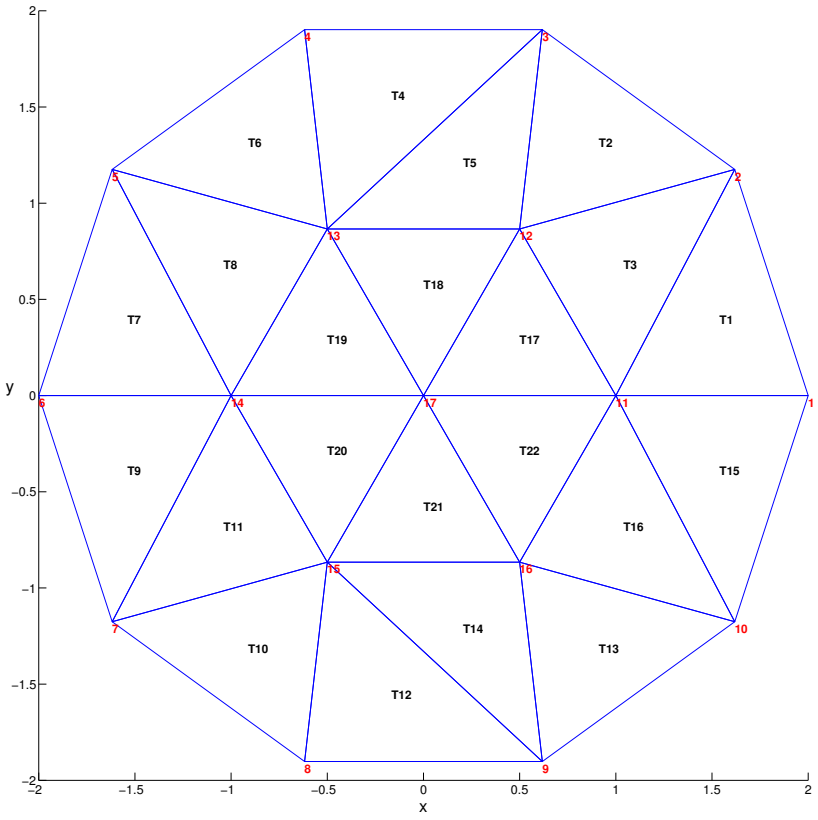

Figure 6.9: Test 1, mesh 1 (10,6,1)

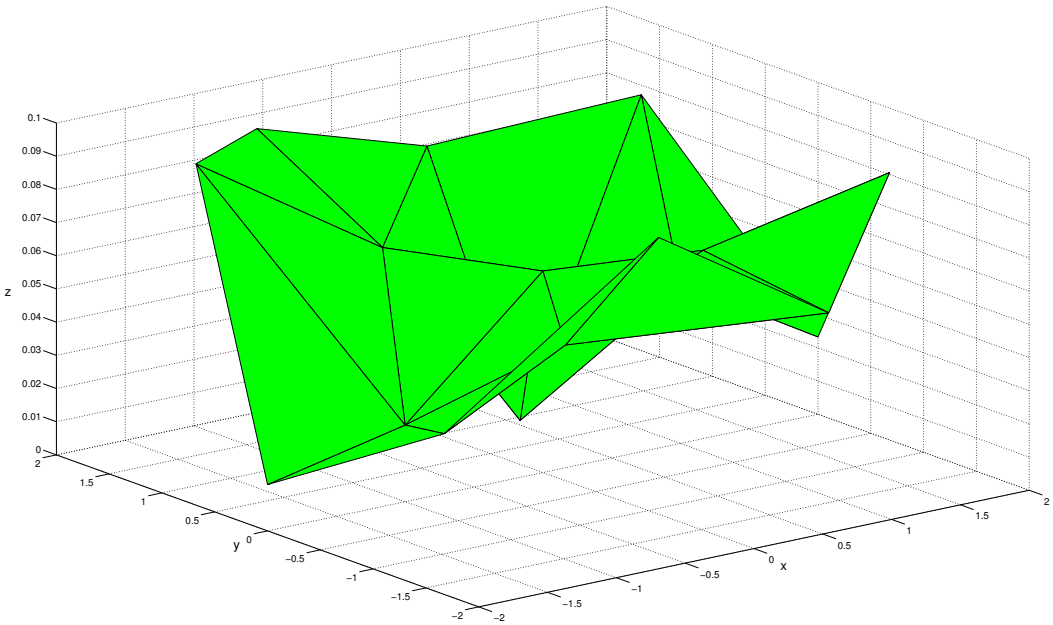

(a) z-axes perturbation, $\epsilon = 0.1$

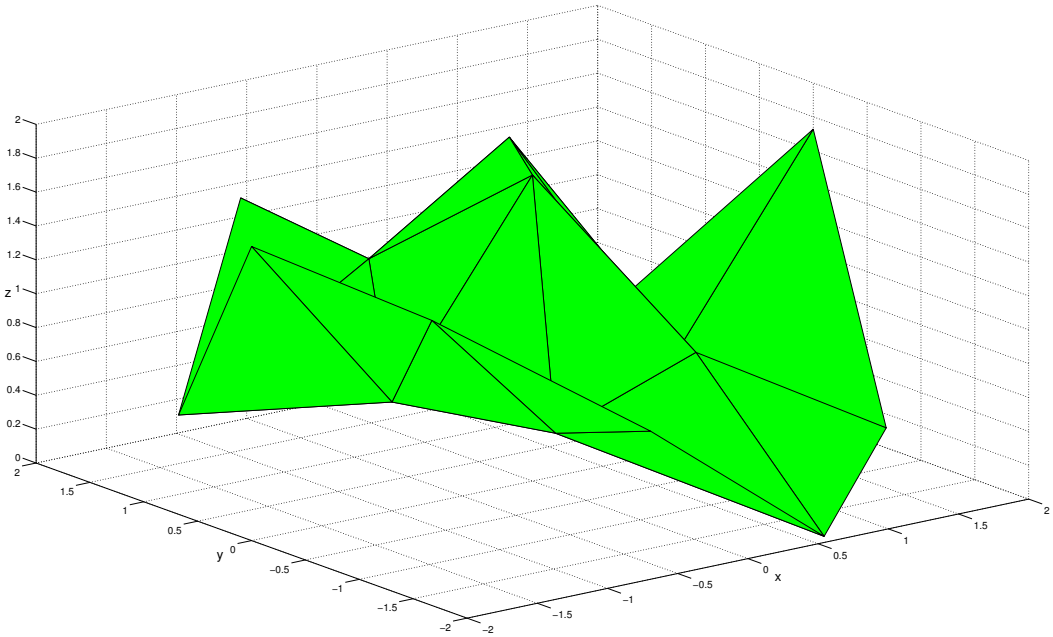

(b) z-axes perturbation, $\epsilon = 2$

Figure 6.10: The embedding for test 1, mesh 1 for two different z-axes perturbations.

ϵ	Convergence	Iterations	$f(x)$
0.1	Yes	8	5.01537e-23
0.5	Yes	8	1.1763e-23
1	Yes	8	3.16884e-24
2	Yes	9	1.4231e-23
3	Yes	13	4.05931e-17
3.5	Yes	11	4.11452e-16
4	No		

Table 6.2: Test 1, mesh 2, 3-layered circular mesh.

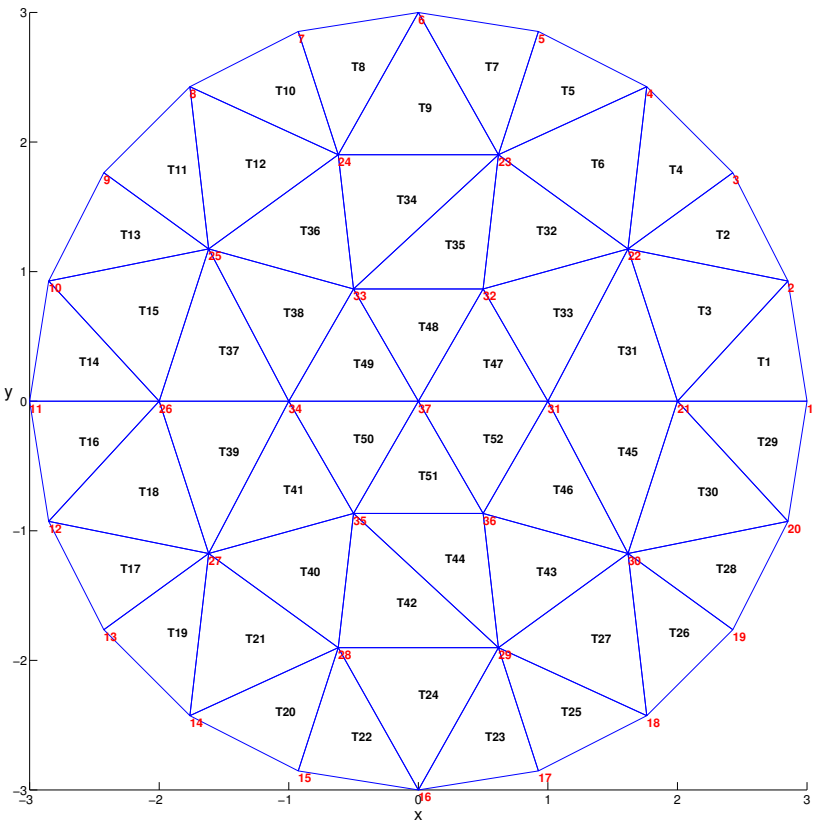

Figure 6.11: Test 1, mesh 2 (20,10,6,1)

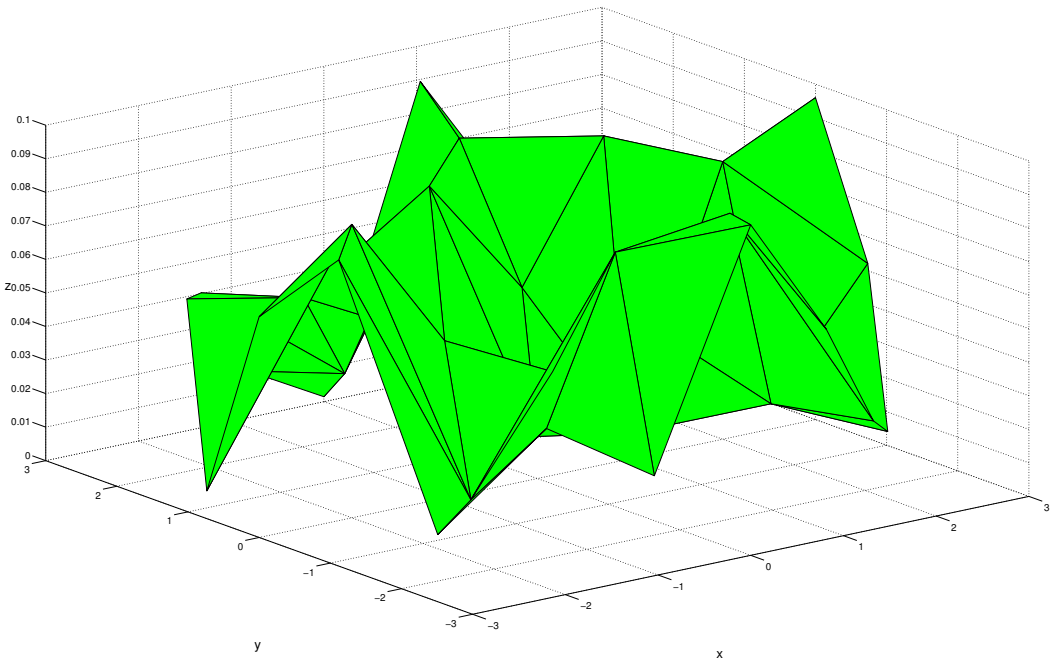

(a) z-axes perturbation, $\epsilon = 0.1$

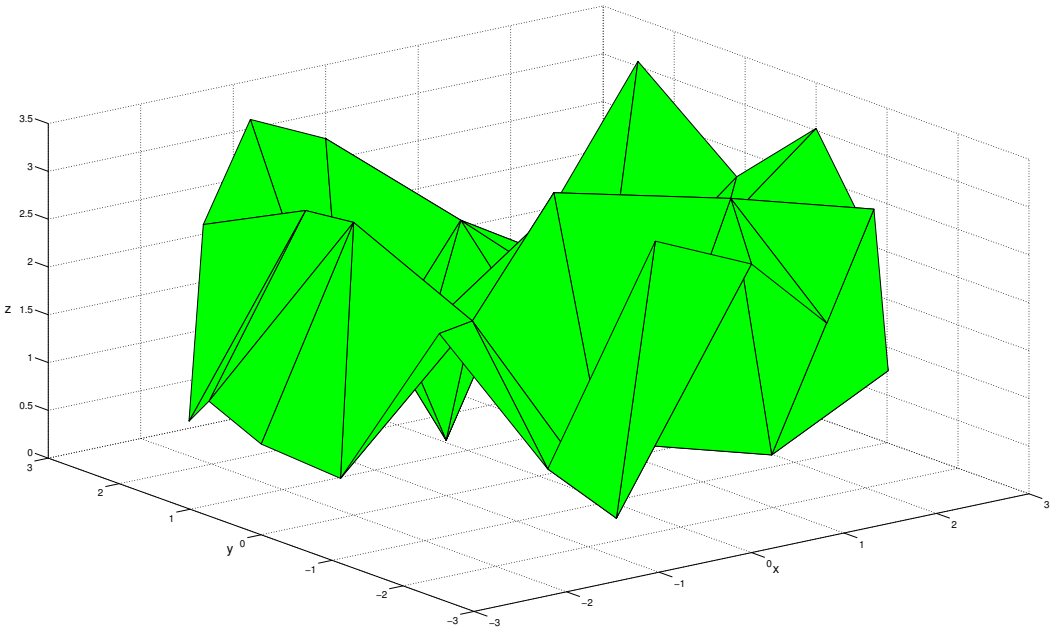

(b) z-axes perturbation, $\epsilon = 3.5$

Figure 6.12: The embedding for test 1, mesh 2 for two different z-axes perturbations.

Test 2 - Perturbation of the edge conductances

For the second test we use the same meshes as before but this time we also perturb by ϵ the edge conductances. The perturbations is done by adding a small random number. Tables 6.3-6.4 show the results for various perturbations. Figures 6.13-6.14 show the calculated embedding for selected perturbations.

ϵ	Convergence	Iterations	$f(x)$
0.001	Yes	7	2.71318e-16
0.005	Yes	7	1.82809e-13
0.01	Yes	8	1.82856e-16
0.03	Yes	8	6.77153e-20
0.04	Yes	8	3.49765e-16
0.05	No		

Table 6.3: Test 2, mesh 1, 2-layered circular mesh.

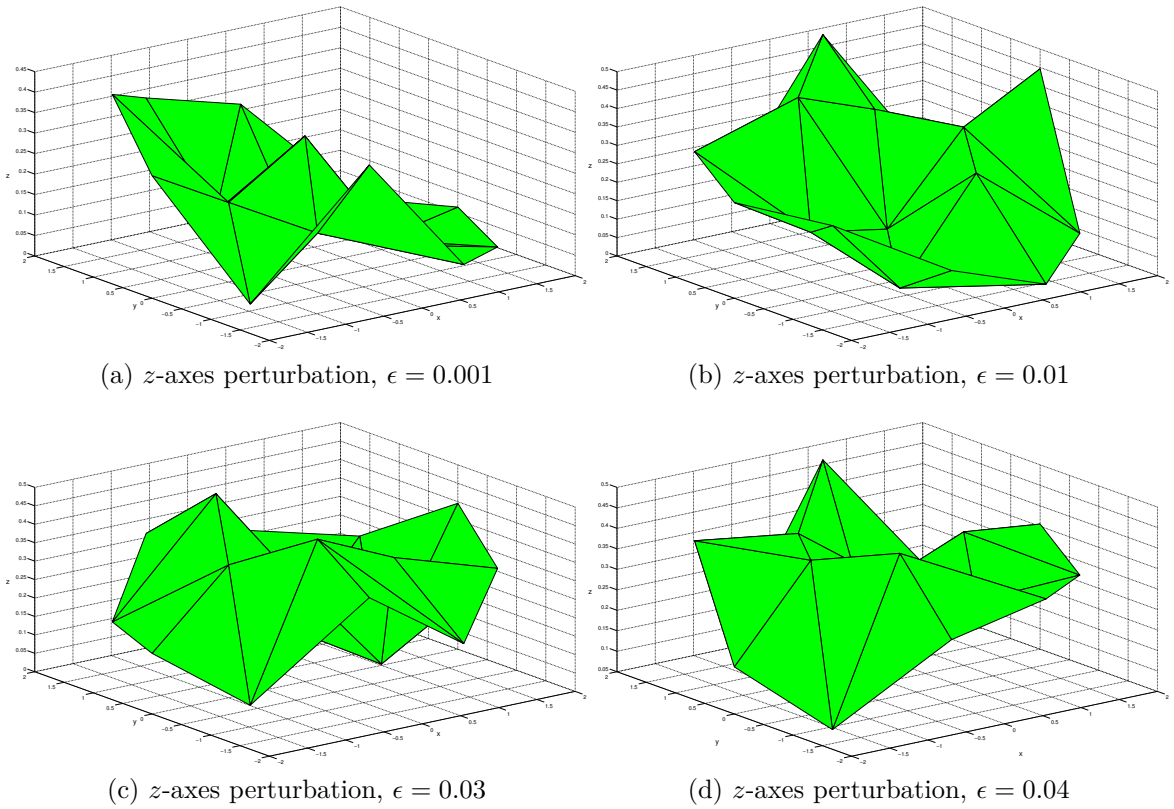

(a) z-axes perturbation, $\epsilon = 0.001$

(b) z-axes perturbation, $\epsilon = 0.01$

(c) z-axes perturbation, $\epsilon = 0.03$

(d) z-axes perturbation, $\epsilon = 0.04$

Figure 6.13: The embedding for test 2, mesh 1 for four different perturbations of the edge conductances

ϵ	Convergence	Iterations	$f(x)$
0.1	Yes	7	4.33005e-18
0.3	Yes	7	5.08211e-14
0.5	Yes	9	1.56302e-23
0.7	Yes	10	4.42493e-24
0.9	No		

Table 6.4: Test 2, mesh 2, 3-layered circular mesh.

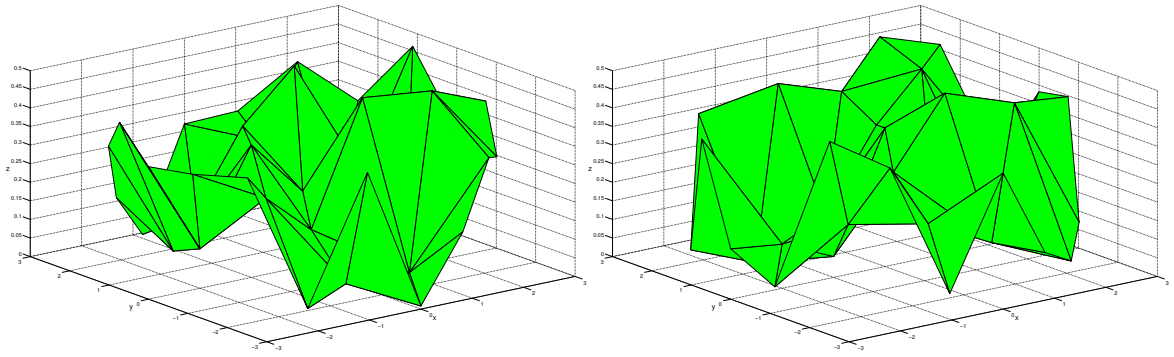

(a) z-axes perturbation, $\epsilon = 0.1$

(b) z-axes perturbation, $\epsilon = 0.3$

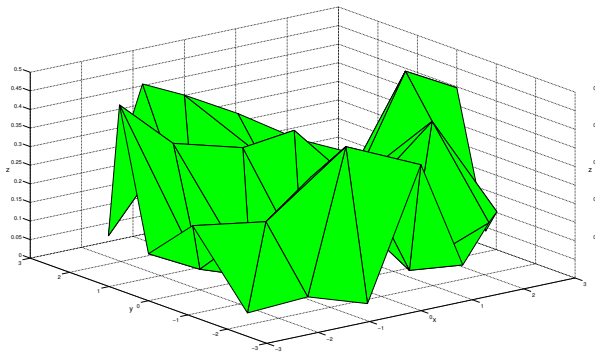

(c) z-axes perturbation, $\epsilon = 0.5$

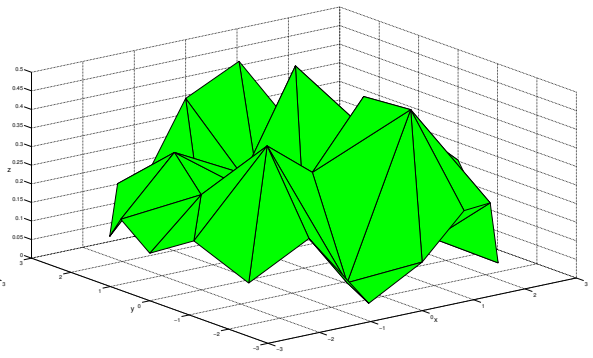

(d) z-axes perturbation, $\epsilon = 0.7$

Figure 6.14: The embedding for test 2, mesh 2 for four different perturbations of the edge conductances

Test 3 - Perturbation x, y and z directions

As a final test we retain the mesh size and we perturb in the x, y and z directions by ϵ. We perform a uniform perturbation in all directions by adding a small random number generated with MATLAB's rand command Tables 6.5-6.6 show the results for various perturbations. Figures 6.15-6.16 show the calculated embedding for selected perturbations.

ϵ	Convergence	Iterations	$f(x)$
0.2	Yes	9	2.52577e-24
0.4	Yes	8	8.39721e-22
0.6	Yes	9	1.58627e-19
0.8	Yes	12	5.37161e-24
0.9	Yes	9	5.84231e-25
1.0	Yes	9	1.81296e-14
1.1	No		

Table 6.5: Test 3, mesh 1, 2-layered circular mesh.

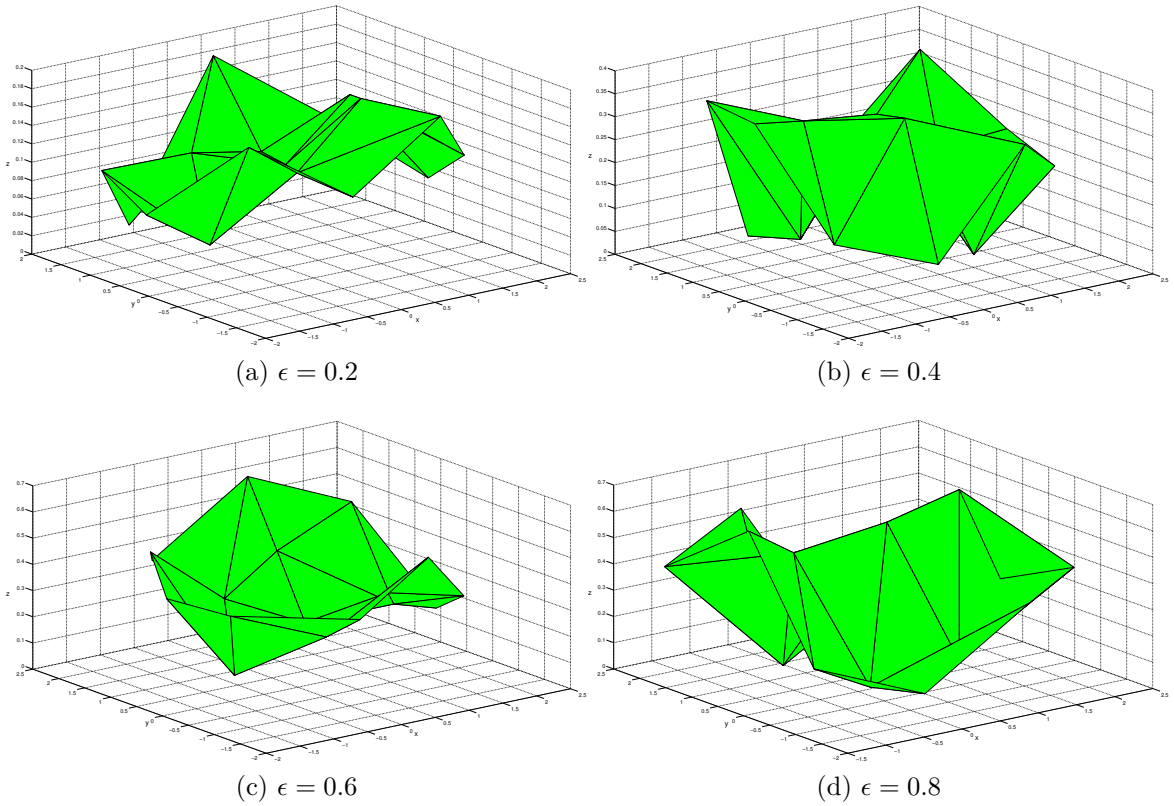

(a) $\epsilon = 0.2$ (b) $\epsilon = 0.4$

(c) $\epsilon = 0.6$ (d) $\epsilon = 0.8$

Figure 6.15: The embedding for test 3, mesh 1 for four different perturbations of the x, y and z coordinates

ϵ	Convergence	Iterations	$f(x)$
0.1	Yes	8	3.99272e-24
0.2	Yes	7	1.4783e-12
0.3	Yes	8	2.20596e-19
0.4	Yes	8	4.9427e-15
0.5	Yes	8	1.62959e-16
0.6	Yes	9	3.0554e-21
0.7	Yes	10	4.22376e-16
0.8	No		

Table 6.6: Test 3, mesh 2, 3-layered circular mesh.

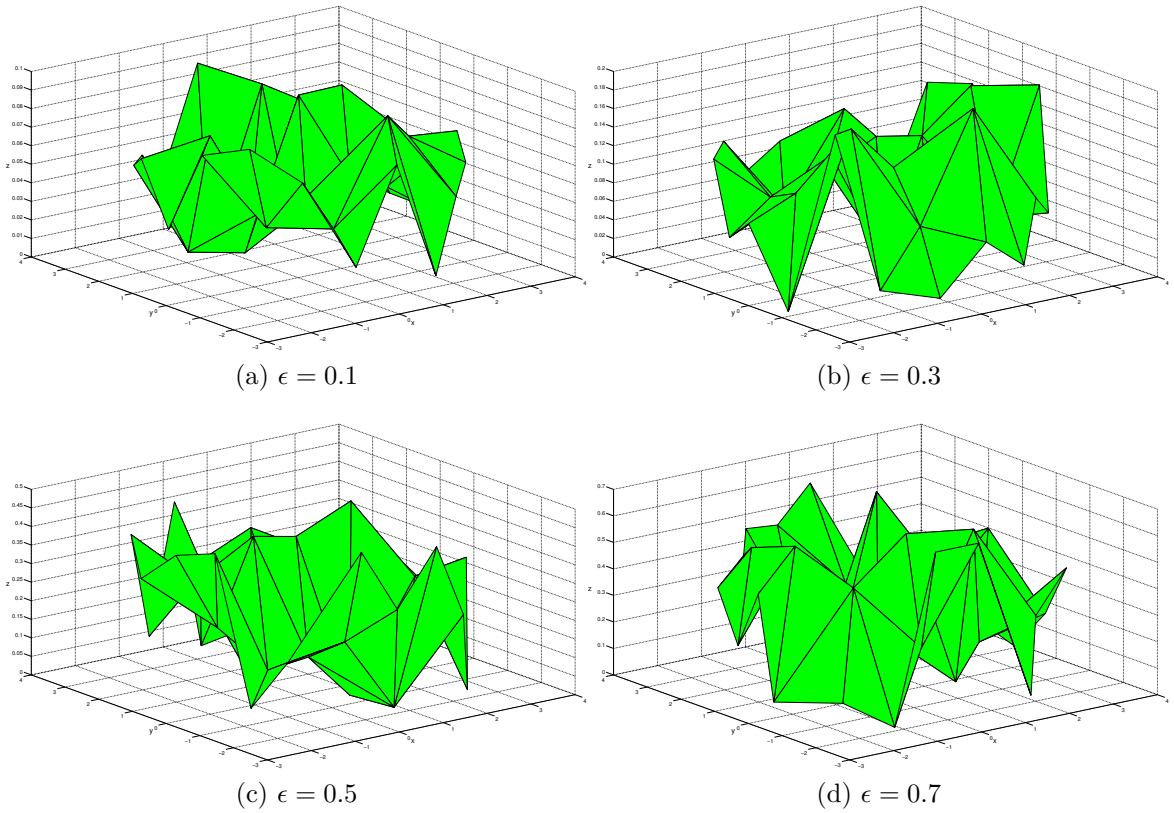

(a) $\epsilon = 0.1$ (b) $\epsilon = 0.3$

(c) $\epsilon = 0.5$ (d) $\epsilon = 0.7$

Figure 6.16: The embedding for test 3, mesh 2 for four different perturbations of the x, y and z coordinates

6.9 Using resistor networks in practical problems

In practice resistor networks might be used to solve various inverse problems. For anisotropic problems the obvious procedure is to assume that the conductivity is constraint by knowing the directions of the eigenvectors and afterwards solve the problem on a resistor network. Then the idea is to find an embedding consistent with the a priori information we have provided. More specifically, say that two eigenvalues are the same but unknown and an eigenvector is known and then you try to find an embedding consistent with these information. Note that this is a relatively common case and it can be found in sheet materials and fibre materials.

The problem of recovering the shape is also complex and there is no hope if there is no information about the anisotropy. In the case that the shape is unknown but you know that the medium is isotropic then the embedding is determined up to a small number of parameters. In this case we can reconstruct the conductivity on a resistor mesh and then find an embedding consistent with the conductivity being isotropic and then that would constrain the shape.

6.10 Conclusion

This chapter is dedicated to the problem of determining a three dimensional embedding for a planar resistor network. Our main contribution is the existence and uniqueness theorem as this is described in Section 6.5. The innovative and at the same time beautiful idea here is that we use the dual of the primary graph. This is done by using a circumcircle parameterisation of a triangular graph, hence the logarithm of the radii represent the voltage of the network. This gives rise to a non-linear system of equations to be solved. Then, Duffin's theorem (see Section 6.4) guarantees that a unique solution exists for the non-linear system.

Chapter 7

Conclusion

Δεν ελπίζω τίποτα. Δεν φοβάμαι
τίποτα. Είμαι λεύτερος.[1]

Νίκος Καζαντζάκης

7.1 Summary of this thesis

The main focus of this thesis was to find an embedding consistent with the discrete Laplacian on a triangular graph. Indeed in Chapter 5 and Chapter 6 we investigate this extensively. In addition to this we study the inverse conductivity problem with anisotropic conductivity (Chapter 3) and the problem of shape deformations in EIT (Chapter 4).

In Chapter 3 we looked at the non-uniqueness problem of EIT with anisotropic conductivity. Here we explored the problem of recovering an anisotropic conductivity from the FE system matrix. The maximum number of degrees of freedom is the number of edges in the mesh. An anisotropic conductivity is naturally represented by a symmetric matrix on each element, so this gives six times the elements degrees of freedom. It is clear then that even with full knowledge of the FE system matrix, recovering the conductivity on each element uniquely is not possible. By examining the SVD of the linearised forward problem for anisotropic EIT we verified that the problem of finding the edge conductances is as ill-conditioned as the isotropic problem.

[1] "I hope nothing. I fear nothing. I am free". Epitaph on the grave of Nikos Kazantzakis.

Chapter 4 involved the study of the important issue of shape deformations. In this chapter after we reviewed the current state of research, we explained the problem of shape deformations and how this appears in EIT. We then used the two dimensional work of Boyle et al. [25], [26] to construct a Möbius transformation vector. From this vector we can construct other independent Möbius vector fields, and obtain a basis of the conformal vector fields. According to theory, complete boundary data determine any vector field orthogonal to the space of Möbius vector fields. In our case, where we apply a Möbius vector field distortion the produced data will be consistent with an isotropic conductivity distribution, which is distorted from the true one by the Möbius vector field.

In Chapter 5 we used n-port theory to give a consistency condition on transfer resistance matrices of networks. To use Cederbaum's paramountcy condition in EIT we chose a subset of measurements so that an n-port open circuit resistance matrix is defined. This gives a consistency condition for EIT data and ensures that the open circuit resistance matrix for the chosen electrodes subset is paramount. Moreover, the case of planar networks was studied. The generalised inverse $\mathbf{A}$ of a planar network's resistance matrix satisfies $\det(-1)^k \mathbf{A}_{P,Q} > 0$, where $\mathbf{A}_{P,Q}$ is restricted in a certain way. These conditions are necessary and sufficient for a matrix to be the transfer conductance of a planar resistor network. This chapter gives rise to an important question, "which resistor networks correspond to some FEM?".

Answering the previous question was our objective in Chapter 6. We built our theory using ideas of Al Humaidi [52] and Duffin [40] to prove that a unique embedding can be calculated. Of course there are conditions to be satisfied. Namely, for a mesh with n triangles, we have

- a π constraint per triangle,
- a sine constraint per interior vertex, and
- a cot formula per edge.

For convenience we used a circumcircle representation for the triangular mesh, and more precisely the log of the radii ratio. Finally, using Duffin's result for non-linear resistor networks we were able to prove the embedding uniqueness. An algorithm to calculate the embedding (Appendix D) was also given.

7.2 Future work

Some ideas for future work and extensions are outlined below:

1. Embedding determination

   (a) The numerical implementation of our existence and uniqueness theorem is probably the next to try. We know that Duffin's Theorem guarantees a solution, even if this is not in the region of interest. Finding a solution in the region of H we have linearly extended is not unwelcome as we can still try to fit the conductivity so that we can "force" the solution in our region of interest. A second implementation could also act as a validation for the results we have so far.

   (b) Though we have some understanding when the numerics fail, we still need to investigate this further and find possible solutions. The obvious cause of these failures are the obtuse angles, either on the initial mesh due to the perturbation or when finding the solution during the optimization process. It is possible that the numerics sometimes fail for other reasons that we need to determine.

   (c) The three dimensional equivalent of the constraints is something that should be investigated. The main problem is to find a sine consistency condition for tetrahedral meshes.

2. The problem of anisotropy

   The non-uniqueness resulting from the undetermined diffeomorphism should be reintroduced in the numerical representation. One way to do this is to reconstruct edge conductances on a mesh, then use a priori information, for example about the orientation of muscle fibres, to constrain the mapping of the abstract resistor mesh, that has no geometric information, to the vertex positions and hence conductivities.

3. Shape deformations

   In addition to shape deformation, electrode movement must be studied. Fixed electrodes do not represent real tests and correct modelling might give better reconstructions with less artefacts.

7.3 Final remarks

The original programme of work for this thesis has changed significantly over the past four years. Our initial aim was to study exclusively the inverse conductivity problem for anisotropic media and answer some of the numerous open questions. This thesis spans from the study of resistor network to the problem of shape deformations in EIT. Though we do touch the problem of anisotropy our main contribution is in the area of resistor networks. We believe that there is still a lot to be done in all three topics we address but we hope that this thesis will help and motivate other researchers.

Bibliography

[1] Juan-Felipe P. J. Abascal, *The anisotropic conductivity problem*, Master's thesis, University of Manchester, Manchester, United Kingdom, 2003.

[2] Juan-Felipe P. J. Abascal, Simon R. Arridge, David Atkinson, Raya Horesh, Lorenzo Fabrizi, Marzia De Lucia, Lior Horesh, Richard H. Bayford, and David S. Holder, *Use of anisotropic modelling in electrical impedance tomography; description of method and preliminary assessment of utility in imaging brain function in the adult human head*, Neuroimage **43** (2008), no. 2, 258–268.

[3] Ralph Abraham, Jerrold E. Marsden, and Tudor S. Ratiu, *Manifolds, tensor analysis and applications*, 2nd ed., Applied mathematical sciences ; v.75, Springer-Verlag, New York ; London, c1988.

[4] Andy Adler, Marcelo B. Amato, John H. Arnold, Richard Bayford, Marc Bodenstein, Stephan H. Böhm, Brian H. Brown, Inéz Frerichs, Ola Stenqvist, Norbert Weiler, and Gerhard K. Wolf, *Whither lung EIT: Where are we, where do we want to go and what do we need to get there?*, Physiological Measurement **33** (2012), no. 5, 679.

[5] Andy Adler, John H. Arnold, Richard Bayford, Andrea Borsic, Brian Brown, Paul Dixon, Theo J. C. Faes, Inéz Frerichs, Hervé Gagnon, Yvo Gärber, Bartłomiej Grychtol, Günter Hahn, William R. B. Lionheart, Anjum Malik, Robert P. Patterson, Janet Stocks, Andrew Tizzard, Norbert Weiler, and Gerhard K. Wolf, *GREIT: a unified approach to 2D linear EIT reconstruction of lung images*, Physiological Measurement **30** (2009), no. 6, S35.

[6] Andy Adler, Robert Guardo, and Yves Berthiaume, *Impedance imaging of lung*

ventilation: do we need to account for chest expansion?, IEEE Transactions on Biomedical Engineering **43** (1996), no. 4, 414–420.

[7] Andy Adler and William R. B. Lionheart, *Uses and abuses of EIDORS: an extensible software base for EIT*, Physiological Measurement **27** (2006), no. 5, Sp. Iss. SI, S25–S42 (English), 6th Conference on Biomedical Applications of Electrical Impedance Tomography, London, England, Jun 22-24, 2005.

[8] Lars Valerian Ahlfors, *Complex analysis : an introduction to the theory of analytic functions of one complex variable*, 3rd ed., International series in pure and applied mathematics, McGraw-Hill, New York ; London, 1979, Previous ed.: 1966.

[9] Giovanni Alessandrini, *Singular solutions of elliptic equations and the determination of conductivity by boundary measurements*, Journal of Differential Equations **84** (1990), no. 2, 252–272.

[10] Louis A. Allaud and Maurice H. Martin, *Schlumberger: the history of a technique*, A wiley-interscience publication, Wiley, 1977.

[11] Kari Astala and Lassi Päivärinta, *Calderón's inverse conductivity problem in the plane*, Annals of Mathematics. Second Series **163** (2006), no. 1, 265–299.

[12] David C. Barber and Brian H. Brown, *Applied potential tomographty*, Journal of Physics e-scientific Instruments **17** (1984), no. 9, 723–733.

[13] ———, *Errors in reconstruction of resistivity images using a linear reconstruction technique*, Clinical Physics and Physiological Measurement **9** (1988), no. 4A, 101.

[14] ———, *Reconstruction of impedance images using filtered back–projection*, Proceedings of the European Community concerted action on Electrical Impedance Tomography (Copenhagen, Denmark), 1990, pp. 1–8.

[15] David C. Barber, Brian H. Brown, and Ian L. Freeston, *Imaging spatial distributions of resistivity using applied potential tomography*, Electronics Letters **19** (1983), no. 22, 933 –935.

[16] David C. Barber and Andrew D. Seagar, *Fast reconstruction of resistance images*, Clinical Physics and Physiological Measurement **8** (1987), no. 4A, 47.

[17] Claude Berge, *Graphs and hypergraphs*, North-Holland Mathematical Library, North-Holland Publishing Company, 1976.

[18] Mario Bertero and Patrizia Boccacci, *Introduction to inverse problems in imaging*, Institute of Physics Publishing, Bristol, 1998.

[19] Norman Biggs, *Algebraic potential theory on graphs*, Bulletin of the London Mathematical Society **29** (1997), no. 6, 641–682.

[20] Philippe Blanchard and Erwin Brüning, *Mathematical methods in physics*, Progress in Mathematical Physics, vol. 26, Birkhäuser Boston Inc., Boston, MA, 2003.

[21] Alexander I. Bobenko and Ivan Izmestiev, *Alexandrov's theorem, weighted delaunay triangulations, and mixed volumes*, `http://arxiv.org/abs/math/0609447v1`, 2008.

[22] Béla Bollobás, *Modern graph theory*, Graduate Texts in Mathematics, Springer, 1998.

[23] Liliana Borcea, Vladimir Druskin, and Alexander V. Mamonov, *Circular resistor networks for electrical impedance tomography with partial boundary measurements*, Inverse Problems **26** (2010), no. 4, 045010.

[24] Liliana Borcea, Vladimir Druskin, and Fernando Guevara Vasquez, *Electrical impedance tomography with resistor networks*, Inverse Problems **24** (2008), no. 3, 035013.

[25] Alistair Boyle, William R.B. Lionheart, and Andy Adler, *Artifacts due to conformal deformations in electrical impedance tomography*, Proceedings of the Electrical Impedance Tomography Conference 2009, University of Manchester, Manchester, UK, 16-19 June 2009.

[26] Alistair Boyle, William R.B. Lionheart, Camille Gomez-Laberge, and Andy Adler, *Evaluating deformation corrections in electrical impedance tomography*, Proceedings of the Electrical Impedance Tomography Conference 2008, Dartmouth College, NH, USA, 16-18 June 2008, pp. 175–178.

[27] Brian H. Brown and Andrew D. Seagar, *The Sheffield data collection system*, Clinical Physics and Physiological Measurement **8** (1987), no. 4A, 91.

[28] Alberto P. Calderón, *On an inverse boundary value problem*, Seminar on Numerical Analysis and its Applications to Continuum Physics (Rio de Janeiro, 1980), Soc. Brasil. Mat., Rio de Janeiro, 1980, pp. 65–73.

[29] Israel Cederbaum, *Applications of matrix algebra to network theory*, IRE Transactions on Circuit Theory **6** (1959), no. 5, 127 – 137.

[30] Yves Colin de Verdière, *Réseaux électriques planaires. I*, Comment. Math. Helv. **69** (1994), no. 3, 351–374.

[31] Yves Colin de Verdière, Isidoro Gitler, and Dirk Vertigan, *Réseaux électriques planaires. II*, Comment. Math. Helv. **71** (1996), no. 1, 144–167.

[32] E. Curtis, E. Mooers, and J. Morrow, *Finding the conductors in circular networks from boundary measurements*, Mathematical Modelling and Numerical Analysis **28** (1994), no. 7, 781–814.

[33] Edward. B. Curtis, David Ingerman, and James. A. Morrow, *Circular planar graphs and resistor networks*, Linear Algebra Appl. **283** (1998), no. 1-3, 115–150.

[34] Edward B. Curtis and James A. Morrow, *Determining the resistors in a network*, SIAM J. Appl. Math. **50** (1990), no. 3, 918–930.

[35] ———, *The dirichlet to neumann map for a resistor network*, SIAM J. Appl. Math. **51** (1991), no. 4, 1011–1029.

[36] ———, *Inverse problems for electrical networks.*, Series on Applied Mathematics (Singapore) 13. River Edge, NJ: World Scientific. xi, 184 p., 2000.

[37] Dennis M. DeTurck and Deane Yang, *Strains and triply orthogonal systems*, Duke Mathematical Journal **51** (1984), no. 2, 243–260.

[38] Boris A. Dubrovin, Anatoly T. Fomenko, and Sergei P. Novikov, *Modern geometry: methods and applications.*, Part 2, vol. The geometry and topology of manifolds, Springer, Berlin, 1982.

[39] Richard J. Duffin, *Nonlinear networks. IIa*, Bull. Amer. Math. Soc. **53** (1947), 963–971.

[40] ———, *Nonlinear networks. IIb*, Bull. Amer. Math. Soc. **54** (1948), 119–127.

[41] ———, *Distributed and lumped networks*, Journal of Mathematics and Mechanics **8** (1959), 793–826.

[42] Inéz Frerichs, Sven Pulletz, Gunnar Elke, Barbara Gawelczyk, Alexander Frerichs, and Norbert Weiler, *Patient examinations using electrical impedance tomography – sources of interference in the intensive care unit*, Physiological Measurement **32** (2011), no. 12, L1.

[43] Hervé Gagnon, Martin Cousineau, Andy Adler, and Alzbeta E. Hartinger, *A resistive mesh phantom for assessing the performance of EIT systems*, IEEE Transactions on Biomedical Engineering **57** (2010), no. 9, 2257 –2266.

[44] David B. Geselowitz, *An application of electrocardiographic lead theory to impedance plethysmography*, IEEE Transactions on Biomedical Engineering **18** (1971), no. 1, 38–41.

[45] Hugh Griffiths, *A phantom for electrical impedance tomography*, Clinical Physics and Physiological Measurement **9** (1988), no. 4A, 15.

[46] Bartołomiej Grychtol, William R. B. Lionheart, Marc Bodenstein, Gerhard K. Wolf, and Andy Adler, *Impact of model shape mismatch on reconstruction quality in Electrical Impedance Tomography*, IEEE Transactions on Medical Imaging **31** (2012), no. 9, 1754 –1760.

[47] Jacques Hadamard, *Sur les problèmes aux dérivés partielles et leur signification physique*, Princeton University Bulletin **13** (1902), 49–52.

[48] Frank Harary, *Graph theory*, Addison-Wesley Series in Mathematics, Addison-Wesley Publishing Company, 1969.

[49] Ross P. Henderson and John G. Webster, *An impedance camera for spatially specific measurements of the thorax*, IEEE Transactions on Biomedical Engineering **25** (1978), no. 3, 250 –254.

[50] David S. Holder and Institute of Physics., *Electrical impedance tomography : methods, history and applications*, Series in medical physics and biomedical engineering, Institute of Physics Pub., Bristol; Philadelphia, c2005., Formerly CIP.

[51] Ping Hua, Eung Je Woo, John G. Webster, and Willis J. Tompkins, *Using compound electrodes in electrical impedance tomography*, IEEE Transactions on Biomedical Engineering **40** (1993), no. 1, 29 –34.

[52] Abdulaziz Al Humaidi, *Resistor networks and finite elelment models*, PhD, University of Manchester, 2011.

[53] IMT, *Impedance medical technologies*, `http://medimpedance.com/products.html`, Accessed: 15/08/2012.

[54] David Ingerman and James A. Morrow, *On a characterization of the kernel of the Dirichlet-to-Neumann map for a planar region*, SIAM Journal on Mathematical Analysis **29** (1998), no. 1, 106–115.

[55] Maltron International, *The Maltron Sheffield Mk 3.5*, `http://www.maltronint.com/eit/msmk35.php`, Accessed: 15/08/2012.

[56] Victor Isakov, *Uniqueness and stability in multi-dimensional inverse problems*, Inverse Problems **9** (1993), no. 6, 579–621.

[57] ———, *Inverse problems for partial differential equations*, 2nd ed., Applied Mathematical Sciences, 127 0066-5452, Springer, New York, c2006.

[58] J. Just, M. Dittmar, G. Quintel, and Hahn, *Constructing resistive mesh phantoms by an equivalent 2D resistance distribution of a 3D cylindrical object*, Proceedings of the Electrical Impedance Tomography Conference 2011, University of Bath, Bath, UK, 4-6 May 2011.

[59] Nakayama K., Yagi W., and Yagi S., *Fundamental study on electrical impedance CT algorithm utilizing sensitivity theorem on impedance plethysmography*, Proceedings of the 5th International Conference on Electrical Bioimpedance (ICEBI), Tokyo, Japan, 24-26 August 1981, pp. 99–102.

[60] Joseph B. Keller, *Inverse problems*, Amer. Math. Monthly **83** (1976), no. 2, 107–118.

[61] Liliya Kharevych, Boris Springborn, and Peter Schröder, *Discrete conformal mappings via circle patterns*, ACM Trans. Graph. **25** (2006), no. 2, 412–438.

[62] Robert Kohn and Michael Vogelius, *Identification of an unknown conductivity by means of measurements at the boundary*, Inverse problems (New York, 1983), SIAM-AMS Proc., vol. 14, Amer. Math. Soc., Providence, RI, 1984, pp. 113–123.

[63] ———, *Determining conductivity by boundary measurements. II. Interior results*, Comm. Pure Appl. Math. **38** (1985), no. 5, 643–667.

[64] R. E. Langer, *An inverse problem in differential equations*, Bull. Amer. Math. Soc. **39** (1933), no. 10, 814–820.

[65] Matti Lassas, Michael Taylor, and Gunther Uhlmann, *The Dirichlet-to-Neumann map for complete Riemannian manifolds with boundary*, Comm. Anal. Geom. **11** (2003), no. 2, 207–221.

[66] Matti Lassas and Gunther Uhlmann, *On determining a Riemannian manifold from the Dirichlet-to-Neumann map*, Annales Scientifiques de l' École Normale Supérieure **34** (2001), no. 5, 771 – 787.

[67] John M. Lee and Gunther Uhlmann, *Determining anisotropic real-analytic conductivities by boundary measurements*, Comm. Pure Appl. Math. **42** (1989), no. 8, 1097–1112.

[68] Jung Rye Lee, *The law of cosines in a tetrahedron*, J. Korea Soc. Math. Educ. Ser. B Pure Appl. Math. **4** (1997), no. 1, 1–6.

[69] Willian R. B. Lionhear, Kyriakos Paridis, and Andy Adler, *Resistor networks and transfer resistance matrices*, Proceedings of the Electrical Impedance Tomography Conference 2012, Tianjin University, Tianjin, China, 23-25 May 2012.

[70] William R. B. Lionheart, *Boundary shape and electrical impedance tomography*, Inverse Problems **14** (1998), no. 1, 139–147.

[71] William R. B. Lionheart, *Uniqueness, shape, and dimension in EIT*, Electrical Bioimpedance Methods: Applications to Medicine and Biotechology (Riu, PJ and Rosell, J and Bragos, R and Casas, O, ed.), Annals of the New York Academy of Sciences, vol. 873, Int Comm Promot Res Bio Impedance, New York Acad Sciences, 1999, 10th International Conference on Electrical Bio-Impedance, Barcelona, Spain, APR 05-09, 1998, pp. 466–471 (English).

[72] William R. B. Lionheart and Kyriakos Paridis, *Finite elements and anisotropic EIT reconstruction*, Journal of Physics: Conference Series **224** (2010), no. 1, 012022.

[73] Meng H. Loke, *RES2DINV - 2D resistivity & IP inversion software*, GEOTOMO Software, Available from http://www.geoelectrical.com/gs_brochure2d.pdf.

[74] ———, *RES3DINV - 3D resistivity & IP inversion software*, GEOTOMO Software, Available from http://www.geoelectrical.com/gs_brochure3d.pdf.

[75] M.H. Loke and R.D. Barker, *Practical techniques for 3D resistivity surveys and data inversion*, Geophysical Prospecting **44** (1996), no. 3, 499–523.

[76] ———, *Rapid least-squares inversion of apparent resistivity pseudosections by a quasi-newton method*, Geophysical Prospecting **44** (1996), no. 1, 131–152.

[77] Li-Qin Lu and Brian H. Brown, *The electrode and electronic interface in an EIT spectroscopy system*, Innovation and Technology in Biology and Medicine **15** (1994), 97–103.

[78] Dräger Medical, *Technical Data for PulmoVista 500*, `http://www.draeger.com/media/10/08/96/10089606/rsp_pulmovista_500_pi_9066475_en.pdf`, Accessed: 15/08/2012.

[79] Tadakuni Murai and Yukio Kagawa, *Electrical impedance computed tomography based on a finite element model*, IEEE Transactions on Biomedical Engineering **32** (1985), no. 3, 177 –184.

[80] Adrian Nachman, John Sylvester, and Gunther Uhlmann, *An n–dimensional Borg-Levinson theorem*, Communications in Mathematical Physics **115** (1988), 595–605, 10.1007/BF01224129.

[81] Adrian I. Nachman, *Reconstructions from boundary measurements*, The Annals of Mathematics **128** (1988), no. 3, pp. 531–576 (English).

[82] ———, *Global uniqueness for a two-dimensional inverse boundary value problem*, Annals of Mathematics. Second Series **143** (1996), no. 1, 71–96.

[83] Mark E. Nelson, *Electric fish*, `http://nelson.beckman.illinois.edu/electric_fish.html`, Accessed: 08/08/2012.

[84] Kyriakos Paridis and William R. B. Lionheart, *Shape corrections for 3D EIT*, Journal of Physics: Conference Series **224** (2010), no. 1, 012049.

[85] Michael K. Pidcock, Kevin S. Paulson, and William R. Breckon, *A hybrid phantom for electrical impedance tomography*, Clinical Physics and Physiological Measurement **13** (1992), no. A, 155.

[86] Nicholas Polydorides, *Image reconstruction algorithms for soft-field tomography*, PhD, University of Manchester Institute of Science and Techology (UMIST), 2002.

[87] Nicholas Polydorides and William R. B. Lionheart, *A MATLAB toolkit for three-dimensional electrical impedance tomography: a contribution to the electrical impedance and diffuse optical reconstruction software project*, Measurement Science and Technology **13** (2002), no. 12, 1871–1883.

[88] Otmar Scherzer (ed.), *Handbook of mathematical methods in imaging. In 3 volumes.*, Springer Reference. Berlin: Springer. xviii, 1607 p., 2011.

[89] Joachim Schöberl, *Netgen an advancing front 2D/3D-mesh generator based on abstract rules*, Computing and Visualization in Science **1** (1997), no. 1, 41 –52.

[90] Manuchehr Soleimani, Camille Gomez-Laberge, and Andy Adler, *Imaging of conductivity changes and electrode movement in EIT*, Physiol. Meas. **27** (2006), no. 5, S103–S113.

[91] Erkki Somersalo, Margaret Cheney, and David Isaacson, *Existence and uniqueness for electrode models for electric current computed tomography*, SIAM Journal on Applied Mathematics **52** (1992), no. 4, 1023–1040.

[92] John Sylvester, *An anisotropic inverse boundary value problem*, Comm. Pure Appl. Math. **43** (1990), no. 2, 201–232.

[93] John Sylvester and Gunther Uhlmann, *A global uniqueness theorem for an inverse boundary value problem*, Ann. of Math. (2) **125** (1987), no. 1, 153–169.

[94] Eckhard Teschner and Michael Imhoff, *Electrical impedance tomography: The realization of regional ventilation monitoring*, Tech. report, Dräger Medical GmbH, Lübeck, Germany.

[95] Gunther Uhlmann, *Developments in inverse problems since Calderón's foundational paper*, Harmonic analysis and partial differential equations (Chicago, IL, 1996), Chicago Lectures in Math., Univ. Chicago Press, Chicago, IL, 1999, pp. 295–345.

[96] Fernando Guevara Vasquez, *On the parametrization of ill-posed inverse problems arising from elliptic partial differential equations*, PhD, Rice University, Houston, USA, 2006.

[97] Thomas J. Yorkey, *Comparing reconstruction algorithms for electrical impedance tomography*, PhD, University of Wisconsin, 1986.

[98] Thomas J. Yorkey, John G. Webster, and Willis J. Tompkins, *Comparing reconstruction algorithms for electrical impedance tomography*, IEEE Transactions on Biomedical Engineering **34** (1987), no. 11, 843 –852.

Appendix A

Derivation of cot formula

The derivation of (3.3.10) is fairly elementary apart from one step. Consider one tetrahedron T with vertices $x_1, ..., x_4$. The unit normal to plane of vertices $2, 3, 4$ is

$$\mathbf{N}_1 = \frac{(x_2 - x_3) \times (x_2 - x_4)}{|(x_2 - x_3) \times (x_2 - x_4)|} \tag{A.0.1}$$

Hence the nodal basis function on this tetrahedron is

$$\phi_1(x) = \frac{(x - x_2) \cdot (x_2 - x_3) \times (x_2 - x_4)}{(x_1 - x_2) \cdot (x_2 - x_3) \times (x_2 - x_4))} \tag{A.0.2}$$

and

$$\nabla\phi_1 \cdot \nabla\phi_2 |T| = \mathbf{N}_1 \cdot \mathbf{N}_2 \frac{4\text{Area}(234)\text{Area}(134)}{|T|} \tag{A.0.3}$$

Clearly $\mathbf{N}_1 \cdot \mathbf{N}_2 = \cos\theta_{12}$ where θ_{12} is the dihedral angle at the edge 34 and from [68] we see that

$$|T| = \frac{2}{3L_{12}} \text{Area}(234)\text{Area}(134) \sin\theta_{12}$$

where L_{12} is the length of the *opposite* edge 34. The result follows.

Appendix B

Anisotropic Jacobian code

The code is a modification of code derived by Abascal [2] from Polydorides' EIDORS-3D [87] and it calculates the singular values of the Jacobian. The geometric objects' meshes are generated with Netgen [89].

```
function [J,dof_E] = anisotropic(filename)
% Read the mesh generated with NETGEN
% Input
% Filename = The file containing the information exported from NETGEN
% Output
% J     = The Jacobian matrix
% dof_E = The degrees of freedom of the system matrix
%

%-------------------------------------------------------------------------
% val   = Vector containing the six local conductivity values
%         on the form
%         (val_xx,val_yy,val_zz,val_xy,val_xz,val_yz)
%-------------------------------------------------------------------------
%Read the mesh
[srf, simp, vtx] = meshReader(filename);
% vtx=rand(size(vtx,1),3)*1e-5+vtx;
% Clear figures
%clf;

```

```
% Local conductivity matrix
val=[1 1.2 1.3 0.1 0.2 0.3];
% Global conductivity matrix
[mat_ani]=set_hom_mat(simp,val);

% Draw the domain
% trimesh(srf,vtx(:,1),vtx(:,2),vtx(:,3));
% colormap([0 0 0]);
% daspect([1 1 1]);
% hidden off;

% Draw each simplex in a different colour
%%%%%%%%%%%%%%%%%%%%%%%%%%%%%%%%%%%%%%%%%%%%%%
%  colorarray=rand(size(simp,1),3);
% colordef white;
% for i=1:size(srf,1)
%     j=1;
%     while(¬all(ismember(srf(i,:),simp(j,:))))
%         j=j+1;
%     end
% % Exlclude one tetrahedron
% %     if j>size(simp,1)-1
% %         continue;
% %     end
%      switch (mod(j,3))
%         case 0
%             color=[0 0 0];
%         case 1
%             color=[0.5 0.5 0.5];
%         case 2
%             color=[1 1 0];
%      end
%     color=colorarray(j,:);
%     trimesh(srf(i,:),vtx(:,1),vtx(:,2),vtx(:,3),'FaceColor',color);
%     hold on;
% end
```

```
% colormap([0 0 0; 1 0 0; 1 1 0; 0 1 0; 0 0 1]);
% daspect([1 1 1]);
% hidden off;

v_ind_ext = unique(srf);
n_v = size(vtx,1);
n_ve = length(v_ind_ext);
n_s = size(simp,1);

% Define constants
% elec : vtxs where current is injected
elec = 1:n_ve;
n_el = length(elec);
max(vtx);
min(vtx);

% Set current pattern
[I] = set_all_currents_perp_ones(n_el,n_v,elec);

% System matrix
[E,D,Ela] = bld_master_a_basisfunc(vtx,simp,mat_ani);

volsDiag = full(diag(Ela));
vols = volsDiag(1:3:end);

[E,I,E_un] = UniquenessFP(vols,simp,E,I,n_v);

%Er is also possitive definite, check its eigenvalues/singular values
%svds(E)
cond(full(E));

%and calculte the reference forward solution Vref
Vref = E\I;

%The animate the forward solution
 % potplot(vtx,srf,Vref);
```

```
93
94  % Voltage on boundary vertices
95  [v_meas_ref,df] = get_bnd_meas_all_perp_ones(I,elec,Vref,n_el);
96  sum(df);
97
98  % Jacobian
99  v_f = kron(ones(1,length(df)),Vref);
100
101 el_no = n_ve;
102
103 % General tensor:
104 tic
105 [J] = jac_3d_a_2_nonelec_perp_ones(I,elec,vtx,simp,v_f,Vref,df,Ela,D)
106 toc
107 tic
108 Jn=J'*J;
109 toc
110 tic
111 Sn=eig(Jn);
112 S=real(sqrt(Sn));
113 toc
114 % tic,[U,S,V] = svd(J,0);toc
115 %tic,S2= svd(J);toc
116
117 % sv_J = diag(S);
118 % figure; semilogy(sv_J);
119 figure; semilogy(S);
120 % semilogy(S2,'x'), hold on, ...
       semilogy(real(sqrt(Sn(end:-1:1))),'or'), hold off
121 xlabel('vtx #','FontSize',[34]); ylabel('sv','FontSize',[34]);
122 set(gca,'FontSize',30); %Set axis font size
123 % Dof for Ef without ground reference
124 dof_E = (length(nonzeros(E(1:end-1,:)))...
125     -length(nonzeros(diag(E(1:end-1,:))))/2;
126
127 %matrix=kron(eye(size(D,1)),D)*kron(D',eye(size(D,1)))*mat_ani(:);
```

Appendix C

Shape deformations code

```
% function [inhomg_img, demo_img] = netgen_model_play(type)
% [inhomg_img, demo_img] = demo_real;
% DEMO to show usage of EIDORS3D
%
% (C) 2005 Nick Polydorides + Andy Adler. License: GPL version 2 ...
    or version 3
% $Id: demo_real.m,v 1.59 2008/03/19 16:37:25 aadler Exp $
%
% Modified version of demo_real from EIDORS.
% [inhomg_img, demo_img] = mdl_perturb(type);
% Input: type   You can specify the type of perturbation ...
    (conformal, non_conformal)
% Usage: [inhomg_img, demo_img] = mdl_perturb('conformal')
% Kyriakos Paridis 04/03/20010
% Further development 17/05/2012
% Everything seems to work 24/05/2012

%============================================================
% Define the variables.
type='conformal';
inclusion='ball';
cyl=[3,1,[]]; %[height,radius,max_size}
no_elec=16; % per plane
```

```
22 no_pl=2; % Remember to change rings_vert_pos
23 rings_vert_pos=[2.5 0.5];
24 elec_type='rectangular';
25 % choose electrode shape
26     switch elec_type
27          case 'rectangular'
28              elec_shape=[0.2,1,[]]; %[width,height,refinement]
29         case 'circular'
30              elec_shape=[0.2,0,0.2];
31         case 'point'
32              elec_shape=[0,0,0.2];
33         otherwise
34          error('don''t understand electrode type')
35     end
36 protocol='{ad}'; % choose '{ad}' or '{op}'
37 %=============================================================
38 isOctave= exist('OCTAVE_VERSION');
39 eidors_msg('log_level',2); % most messages
40
41 close all
42 disp('step 1: create FEM model structure');
43 % create an inlcusion
44     switch inclusion
45          case 'ball'      % test 1
46              extra={'ball','solid ball = sphere(0.2,0.5,2;0.4);'};
47         case 'cube'       % test 2
48              extra={'cube','solid cube = ...
                    orthobrick(0.5,0.5,0.5;0,0,1.5);'};
49         case 'torus'      % test 3
50              extra={'torus1','solid torus1 = ...
                    torus(0,0,1.2;0,1,0;0.4;0.1);'};
51         otherwise
52          error('don''t understand inclusion options')
53     end
54
55 % create a 'fwd_model' object with name fmdl
```

```
56 [fmdl,mat_idx]= ...
       ng_mk_cyl_models(cyl,[no_elec,rings_vert_pos],elec_shape,extra);
57 img= eidors_obj('image','ball'); img.fwd_model= fmdl;
58 img.elem_data(mat_idx{1}) = 1; img.elem_data(mat_idx{2}) = 1;
59
60 fmdl.name = 'fmdl model';
61 fmdl.nodes= fmdl.nodes;
62 fmdl.elems= fmdl.elems;
63 fmdl.boundary= fmdl.boundary;
64 fmdl.solve=      'np_fwd_solve';
65 fmdl.jacobian=   'np_calc_jacobian';
66 fmdl.system_mat= 'np_calc_system_mat';
67
68 disp('step 2: create FEM model electrodes definitions');
69
70 fmdl.gnd_node=fmdl.gnd_node;
71 fmdl.electrode = fmdl.electrode;
72 fmdl.np_fwd_solve.perm_sym = fmdl.np_fwd_solve.perm_sym;
73
74 disp('step 3: create FEM model stimulation and measurement patterns');
75
76 [stimulations, meas_sel]= mk_stim_patterns(no_elec, no_pl, '{ad}', ...
       '{ad}',{'no_meas_current'}, 1);
77 fmdl.stimulation= stimulations;
78
79 fmdl= eidors_obj('fwd_model', fmdl); %create object
80
81 %============================================================
82 %============================================================
83 disp('step 4: Create purturbed model');
84 fmdl.nodes_new = zeros(size(fmdl.nodes,1),size(fmdl.nodes,2));
85     switch type
86       case 'non_conformal'
87 % non-conformal perturbation
88         const=1e-1; % For non-conformal const=1e-1
```

```
89          fmdl.nodes_new(:,1) = fmdl.nodes(:,1) + ...
                const*(fmdl.nodes(:,1).*((fmdl.nodes(:,3)+3))/3);
90          fmdl.nodes_new(:,2) = fmdl.nodes(:,2) + ...
                const*(fmdl.nodes(:,2).*(-fmdl.nodes(:,3)+6)/3);
91          fmdl.nodes_new(:,3) = fmdl.nodes(:,3);
92
93        case 'conformal'
94  % Conformal perturbation
95          const=1e-4; % For conformal const=1e-4
96          fmdl.nodes_new(:,1) = fmdl.nodes(:,1) + ...
                const*((-fmdl.nodes(:,1).^2 + fmdl.nodes(:,2).^2 + ...
                fmdl.nodes(:,3).^2 - 1)/2);
97          fmdl.nodes_new(:,2) = fmdl.nodes(:,2) + ...
                const*(-fmdl.nodes(:,1).*fmdl.nodes(:,2));
98          fmdl.nodes_new(:,3) = fmdl.nodes(:,3) + ...
                const*(-fmdl.nodes(:,1).*fmdl.nodes(:,3));
99
100         otherwise
101          error('don''t understand type options')
102     end
103
104 fmdl_perturbed.name = 'demo model';
105 fmdl_perturbed.nodes= fmdl.nodes_new;
106 fmdl_perturbed.elems= fmdl.elems;
107 fmdl_perturbed.boundary= fmdl.boundary;
108 fmdl_perturbed.solve=      'np_fwd_solve';
109 fmdl_perturbed.jacobian=   'np_calc_jacobian';
110 fmdl_perturbed.system_mat= 'np_calc_system_mat';
111
112 disp('step 4.1: create FEM purturbed model electrodes definitions');
113
114 fmdl_perturbed.gnd_node = fmdl.gnd_node;
115 fmdl_perturbed.electrode = fmdl.electrode;
116 fmdl_perturbed.np_fwd_solve.perm_sym = fmdl.np_fwd_solve.perm_sym;
117
```

```
118 disp('step 4.2: create FEM purturbed model stimulation and ...
        measurement patterns');
119
120 [stimulations]= mk_stim_patterns(no_elec, no_pl, protocol, ...
        protocol,{}, 1); %'no_meas_current'
121 fmdl_perturbed.stimulation= stimulations;
122 fmdl_perturbed= eidors_obj('fwd_model', fmdl_perturbed); %create ...
        object
123 %=============================================================
124 %=============================================================
125
126 % create a homogeneous image
127 mat= ones( size(fmdl.elems,1) ,1);
128
129 homg_img= eidors_obj('image', 'homogeneous image', ...
130                      'elem_data', mat, ...
131                      'fwd_model', fmdl );
132
133 homg_data=fwd_solve( fmdl, homg_img);
134 disp('step 5: simulate data for inhomogeneous medium');
135
136 % create an inhomogeneous image
137 % A are Indices of the elements to represent the inhomogeneity
138 A=mat_idx{2};
139 mat(A)= mat(A)+0.15;
140 inhomg_img= eidors_obj('image', 'inhomogeneous image', ...
141                        'elem_data', mat, ...
142                        'fwd_model', fmdl_perturbed );
143
144 figure;show_fem( inhomg_img );
145 view(-14,13); axis tight; axis equal;
146 % print_convert('inhomg_img.png');
147
148 inhomg_data=fwd_solve( fmdl_perturbed, inhomg_img); % ANOTHER CHANGE
149
150 disp('step 6: add noise to simulated data');
```

```
151
152 inhomg_data.meas = inhomg_data.meas + ...
       1e-5*randn(size(inhomg_data.meas));
153   homg_data.meas =   homg_data.meas + 1e-5*randn(size(  ...
         homg_data.meas));
154
155 % xax= 1:length(homg_data.meas);
156 % hh= plotyy(xax,[homg_data.meas, inhomg_data.meas], ...
157 %             xax, homg_data.meas- inhomg_data.meas );
158 % set(hh,'Xlim',[1,max(xax)]);
159
160 disp('step 7: create inverse model');
161
162 % create an inv_model structure of name 'fmdl_inv'
163 fmdl_inv.name= 'Nick Polydorides EIT inverse';
164 fmdl_inv.solve=       'np_inv_solve';
165 fmdl_inv.hyperparameter.value = 1e-3;
166 fmdl_inv.R_prior= 'np_calc_image_prior';
167 fmdl_inv.np_calc_image_prior.parameters= [3 1]; % see ...
       iso_f_smooth: deg=1, w=1
168 fmdl_inv.jacobian_bkgnd.value= 1;
169 fmdl_inv.reconst_type= 'difference';
170 fmdl_inv.fwd_model= fmdl;
171 fmdl_inv= eidors_obj('inv_model', fmdl_inv);
172
173 disp('step 8: solve inverse model');
174
175 demo_img= inv_solve( fmdl_inv, homg_data, inhomg_data);
176
177 disp('step 9: display results');
178
179 levels=[1 2];
180
181  figure;  show_slices( inhomg_img, levels' * [inf,inf,1] );
182  axis tight; axis equal;
183  print_convert('inhomg_img_levels.png');
```

```
184  figure; show_3d_slices(inhomg_img, [1,2], [0.5],[0.5]);
185  view(-14,13); axis tight; axis equal;axis off;
186  print_convert('inhomg_img_3d.png');
187
188 demo_img.name= 'Reconstructed conductivity distribution';
189  figure; show_slices( demo_img, levels' * [inf,inf,1] );
190  axis tight; axis equal;
191  print_convert('rec_img_levels.png');
192  show_fem(demo_img);
193  print_convert('rec_img.png');
194  show_3d_slices(demo_img, [1,2], [0.5],[0.5]);
195  view(-14,13); axis tight; axis equal;
196  print_convert('rec_img_3d.png');
197
198 %elec : The electrodes matrix.
199 %np_pl : Number of electrode planes (in planar arrangements)
200 %protocol : Adjacent or Opposite or Customized.
201 %zc : Contact impedances of the electrodes
202 %perm_sym : Boolean entry for efficient forward computations
203 %perm_sym='{n}';
204 zc=[fmdl.electrode.z_contact]';
205 e=[fmdl.electrode.nodes];
206 elec=reshape(e,length(fmdl.electrode(1,1).nodes),...
207         length(fmdl.electrode))';
208 for i=1:length(zc)
209     electrodes(i).z_contact= zc(i);
210     electrodes(i).nodes=     unique(elec(i,:) );
211 end
212  perm_sym='{n}';
213
214 % % get the current stimulation patterns
215 [I,Ib] = set_3d_currents(protocol, ...
216                          elec, ...
217                          fmdl.nodes, ...
218                          fmdl.gnd_node, ...
219                          no_pl);
```

```
220
221 % get the measurement patterns, only indH is used in this model
222 %   here we only want to get the meas pattern from 'get_3d_meas',
223 %   not the voltages, so we enter zeros
224 [jnk,jnk,indH,indV,jnk] = get_3d_meas( ...
225                   elec, fmdl.nodes, ...
226                   zeros(size(I)), ... % Vfwd
227                   Ib, no_pl );
228 n_elec= size(elec,1);
229 n_meas= size(indH,1) / size(Ib,2);
230 for i=1:size(Ib,2)
231     stimulations(i).stimulation= 'mA';
232     stimulations(i).stim_pattern= Ib(:,i);
233     idx= ( 1+ (i-1)*n_meas ):( i*n_meas );
234     meas_pat = sparse( (1:n_meas)'*[1,1], ...
235                        indH( idx, : ), ...
236                        ones(n_meas,2)*[1,0;0,-1], ...
237                        n_meas, n_elec );
238     stimulations(i).meas_pattern= meas_pat;
239 end
240
241 %%%%%%%%%%%%%%%%%%%%%%%%%%%%%%%%%%%%%%%%%%%%
242 % This is part of the EIDORS suite.
243 % Copyright (c) N. Polydorides 2003
244 % Copying permitted under terms of GNU GPL
245 % See enclosed file gpl.html for details.
246 % EIDORS 3D version 2.0
247 % MATLAB version 6.1 R12
248 %%%%%%%%%%%%%%%%%%%%%%%%%%%%%%%%%%%%%%%%%%%%
```

Appendix D

Embedding code

D.1 Embedding main code

```
% Test code for embedding
% Kyriakos Paridis
%%%%%%%%%%%%%%%%%%%%%%%%%%%%%%%%%%%%%%%%%%%%%%%%%%%%%%%%
% g is the x and y coordinates of vertices
% H is the topology

% Global variables passed to the optimization function
global H vtoe intverts nedges twinelts edges Conductivity
global EdgeCond corner_to_x angles3d
%%%%%%%%%%%%%%%%%%%%%%%%%%%%%%%%%%%%%%%%%%%%%%%%%%%%%%%%

% Radii of each ring
r =[1.5, 1, 0.5, 0];
% Numbers of vertices in each ring
N =[20, 10, 6, 1];
eI =[1 ,0];

% Make a mesh
[g,gp,H,E]= cirgrid_eit(r,N,eI);
H = orientH(H,g);

```

```
% Plot the mesh
figure, plcigrid(g,H);
bdryverts = 1:N(1);

% Centroid for each triangle
centroids =(g(H(:,1),:)+g(H(:,2),:)+g(H(:,3),:))/3;

% Number of interior vertices
nvint = size(g,1)-length(bdryverts);
intverts = setdiff (1:size(g,1),bdryverts);
% Now our conductivites are one per interior vertex
% We need a matrix to multiply the conductivities
% at each int vertex to give us a conductivity
% on each element (i.e. the average)
Xtocond = zeros(size(H,1),nvint);

for ie = 1:size(H,1)
    for iv = 1:nvint ; % non boundary verts
        if ismember (intverts(iv),H(ie,:))
            Xtocond(ie,iv)=1;
        end
    end;
end;

sums = sum(Xtocond,2)';
% row sum
for ie =1:size(H,1)
    if(sums(ie)~=0)
        Xtocond(ie,:) = Xtocond(ie,:)./sums(ie);
    end;
end;

vcond = ones(size(intverts));
Conductivity = Xtocond * vcond';
K = zeros(size(g,1),size(g,1));
z = size(g,1);
```

```
58 vtoe = cell([z,1]);
59 angles2d=zeros(size(H,1),3);
60 for ie=1:size(H,1)
61     for k=1:3
62         b = H(ie,k);
63         vtoe{H(ie,k)}=[vtoe{b},ie];
64         side1 = g(H(ie,mod(k,3)+1),:) - g(H(ie,k),:);
65         side2 = g(H(ie,mod(k-2,3)+1),:) - g(H(ie,k),:);
66         %Calculate the angles2d for the 2D mesh
67         angles2d(ie,k) = acos(side1*side2'/(norm(side1)*norm(side2)));
68     end
69 end
70 %%%%%%%%%%%%%%%%%%%%%%%%%%%%%%%%%%%%%%%%%%%%%%%%%%%%%%%%%%%%%%%%%%%%
71
72 % Calculate the angles for the 3D mesh
73 X3d=[g 0.1*rand(size(g,1),1)];
74
75 %Calculate the 3D mesh angles
76 vtoen = cell([size(g,1),1]);
77 angles3d=zeros(size(H,1),3);
78 for ie=1:size(H,1)
79     for k=1:3
80         b = H(ie,k);
81         vtoen{H(ie,k)}=[vtoen{b},ie];
82         side1 = X3d(H(ie,mod(k,3)+1),:) - X3d(H(ie,k),:);
83         side2 = X3d(H(ie,mod(k-2,3)+1),:) - X3d(H(ie,k),:);
84         angles3d(ie,k) = acos(side1*side2'/(norm(side1)*norm(side2)));
85     end
86     K(H(ie,1),H(ie,2)) = ...
       K(H(ie,1),H(ie,2))+Conductivity(ie)*cot(angles3d(ie,3))/2;
87     K(H(ie,2),H(ie,3)) = ...
       K(H(ie,2),H(ie,3))+Conductivity(ie)*cot(angles3d(ie,1))/2;
88     K(H(ie,3),H(ie,1)) = ...
       K(H(ie,3),H(ie,1))+Conductivity(ie)*cot(angles3d(ie,2))/2;
89 end
90
```

```
K = K+K';
rowsums = sum(K,1);
Ksu = sparse(triu(K) - diag(diag(K)));
Ks = sparse(K);
[ied,jed,s]= find(Ksu);
edges =[ied,jed];
nedges = size(edges,1);

% Edge conductances
EdgeCond=zeros(1,nedges);
for ie = 1:nedges
    EdgeCond(ie) = K(edges(ie,1),edges(ie,2));
end;
%%%%%%%%%%%%%%%%%%%%%%%%%%%%%%%%%%%%%%%%%%%%%%%%%%%%%%%%%%%%%%%%
% we need to know the indices of the two angles in each edge
btris =[]; % outward facing triangles with no partner
for ied=1:nedges
    [r1,~] = find(H==edges(ied,1));
    [r2,~] = find(H==edges(ied,2));
    twinelt = intersect(r1,r2);
    if length(twinelt)==1
        btris = [btris,twinelt]; % it is only one!
    else
        twinelts(ied,:) = twinelt;
    end;
end
btris = unique(btris);

corner_to_x = ones(size(H));
nbtris = length(btris);
for ibt = 1:nbtris %miss off the first
    insideone = setdiff(H(btris(ibt),:),bdryverts);
    ind = find(H(btris(ibt),:)==insideone);
    % Now triangle btris(ibt) has angle ind facing outwards
    corner_to_x(btris(ibt),ind)=0;
end
```

```
127
128 count_angles = 0;
129 for ie=1:size(H,1)
130     for k=1:3
131         if corner_to_x(ie,k)==1
132             count_angles = count_angles+1;
133             corner_to_x(ie,k) = count_angles;
134         end
135     end
136 end
137
138 %%%%%%%%%%%%%%%%%%%%%%%%%%%%%%%%%%%%%%%%%%%%%%%%%%%%%%%%%%%%%%%%%%%%%%%
139 % Vectorize the variying angles
140 clear angles_vec
141 for ie=1:size(H,1)
142     for k=1:3
143         if corner_to_x(ie,k)≠0
144         angles_vec(ie,k) = angles3d(corner_to_x(ie,k));
145         end
146     end
147 end
148 angles_vec=angles_vec(angles_vec≠0);
149
150 %%%%%%%%%%%%%%%%%%%%%%%%%%%%%%%%%%%%%%%%%%%%%%%%%%%%%%%%%%%%%%%%%%%%%%%
151 % Calculate and plot the singular values
152 [F,J] = myfunc(angles_vec);
153 figure
154 s = svd(J);
155 plot(s);
156 title('Singular values of Jacobian');
157
158 %%%%%%%%%%%%%%%%%%%%%%%%%%%%%%%%%%%%%%%%%%%%%%%%%%%%%%%%%%%%%%%%%%%%%%%
159 % Calculate the new angles
160 if exist('fsolve','file')
161     options = optimset('Algorithm','levenberg-marquardt',...
162         'Jacobian','on','DerivativeCheck','on','FunValCheck','on',...
```

```
163         'Display','iter','MaxFunEvals',1000);
164     [Xnew,fval,exitflag]=fsolve(@myfunc,angles_vec,options);
165 else
166     Xnew = myfsolve(@myfunc,angles_vec);
167 end
168 
169 %%%%%%%%%%%%%%%%%%%%%%%%%%%%%%%%%%%%%%%%%%%%%%%%%%%%%%%%%%%%
170 % Create the matrix containing the angles (add the fixed angles)
171 angsnew = zeros(size(H,1),3);
172 count_angles = 0;
173 for ie=1:size(H,1)
174     for k=1:3
175         if corner_to_x(ie,k)≠0
176         count_angles = count_angles+1;
177         angsnew(ie,k) = Xnew(count_angles);
178         else
179         angsnew(ie,k) = angles3d(ie,k);
180         end
181     end
182 end
```

D.2 Constraints function code

```
1  function [F,J] = myfunc(anglesvec)
2  % Modified version of Al Humaidi's code
3  % Kyriakos Paridis
4  % 14/09/2012
5  %%%%%%%%%%%%%%%%%%%%%%%%%%%%%%%%%%%%%%%%%%%%%%%%%%%%%%%%%%%%
6  % anglesvec are the varying angles
7  
8  global H vtoe intverts nedges twinelts edges Conductivity
9  global EdgeCond corner_to_x angles3d
10 % F function values
11 % J jacobian
```

```
fnum =1; % number of equations
angles=angles3d;
for ie=1:size(H,1)
    for k=1:3
        if corner_to_x(ie,k)≠0
        angles(ie,k) = anglesvec(corner_to_x(ie,k));
        end

    end
end

% First sum of angles in each triangle
for el=1:size(H,1)
    F(fnum) = angles(el,1)+angles(el,2)+angles(el,3)−pi;
        for k=1:3
            if corner_to_x(el,k)≠0
            J(fnum,corner_to_x(el,k))=1;
            end
        end
        fnum = fnum +1;
end

% Now the sine rule formulae around interior vertices.
for iv = intverts ; % We need just the interior vertices
    vinele = vtoe{iv}; % List of elements around this vertex
    logsinsum = 0;
    for el=vinele % all the elements that include this vertex
    % Within this element which two vertices are not iv?
    outsideverts = find(H(el,:)≠iv);
        if outsideverts(1)==1 && outsideverts(2)==3
        outsideverts = outsideverts([2,1]); % keep cyclic ordering
        end
    logsinsum = logsinsum+log(sin(angles(el,outsideverts(2)))) ...
        −log(sin(angles(el,outsideverts(1))));
% as the cyclic order of the vertices in each triangel is
% anticlockwise the first is plus and the second is minus
```

```
48          if corner_to_x(el,outsideverts(1))≠0 %those not fixed
49          J(fnum,corner_to_x(el,outsideverts(1)))= ...
50                  -cot(angles(el,outsideverts(1)));
51          end
52          if corner_to_x(el,outsideverts(2))≠0
53          J(fnum,corner_to_x(el,outsideverts(2)))= ...
54              cot(angles(el,outsideverts(2)));
55          end
56      end
57  F(fnum)=logsinsum ; % should be zero
58  fnum = fnum +1;
59  end
60
61  % Now the cot formulae
62  % We have to loop over edges that share two triangles
63  for ied =1:nedges
64      if twinelts(ied,1)≠0 && twinelts(ied,2)≠0
65      t1 = twinelts(ied,1);
66      t2 = twinelts(ied,2);
67      tl1 = H(t1,:);
68      tl2 = H(t2,:);
69      ti1 = find(setdiff(tl1,edges(ied,:))==H(t1,:));
70      ti2 = find(setdiff(tl2,edges(ied,:))==H(t2,:));
71      a1 = angles(t1,ti1);
72      a2 = angles(t2,ti2);
73      F(fnum) = Conductivity(t1)*cot(a1)/2+...
74                  Conductivity(t2)*cot(a2)/2-EdgeCond(ied) ;
75      J(fnum,corner_to_x(t1,ti1)) = -Conductivity(t1)/(2*(sin(a1))^2);
76      J(fnum,corner_to_x(t2,ti2)) = -Conductivity(t2)/(2*(sin(a2))^2);
77      fnum = fnum+1;
78      end
79  end
```

Appendix E

Netgen mesh reader code

The following code reads the mesh files generated by Netgen [89] (stored in a .vol file) and imports the required variables in MATLAB. The code was developed in 2009 when Netgen was not incorporated into EIDORS as it is with the latest version 3.6. The code can be considered redundant now but it might be of use to some people in the case where the required geometry cannot be constructed using EIDORS functions. This is the reason for including the code in this thesis.

```
1  function [srfElements, volElements, points] = meshReader(filename)
2 %%%%%%%%%%%%%%%%%%%%%%%%%%%%%%%%%%%%%%%%%%%%%%%%%%%%%%%%%%%%%%%%
3 %[volElements, points] = meshReader(filename)
4 % Reads the surface and volume elements and the point from a file
5 % generated by NETGEN mesher.
6 % Kyriakos Paridis & David Szotten
7 % 11/12/2009
8 %%%%%%%%%%%%%%%%%%%%%%%%%%%%%%%%%%%%%%%%%%%%%%%%%%%%%%%%%%%%%%%%
9
10 fid=fopen(filename,'r');
11 tmp = '';
12
13 while ¬strcmp(tmp,'surfaceelements')
14     tmp = fgetl(fid);
15 end
16 nPoints = str2double( fgetl(fid));
```

```
17 srfElements = fscanf(fid, '%d', nPoints * 8);
18
19 srfElements = reshape(srfElements,8,[])';
20 srfElements = srfElements(:,6:8);
21
22 while ¬strcmp(tmp,'volumeelements')
23     tmp = fgetl(fid);
24 end
25 nPoints = str2double( fgetl(fid));
26 volElements = fscanf(fid, '%d', nPoints * 6);
27
28 volElements = reshape(volElements,6,[])';
29 volElements = volElements(:,3:6);
30
31
32 while ¬strcmp(tmp,'points')
33     tmp = fgetl(fid);
34 end
35 nPoints = str2double( fgetl(fid));
36 points = fscanf(fid, '%f', nPoints * 3);
37
38 points = reshape(points,3,[])';
39
40
41 fclose(fid);
```